Investigation into High-Speed Thermal Instability Testing of Synchronous Turbo-Generator Rotors

Amesh Narain Singh

A thesis submitted to the Faculty of Engineering, University of the Witwatersrand, Johannesburg, in fulfilment of the requirements for the degree of Doctor of Philosophy.

Johannesburg, 2017

Declaration

I declare that this thesis is my own, unaided work, other than where specifically acknowledged. It is being submitted for the degree of Doctor of Philosophy at the University of the Witwatersrand, Johannesburg. It has not been submitted before for any degree or examination in any other university.

Signed this _____day of _____ 20_____.

_____

Amesh Narain Singh

Abstract

The research presented in this thesis conclusively shows that the most effective method to perform synchronous turbo-generator rotor Thermal Instability Testing is by utilising the current injection method of condition assessment. Analysis of the experiences of a local utility for well over a decade has uncovered a high number of rotors failing thermal instability testing in recent years. This trend has brought the current testing methodology into question. Two different assessment modes of testing have been found to be utilised internationally without preference, namely, current injection and friction/windage. By determining the method that is best suited to detect a thermally sensitive rotor a service provider can benefit by improved rotor reliability as well as cost saving. The evaluation is accomplished by utilising a scaled down experimental setup based on the model of a local testing facility as well as a 600 MW turbo-generator rotor. A direct thermal mapping technique has been devised utilising infrared thermography to capture the thermal distribution of the rotor surface under different test conditions. The results obtained have shown that the methods differ substantially with the friction method exhibiting a uniform surface distribution and the current-injection method exhibiting areas of higher temperature concentration around the rotor pole faces. However, weaknesses do exist in present-day testing techniques in the form of inaccurate temperature measurements during testing as well as little consideration given to external factors such as the interaction between the slip-ring and brush-gear that have the potential to influence test outcomes. A presented augmented method of performing thermal sensitivity testing taking advantage of infrared thermography is found to improve testing accuracy and aid in fault detection and location. Current thermal instability testing coupled with the direct thermal mapping method has been demonstrated to be the most effective means for performing rotor thermal sensitivity testing.

To Rasa, Caitanya and Nitai – my life.

Acknowledgements

I would like to express my gratitude to Prof. Willie Cronje for his guidance and patience.

To Rasa Parayani devi dasi for your constant support, encouragement and love.

To Krsna Krpa das, Radha Krpa devi dasi and Sri Govinda das for believing in me.

To their Lordships Sri Sri Nitai Gaurahari for the mercy bestowed unto me.

A special thank you to all the dedicated individuals who contributed to this research.

Finally I would like to acknowledge Dr. Wesley Doorsamy for his guidance, support and friendship.

List of Publications

The author has contributed to the following academic publications by drawing from the research:

1. A. Narain Singh and W. Cronje, "Improved Understanding of Instability Failures Under Thermal Stress Testing of Repaired Generator Rotors," in *Iris Rotating Machine Conference, Nashville*, Tennessee, 2015.

2. A. Narain Singh, W. Doorsamy and W. Cronje, "Thermal Instability Analysis of a Synchronous Generator Rotor using Direct Mapping," in *Southern African Universities Power Engineering Conference*, Johannesburg, South Africa, 2016.

3. A. Narain Singh, W. Doorsamy and W. Cronje, "Analysis of Thermal Instability Test Methodologies for Synchronous Generator Rotors," in *South African Universities Power Engineering Conference*, Stellenbosch, South Africa, 2017, pp. 100-107.

4. A. Narain Singh, W. Doorsamy and W. Cronje, "Investigation of Thermal Instability Testing on Synchronous Generator Rotors using an Experimental Direct Mapping Method," in *IEEE 26th International Symposium on Industrial Electronics*, Edinburgh, Scotland, 2017, pp. 321-328.

5. A. Narain Singh, W. Doorsamy and W. Cronje, "Thermal Instability Analysis of a Synchronous Generator Rotor using Direct mapping," *in SAIEE Africa Research Journal*, Manuscript ID 2016-68, 2017.

Research outputs have also been presented at the South African Institute of Electrical Engineers Rotating Machines Technical Forum.

Contents

List of Figures

List of Tables

List of Symbols

ω	Angular velocity
$R_{t\text{-}a}$	Axial thermal resistance through a cylindrical shell
k_{fr}	Bearing coefficient of friction
F	Bearing dynamic load
d_b	Bearing inner diameter
P_b	Bearing losses
q_{cond}	Conduction heat transfer
q_{conv}	Convection heat transfer
h	Convection heat transfer coefficient
P_c	Copper losses
A	Cross sectional area
I	Current
ρ	Density
ρ_a	Density of air
k	Fluid conduction coefficient
T_∞	Fluid temperature
F	Force
q_x	Heat rate
r_1	Inner radius
L	Length
L_g	Length of airgap
m	Mass
Nu	Nusselt number

r_2	Outer radius
L	Plain layer thickness
Pr	Prandl Number
R_{t-r}	Radial thermal resistance through a cylindrical shell
r	Radius
q_x''	Rate of heat flux
T_{COLD}	Reference temperature
R	Resistance
R_e	Reynolds Number
d	Rotor outside diameter
r_r	Rotor radius
c	Specific heat
k_s	Surface roughness
T_s	Surface temperature
T_a	Taylor Number
T	Temperature
k	Thermal conductivity
R_{t-x}	Thermal resistance through a plain layer
C_M	Torque coefficient
$\dot{q}$	Volumetric rate of heat generation
P_w	Winding losses
R_{COLD}	Winding resistance at reference temperature
R_{HOT}	Winding resistance at test point
T_{HOT}	Winding temperature

List of Abbreviations

CFD	Computational fluid dynamics
CRR	Convection heat transfer
CTIT	Current thermal instability testing
DFOV	Diagonal field of view
DE	Drive end
FEA	Finite element analysis
FTIT	Friction thermal instability testing
HV	High voltage
HFO	Horizontal field of view
IR	Infrared
IFOV	Instantaneous field of view
L	Length
LPTN	Lumped-parameter thermal network
MWT	Mean winding temperature
NDE	Non-drive end
OEM	Original equipment manufacturer
RSO	Recurrent surge oscillograph
RTD	Resistance temperature detector
TIT	Thermal instability testing
VFOV	Vertical field of view

Chapter 1 | General Introduction

1.1   Overview

Service providers utilise a wide range of condition-assessment techniques during the construction, repair and overhaul of large turbo-generator rotors. These techniques vary in purpose, complexity and economic considerations. Their fundamental purpose is to timeously identify problems during the overhaul/repair/construction process. This proactive approach reduces the possibility of the finally commissioned generating unit failing during operation, in other words, increasing the reliability of trouble free operation.

Although many diagnostic techniques are used, these are generally specific to different components of the turbo-generator rotor, for example, tests that evaluate the insulation or detect inter-turn short-circuits. A final proving test known as Thermal Instability Testing (TIT) is performed to evaluate the rotor functionality in its entirety. The test evaluates the rotor vibrational behaviour under simulated operating conditions at 3000 rpm within a specialised balancing facility. Although TITs potential capability and usefulness in evaluating a turbo-generator rotor have been recognised, two distinctly different testing modes can be employed. The rotor under test can be 'excited' using either current or friction/windage, referred to as Current Thermal Instability Testing (CTIT) and Friction Thermal Instability Testing (FTIT), respectively. The mode best suited to TIT has yet to be determined, a situation exacerbated by complexities surrounding the lack of international standards, unclear testing procedures, the limitations of testing facilities, and the high capital cost of required testing facilities as well as test interpretation [1], [2]. This is further compounded by the small community of service providers that perform such testing and who regard their experience as intellectual property, resulting in a lack of knowledge in the public domain.

The research presented in this thesis aims to improve the understanding of turbo-generator rotor TIT. In particular, it seeks to determine the differences between FTIT and CTIT and thereby derive the most reliable method for the performance of TIT. In order to achieve this, the thermal behaviour of the rotor must be analysed under each test condition. An experimental approach using contemporary methods is used. This is achieved by constructing a novel experimental setup capable of directly mapping the thermal distribution of the surface of a generator rotor. Thereafter, a temperature map of the rotor under different scenarios of FTIT and CTIT is created. A comparison of these scenarios is assessed to determine the differences to ascertain which mode is better suited to performing TIT. Furthermore, the capability of the direct mapping method to detect a fault condition is evaluated to improve the localisation of thermal instability related failure.

1.2 Problem description

The increased demand for energy globally has resulted in many utilities operating within diminished reserve margins. This demand has led to increased pressure on service providers to perform manufacturing and conduct overhauls and repairs to a high degree of reliability within constrained turn-around times to maximise plant availability. The foremost motivations for performing TIT are as follows:

- Providing a mechanism for the early detection of turbo-generator rotor incipient problems.
- Executing remedial action and retesting to assess outcomes.
- Meeting the need for component reliability driven by lower reserve margins, aging generating units and high failure rates.
- Avoiding economic loses that may have resulted from commissioning and subsequent failure of a thermally sensitive turbo-generator rotor.

In order for the aforementioned motivations to have relevance, the chosen test procedure must be able to meet these requirements. The turbo-generator rotor is a critical component of the power generation infrastructure and is subjected to a stringent operating regime that can exacerbate weaknesses introduced during repair/overhaul/assembly activities that can lead to failure [3]. Doubts related to the effectiveness of the two testing modes and which of them to utilise can lead to compromises in reliability and loss of capital by service providers. The potential of utilising TIT to detect undesirable operation as a final proving test has been demonstrated in previous works including [4] and [5]. These works cover two different approaches to TIT: one as a final proving test within a testing facility and the other an online test while the unit is commissioned. No specific detail is given regarding the preferred technique, nor is there any detail covered regarding different techniques. Furthermore, the lack of detail presented in TIT-related publications is hampering progress in testing techniques and understanding. This lack is attributed to intellectual property limitations, as a number of publications originate from Original Equipment Manufacturers (OEMs).

The limited experiences shared by different service providers have contributed to a better understanding of thermal sensitivity; however, there is still a significant absence of practical knowledge associated with TIT modes. Through consultation with service providers, utilities and practitioners, and the review of previous work, the following have been identified as major hindrances to the understanding of the different modes of TIT:

- The lack of progress and improvement of testing methodologies.
- Intellectual property limitations leading to limited readily available information and experience related to TIT.

- The absence of an international standard and acceptance criteria.

- Differences in turbo-generator rotor designs can influence TIT methods and acceptance criteria but form part of the manufacturer's intellectual property and are therefore not readily available to repairers/utilities.

- TIT being a specialised testing technique requires a capital-intensive plant, which influences the preferred test technique i.e. CTIT requires higher capital investment than FTIT.

1.3   Aims and objectives

The presented research aims to utilise modern methods to comparatively analyse FTIT and CTIT with the goal of ultimately determining the most effective method for performing TIT.
The main objectives of the research are as follows:

- Develop a modern experimental framework to evaluate TIT by FTIT and CTIT.

- Develop a method which suitably captures and displays the thermal behaviour of a rotor surface and as well as to directly capture the temperature of the winding.

- Qualitatively and quantitatively investigate the merits of FTIT and CTIT.

- Evaluate shortcomings of current frameworks and improvements to TIT.

- Evaluate the experimental framework to aid in fault detection and location during TIT.

Meeting the aforementioned objectives will considerably enhance TIT and yield a valuable contribution to the testing and maintenance of modern turbo-generator rotors.

1.4   Thesis structure

1.4.1   Thermal instability prominence

Chapter 2 presents the fundamentals of turbo-generator rotor breakdown, refurbishment and testing. The chapter relates the experiences of a local repairer in regard to TIT. Details of an investigation into the testing history regarding TIT, of the local repairer, for an eight year period are presented. A global perspective of the different TIT modes is also presented. The adopted methodology for the local TIT process is described.

1.4.2   Thermal sensitivity of turbo-generator rotors

Chapter 3 presents a background into generator-rotor thermal sensitivity. The unique construction features that make a large turbo-generator rotor susceptible to thermal sensitivity are outlined. The causes of rotor vibration, both mechanically and electrically, are discussed. Furthermore, the types and causes of thermal sensitivity are presented. Online, off-line current and off-line friction methods utilised to detect latent thermal sensitivity are described, including an evaluation for suitability. Solutions to the problem of thermal sensitivity that have been used over the years as well as the history related to TIT are finally presented.

1.4.3   Development of a model to evaluate TIT techniques

In Chapter 4, a practical framework for the development of a suitable experimental test setup and the construction thereof is presented. The developed framework is designed to address the shortcomings related to TIT testing techniques outlined in the previous chapter. Initially, the theoretical thermal parameters that govern TIT are described. Consideration was given to different approaches to simulate the different techniques namely analytical techniques as well as numerical methods. Finally, an experimental setup utilising a scaled model of the local balancing facility with a scale model of a 600 MW mini-rotor was developed. A direct thermal mapping method is developed and presented. The performance of the experimental setup is assessed to develop a temperature map of the surface of the mini-rotor.

1.4.4   Thermal instability testing experimental results and analysis

Chapter 5 presents the results of the experimental scenarios carried out utilising the direct thermal mapping method to evaluate FTIT and CTIT. The aim of the experiments were to be able to differentiable between FTIT and CTIT, thereby determining the best suited method for TIT. Utilising the direct thermal mapping method, temperature maps and associated temperature data are presented for FTIT and CTIT. Thereafter, the ability of the experimental setup to aid in fault finding is evaluated. This is followed by a quantitative and qualitative analysis of the experimental results.

1.4.5   General conclusions

Chapter 6 offers closing remarks on the presented research as well as future research suggestions. Refer to Figure 1.1 (below) for an overview of the research methodology.

1.4.6   Appendices

A number of Appendices are presented: Appendix A details the condition assessment of the mini-rotor prior to testing. The experimental setup construction dimensions can be found in Appendix B. Datasheets and calibration certificates for the infrared (IR) camera and infrared pyrometer are detailed in Appendices C and D. Thermal data captured for the entire test duration for the three different scenarios: FTIT, FTIT – brushless and CTIT are presented in Appendices E, F and G.

Augmented Current Thermal Instability Testing as a preferred mode

(Chapter 6)

| Prominence of thermal sensitivity (Chapter 2) | Thermal sensitivity reviewed (Chapter 3) | Direct Thermal Mapping (Chapter 4) | Augmented CTIT (Chapter 5) |

Inevitability of rotor failure or routine maintenance

Influence of rotor design on thermal sensitivity

LPTN unsuitable for complex analysis

FTIT simulates ideal thermal performance which is unrealistic

System specific condition assessment

Varied causes of thermal sensitivity

FEA unable to analyse fluid flow

CTIT simulates operational conditions

Holistic evaluation required – Thermal Instability Testing

No clear preference for TIT method

CFD is complex and capital intensive

Brush gear losses influence thermal distribution

High TIT failure rate experienced locally

Impractical solutions to TIT

Detailed specifications required for analytical methods

Shortcomings of contemporary TIT modes

Two distinct methods utilised globally

Lack of literature regarding TIT

Practical approach required

Figure 1.1: Summary of the research methodology adopted for the evaluation of TIT techniques

Chapter 2 | Thermal Instability Prominence

2.1 Introduction

The fundamental design of generating units utilised worldwide have not changed significantly since the inception of the turbo-generator. The horizontal mounted stator-rotor combination has become common place in the generating fleets of many utilities. The ever increasing demand for cheaper, more reliable power has given rise to supply shortages in many countries. Utilities are struggling to meet these demands. Most of the installed capacity is from older units, which are being driven harder than before, increasing the frequency for maintenance.

Shrinking reserve margins require that any maintenance being performed must be done efficiently and to a high standard of reliability. Being a fixed component at the generating station, the stator undergoes all maintenance activities on site, while the generator rotor in many circumstances requires more specialised overhaul techniques and testing that can only be conducted at a facility that is remote to the generating station. The running life of a generator rotor tends to be shorter than that of the stator, and in many instances rewinds occur at intervals of around 10 to 15 years of operation [6].

Performing maintenance or refurbishment work on a generator rotor requires a thorough understanding of the failure modes, which will determine what corrective action must be taken. For example, an intern-turn fault would only require a partial rewind, while a cracked coil retaining ring would require replacement. During the refurbishment process, a number of condition-based tests are required to fault find and ensure quality.

This chapter focuses on different aspects of generator rotor failure, refurbishment and testing. Section 2.2 briefly reviews rotor failure modes, while section 2.3 focuses on refurbishment techniques. Section 2.4 touches on basic rotor testing techniques. Sections 2.5 and 2.6 present the experiences of a local utility that performs a test known as Thermal Instability Testing. These experiences have highlighted the need for a detailed/further investigation into this particular test.

2.2 Rotor failure

The fundamental role of the rotor subjects it to a harsh operating regiment, operating at high thermal and centrifugal loads, although designed to withstand these tremendous forces. This regime contributes to its short lifespan. The major components of a generator rotor are delineated in Figure 2.1 (below). The predominant causes of rotor failure are as follows: design weaknesses, defective materials, material yield and breakdown, contamination, component migration, and stray currents. These failure modes are manifested when breakdown occurs. The breakdown can affect the

insulation system, the winding or the rotor body. Depending on the degree of breakdown and effect on operation, some level of refurbishment may be required.
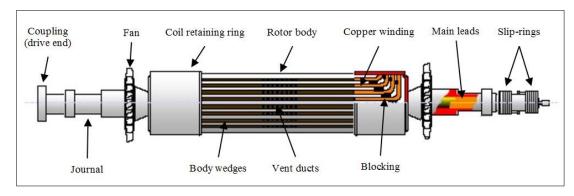
Figure 2.1: Synchronous turbo-generator rotor schematic illustrating major components

2.2.1 Insulation system

Shorted turns are the most common failure experienced on rotor windings. These are caused when there is a breakdown in inter-turn insulation, creating a shorted turn. A number of inter-turn shorts in a coil are shown in Figure 2.2 (below). These lead to severe burning of the inter-turn insulation. Furthermore, the migration of insulation components can affect the flow of the cooling medium, resulting in thermal asymmetries along the rotor body. An earth fault occurs when the ground wall insulation breaks down, and this can cause severe damage to the windings, coil retaining rings and steel forging. An early sign of an inter-turn short burning through the ground wall insulation is depicted in Figure 2.2. Left undetected, this would have resulted in an earth fault occurring.
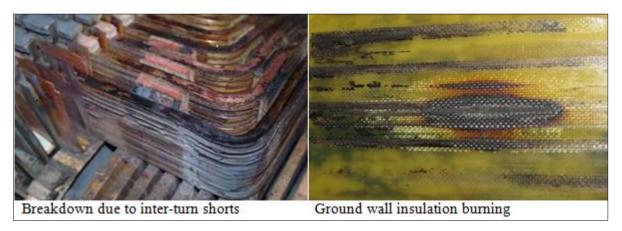
Figure 2.2: Common turbo-generator rotor insulation system failures: inter-turn shorts

2.2.2 Winding

The low yield point of copper introduces a susceptibility to distortion owing to high mechanical stresses experienced during operation. The degree of coil distortion can result in either minor inter-turn shorts or a major short of entire coils, creating undesired magnetic and electrical anomalies. Figure 2.3 (below) illustrates two cases of extreme coil distortion in the rotor overhang area. A more severe case can arise when a turn break occurs, as shown in Figure 2.3. During this occurrence, the

current does not immediately stop, but an arc persists between the break generating intense heat. The heat generated can damage insulation, cause an earth fault or damage the coil retaining rings. A more unique problem called copper dusting, also depicted in Figure 2.3, affects only specific rotor designs and is experienced when the rotor operates at low barring speeds. The abrasive action between the coils and insulation result in copper dust being generated. This can lead to the contamination of the winding, resulting in electrical faults.
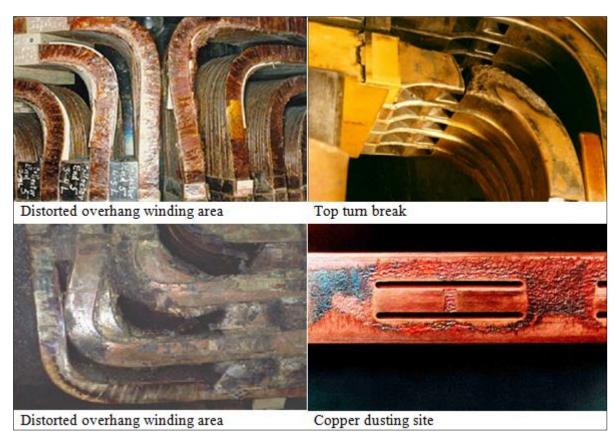
Figure 2.3: Common turbo-generator rotor winding failures: distortion, turn-break, copper dusting

2.2.3   Rotor body

Depending on the material composition of the coil retaining ring (CRR) and the environment in which it operates, cracking can propagate, as seen in Figure 2.4 (below). If this condition continues undetected, the crack will propagate further until a catastrophic failure occurs. Loss of the entire generating unit and consequential plant damage is an expected result. Surface currents induced by incorrect operation can destroy wedges, the steel body and the coil retaining rings, as illustrated in Figure 2.4. Cracking of the forging may also be experienced owing to design weaknesses, incorrect operation or material yield [7] - [10].

Rotor failure is unavoidable and will affect a generating unit at some point within its lifecycle. When a failure is experienced, the outcome will necessitate a process of refurbishment, as detailed below.

CRR surface crack

CRR arcing damage

Arcing damage on rotor body CRR landing Arcing damage on body wedges

Figure 2.4: Common turbo-generator rotor body failures: cracking, arcing

2.3   Rotor refurbishment

Rotor refurbishment methodology will differ with respect to design variations. A generic procedure is therefore not possible, but the basic principles of refurbishment do apply. Different refurbishment options exist based on the condition of the rotor. A rotor may either undergo component replacement, partial rewind or complete rewind. A generic process flow diagram for common maintenance tasks is illustrated in Figure 2.5 (below) and discussed briefly in sections 2.3.1 to 2.3.3.

2.3.1   Component replacement

Components may be replaced to improve material properties, fix defects related to design flaws or comply with routine maintenance. Coil retaining rings are replaced to improve material properties and enhance reliability, as newer materials are less susceptible to cracking and failure. Wedges may also be changed to improve material properties and adjust interference fits. Slip-ring assemblies as well as stalk bolts and main leads may also need to be replaced owing to failure or wear.

2.3.2   Partial rotor rewind

A partial rotor rewind refers to a small-scale but potentially very complex specialised repair on a specific area of concern on the rotor. It is performed to solve inter-turn faults, migrating insulation components, ground wall insulation breakdown, coil distortion and turn breaks. The repair procedure can range from replacing sections of insulation or replacing a number of copper turns or a whole coil (or number of coils) if necessary.

9

2.3.3 Complete rotor rewind

A complete rotor rewind takes place when the rotor winding has reached its end of life or when the failure experienced cannot be repaired by performing a partial rewind or a component replacement. In the case where the rotor winding has reached the end of its design life, the copper winding can be evaluated and reused if still in a good condition, whereas the old insulation system is replaced [11].
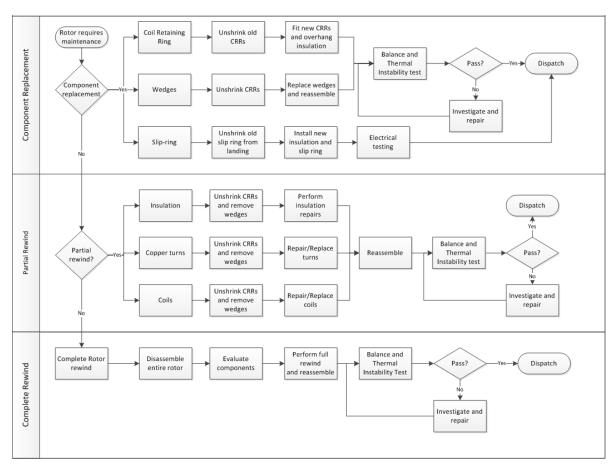
Figure 2.5: Generator rotor refurbishment flow diagram outlining common maintenance processes

2.4 Testing and monitoring during rotor refurbishment

The ongoing cycle of component failure, repair and maintenance must be managed adequately to ensure the security of a utility's generating capacity. All refurbishment activities should not rely exclusively on the adroitness of personnel conducting the work. This needs to be supplemented with a testing regime that ensures the ultimate quality of the finished product. The ability to detect rotor faults during the refurbishment process goes a long way towards ensuring reliability when the unit is commissioned. A number of tests have been devised over the years to assist with rotor fault detection.

2.4.1 Insulation resistance

The insulation resistance test is probably the most common diagnostic tool used to determine problems with the insulation system. It also provides assurance that subsequent high voltage testing can proceed without fear of insulation breakdown. A high DC voltage is applied between two

conductors that are insulated from one another. This provides a measurement for the resistance of the insulation separating the conductors. The resistance for a perfect insulating material should be infinite, but in practice this is not the case as the perfect insulator does not exist. A low resistance value would indicate a problem with the insulation system. Wet, contaminated or damaged insulation would yield a low insulation resistance.

2.4.2   Recurrent Surge Oscillograph

The Recurrent Surge Oscillograph (RSO) test can be used to detect inter-turn shorts, earth faults and any high-resistance connections that may be present in the winding. The principal of operation is based on the fact that a healthy winding is electrically symmetrical viewed from its terminals. Any faults in the winding will result in an asymmetry. Detection is made possible by injecting a steep-fronted step voltage at each terminal. The return signals, when compared, should be identical for a fault-free winding, while a difference would indicate a fault condition. The output waveforms of a RSO test are depicted in Figure 2.6 (below). Waveforms A and B represent the return signals of each respective winding terminal. Waveform M is a comparison of the two waveforms. A difference in symmetry can be observed in waveform M, thus waveforms A and B are not identical indicating an inter-turn fault.
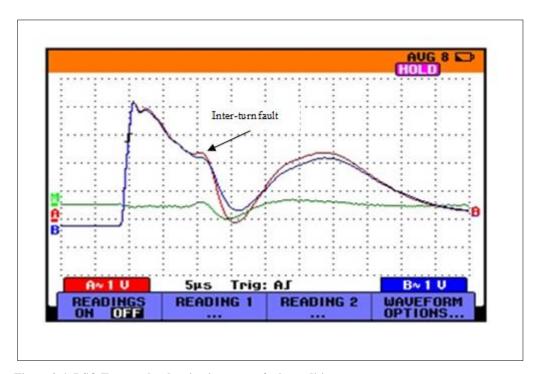
Figure 2.6: RSO Test results showing inter-turn fault condition

2.4.3   Winding resistance

The rotor's total series copper winding resistance is measured. The test can detect inter-turn shorts, poor connections, incorrect connections and circuit discontinuities. The resistance value obtained is generally compared to a previously measured value for the same winding.

2.4.4   High voltage testing

AC, DC or very low frequency AC voltages can be applied to a rotor for high voltage (HV) testing. The purpose of the test is to determine if the winding assembly is capable of withstanding the rated operating voltage as well as any over-voltages and transients that may occur during operation. If the insulation does not break down during the test, the result is considered successful.

2.4.5   Non-destructive testing

The rotor steel body, wedges and coil retaining rings undergo a non-destructive examination to detect any material fatigue and cracking. A number of techniques are used: fluorescent dye penetrant, eddy current and ultrasonic testing. A fluorescent dye penetrant test exposing signs of crack initiation on a CRR is depicted in Figure 2.7 (below) [7] – [9].

Point of surface crack initiation
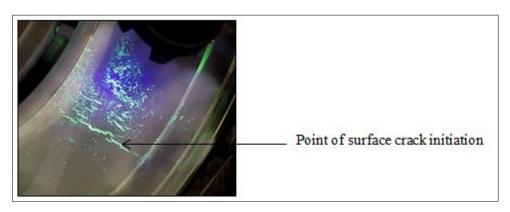
Figure 2.7: Fluorescent dye penetrant test detecting CRR crack initiation

2.4.6   Thermal Instability Testing

A thermal instability test also known as thermal sensitivity testing is performed as the final proving test prior to the rotor being dispatched to the generating station. All the above-mentioned rotor tests in sections 2.4.2 to 2.4.5 target specific areas of the rotor but do not prove that the rotor can function as a whole. All the different components must be able to function homogenously during operation to be considered refurbished and reliable. In essence, thermal instability occurs when a change in the field current causes a corresponding change in vibration levels. A rotor that is both mechanically and electrically balanced is stable and fit for service. Conversely, if a rotor is unbalanced, the resulting uneven loading will lead to bowing of the rotor shaft and increased vibrations. High vibrations result in the rotor being unfit for service and a process of fault finding needs to be followed, as the causes of thermal instability are difficult to pinpoint.

Thermal sensitivity/instability can be commonly caused by the following conditions: shorted turns, coil movement, blocked ventilation slots or inadequate cooling, non-uniform winding, distance blocking variations, ill fitted body wedges, and tight rotor slots. Refer to Chapter 3, section 3.4, for a detailed description of thermal sensitivity.

2.5   Local utility experience of TIT

The utility having experienced a number of TIT-related failures, an analysis is performed to determine the impact and magnitude of test outcomes on the business. The results of a total of 60 thermal instability tests performed on generator rotors are investigated. The time period ranges from the year 2007 to 2014. The rotors are rated from 200 MW to 900 MW and are aged between 20 to 30 years old. Figure 2.8 (below) summarises the test outcomes of the rotors per year. Of the 60 rotors tested during this period, 35 rotors passed and 25 rotors failed, reflecting a high failure rate of 42%.
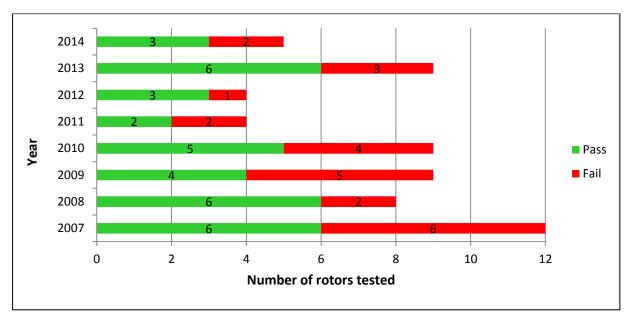
Figure 2.8: Trending of TIT experience of repairer for the period 2007-2014

Figure 2.9 (below) identifies the most prevalent mechanisms of failure for the entire period. Thermal sensitivity constituted the bulk of failures at 88%, inter-turn shorts made up 8%, and earth faults came in at 4%. Most rotors failed due to a combination of coil movement, non-uniform windings, distance blocking variations, ill-fitting body wedges and tight rotor slots. Owing to the uncertainty in distinguishing between these failure mechanisms, thermal sensitivity failure mechanism is used to represent this category. An earth fault is not identified as one of the mechanisms but was experienced.

Analysis of the data indicates an increase in thermal instability failures, which severely affects generating capacity and prolongs the return to service of generating units. This brings the testing methodology into question: Is the testing procedure that has been used for the past 20 years still valid or effective? Global TIT trends and practices have to be determined in order to improve or validate the currently accepted methodology.
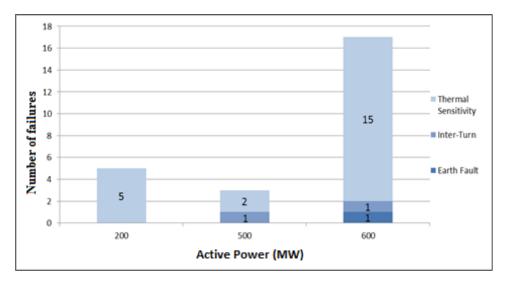
Figure 2.9: TIT failure mechanisms experienced in relation to generator rating

2.6   TIT process

Testing at the local service provider is performed in a specialized 300 t balancing facility designed to accommodate brushless as well as brushed rotors. Different sizes of Faraday cages are also used depending on the rotor length. In brief, the test is conducted by exciting the rotor at different current levels from 400 A to 1500 A, depending on the rotor design. A soaking period is observed for every incremental current. Vibration level, phase and temperature are recorded every five minutes. A rotor that exhibits vibration levels outside prescribed design limits fails the thermal instability test and is not fit for service [12]. Data gathered regarding global TIT preferences is displayed in Figure 2.10 (below) [13] – [21].
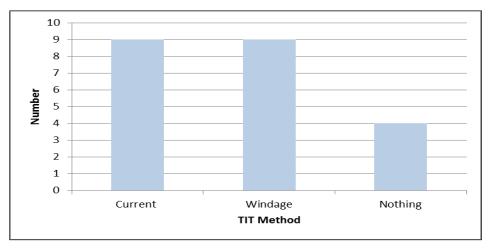
Figure 2.10: Global TIT preferences for current and windage methods for TIT

The data is gathered from OEM and non-OEM service providers that are willing to share information. From the data, it appears that different balancing facilities around the world prefer to use different methods for TIT owing to their own proprietary reasons. Two methods exist: a current injection method used by the local utility and a windage/friction method. There is an even distribution between the two methods of TIT. This lack of a specific preference globally also

14

indicates that a more detailed investigation into which method is better suited to determine rotor thermal instability is required.

2.7   Conclusion

In this chapter, some fundamentals of turbo-generator rotor breakdown, refurbishment and testing are presented. Further to this, TIT is introduced and some experiences regarding TIT are discussed. This information is intended to help the reader understand the purpose of the research and the outcomes presented in further chapters.

Generator rotors operate under harsh conditions and are susceptible to failure. Breakdown can affect the insulation system, the winding or the rotor body. A number of techniques are available to repair such failures based on severity. These techniques can range from simple component replacement to partial or full rotor rewind. To ensure quality and reliability, a condition assessment regime is used throughout the refurbishment process to ensure that faults are detected prior to site commissioning. Techniques utilised generally target specific areas of the rotor construction, while TIT is generally utilised to evaluate the entire rotor under simulated operational conditions.

A number of rotors at a local utility have experienced thermally induced vibrations. This has led to an analysis of the utility's experience of performing such testing for the past 20 years. The result of this analysis is presented and highlights the high failure rate being experienced while performing TIT. This occurrence has brought the test methodology into question. A global perspective related to the test methodology was sought and it was found that two methods of TIT exist: direct current injection and windage/friction. The high failure rate experienced by the utility coupled with the failure to determine a preference in testing methodology has prompted the need for further evaluation and investigation. The disparity in available knowledge related to TIT make the evaluation of the different modes of testing challenging. The current state of knowledge will be examined in the following chapter.

Chapter 3 | Thermal Sensitivity of Turbo-Generator Rotors

3.1 Introduction

The role and impact of performing TIT has been established in Chapter 2. An evaluation into the process and knowledge surrounding TIT is necessary in contributing to a better understanding of the phenomena thereby enabling a process to be formulated for the evaluation of the different modes of TIT. This evaluation will be conducted in the subsequent chapter.

Large-scale turbo-generator plants are commonly fossil and nuclear fuel generation facilities [10]. Global energy demand is forecast to grow by one-third from 2011 to 2035, as outlined in energy policies in [22]. At the end of 2010, coal-fired plants had an installed capacity of 1600 GW with a growth forecast of an additional 1000 GW by 2035 [23]. At the end of 2013, nuclear installed capacity was at 392 GW, with a forecast growth to 624 GW by 2040 [24]. By the year 2040, turbo-generators will be responsible for the generation of an excess of 3000 GW for both nuclear and coal-fired generation. The significance of the turbo-generator is illustrated by these facts. The demand for energy is ever increasing, and the turbo-generator will always form part of core generating capacity alongside other means of energy conversion.

The reliable operation and maintenance of these high-value assets hinge on the ability to effectively test a generator rotor once repaired/overhauled. Specific condition assessment carried out throughout the different stages of repair/assembly will not guarantee trouble-free operation of the entire assembled unit once commissioned. For example, an Insulation Resistance Test will only verify the integrity of the insulation while the rotor is at a standstill and will not take into account the centrifugal and heating effects during operation that may expose weaknesses in the insulation and possible failure. Although regular condition assessment during repair/overhaul is essential, in many instances it is only possible to detect faults specific to that particular testing methodology and not at steady-state behaviour [7]. A more definitive test for evaluating the generator rotor as a whole is necessary. This chapter focuses on the different aspects that relate to the thermal sensitivity of the generator rotor. Section 3.2 briefly reviews the design aspects of the rotor, while the vibration behaviour related to this unique design is outlined in section 3.3. The types and causes of thermally induced vibration are introduced in section 3.4. Three different methods for detecting latent thermal instability within a generator rotor are considered in section 3.5. Section 3.6 presents background information related to thermal sensitivity.

3.2 Review of generator rotor design

Cylindrical rotors are mainly used for applications requiring speeds in excess of 1000 rpm. Electrical networks commonly operate at 50 or 60 Hz; the former will result in the rotor rotating at 3000 rpm and the latter 3600 rpm. The rotor carries the excitation winding and transfers the torque from the

turbine to the electromagnetic reaction at the air-gap [25]. Units have been constructed in excess of 1800 MW, with dimensions ranging from 10 m in length and 5m in diameter [26]. Such generators are typically horizontally mounted and hydrogen cooled. The main components of the rotor are as follows: rotor forging, shaft body, rotor winding and excitation assembly.

3.2.1 Rotor forging

A turbine generator rotor is commonly constructed from a single forging consisting of highly permeable magnetic steel, as illustrated in Figure 3.1 (below). The forging is the basic structure from which the rotor is manufactured. The shaft, rotor body and slots are machined from the blank forging, which must possess excellent mechanical properties and electro-magnetic characteristics. The forging must withstand the centrifugal forces of the rotor operating at rated speed and provide a low reluctance path for the winding flux.

Figure 3.1: Generator rotor rough machined mono-block steel forging

3.2.2 Shaft body

The shaft has two main functions: an electromagnetic function of generating a rotating field and a mechanical function of transferring torque. The shaft is the central structure of the rotor, made of a single forging whose ingot is made in an electric furnace and then vacuum cast. Towards each end, it has a machined journal on which it rotates in the bearings, as well as seal landing areas if the generator is hydrogen cooled, a main coupling to connect the rotor to the turbine on what is referred to as the Drive End (DE) of the rotor, and possibly a smaller coupling on the Non Drive End (NDE) to connect an exciter rotor in certain designs. The NDE may also have slip-rings fitted, through which the DC field current is supplied to the rotor winding.

The body of the rotor has the winding slots milled into what is commonly known as the active zone, with the pole faces in between. In order to equalise the stiffness of the rotor in all planes, radial slits called inertia slits are cut into the pole pace at intervals. A bore hole is often machined in the centre of the forging through its full axial length. The bore hole serves two purposes, firstly to remove material defects (impurities and porosity in the forgings which tend to concentrate at the centre), and secondly to provide access for performing boresonic (ultra-sonic) inspections of the rotor forging from the bore to the surface.

The slots milled into the rotor body are separated by what are known as the slot teeth, which are designed to bear the centrifugal load of the copper coils. Dovetail grooves machined into the top of the slots contain the wedges that transmit the radial centrifugal load of the coils to the teeth. A rotor body with milled slots is depicted in Figure 3.2 (below). The wedges are of a complex design and are highly stressed components. Adding to the complexity of the design, the wedges include radial ventilation holes for cooling gas to enter or escape the copper winding in the slot below.

Figure 3.2: Generator rotor body with final machined winding and cooling slots

The magnetic flux is carried by the rotor in the main body, and is DC in nature. There are two areas which carry the main flux: the solid forging under the winding slots, and the magnetic poles. Leakage flux flows between the rotor teeth and links in the air-gap above each slot.

The shaft design of the rotor is critical in relation to its vibration characteristics. Shaft diameter and length greatly affect the stiffness and consequently the critical speeds and sensitivity of the rotor. The smooth surface of a cylindrical rotor has significantly lower friction in air than salient pole rotors: consequently the losses at the surface of the rotor, known as windage losses, are lower. They are not, however, negligible, and these losses can generate significant heat at the surface of the rotor. The cylindrical shape also results in a more robust structure able to withstand higher centrifugal forces.

As mentioned above, the DE of the rotor has a forged coupling plate bolted to the coupling of the turbine, allowing for the transfer of the torque from the turbine shaft train to the generator rotor. It also facilitates the alignment of the rotors. The coupling has holes machined into it to accommodate the coupling bolts as well as separating holes which allow coupling plate separation during dismantling. The opposite end (NDE) is coupled to an auxiliary machine, depending on the design of the generator. The auxiliary machine may be an exciter, oil pump or starting pony motor.

On each end of the rotor is an axial fan with individual blades mounted on a support ring. The fans create the necessary pressure to ensure the circulation of the cooling medium through the rotor and stator circuits [27].

3.2.3   Rotor winding

The field winding of the rotor is installed in the slots machined into the body. The winding is distributed around the pole faces of the rotor. The winding itself is made up of a number of series-connected concentric coils. There are two main sections of the winding: the winding within the slot area called the slot section, and the winding that protrudes from the ends of the slots, known as the overhang. The winding is insulated from the rotor body; depending on the design, the material properties may vary. Each coil consists of a number of turns, separated by thin layers of insulation. This insulation, despite being relatively thin, must be able to serve its intended insulating purpose and also be able to withstand the mechanical and thermal cycling duty imposed by the rotational forces and thermal variations during operation.

A number of designs are employed to remove the heat produced in the copper turns of the field winding during operation. The copper winding is either cooled directly through contact with the cooling medium, or indirectly in the cases where the heat needs to transfer across the insulation to the rotor body, where it is removed by the cooling medium. In the direct method, cooling ducts are machined into the copper turns, with corresponding holes punched into the insulation, and the cooling gas passes through these ducts to dissipate the heat produced. A key feature of any cooling system design is to slow down the passage of the cooling gas sufficiently to allow the heat time to transfer into the gas and be removed. There are three main cooling designs: axial, radial and air-gap pickup. Combinations of designs are also utilized by many manufacturers as illustrated in Figure 3.3 (below). In an axially cooled winding, the gas is forced axially by the fan along ducts in the conductors. The gas enters the ducts in the overhang section and is then exhausted to the air-gap either at the axial centre of the rotor or in stages along the length of the rotor. In a radially cooled winding, the fans force the gas into sub-slots machined beneath the slots of the rotor at the bottom of each slot. Centrifugal force then forces the gas up radially aligned vent ducts in the winding, to exhaust into the air-gap. In the air-gap pickup method, the wedges are designed in such a way that the surface acts like a scoop, collecting the gas as the rotor rotates and passing it down specially designed ducts in the coils to exhaust through the rear of the wedge.

The rotor windings are supported in the slot section by the slot wedges, but the overhang windings are held in place against centrifugal forces by Coil Retaining Rings (CRRs). The CRRs are composed of high strength non-magnetic steel. Non-magnetic CRRs are used to minimise eddy current formation in the CRRs themselves, and occasionally to better shape the magnetic field produced by the rotor. The CRRs are generally the highest mechanically stressed component in the

generator. They are fitted by heating the CRR until it expands sufficiently to pass over the overhang of the rotor and onto what is known as the landing area of the rotor body. They are designed to have a small interference fit with the landing, and so experience complex stresses both at standstill and during operation, where the centrifugal force can exceed 6000 g. A locking mechanism, typically a snap ring or plungers, or a 'bayonet' type fit, is employed to restrain the CRRs against axial forces due to the expansion of the field winding in service [9].
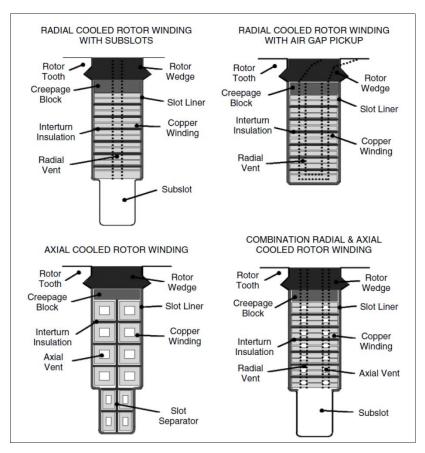
Figure 3.3: Generator rotor winding direct and indirect cooling designs

3.2.4   Exciter assembly

DC current to the field winding is supplied by a number of methods. In the first, current is generated in an auxiliary generator known as an exciter and conducted to the rotor field winding through a slip-ring or collector that consists of two stainless steel rings (one for each polarity of the DC current) mounted on the rotor shaft. The current is transferred from the excitation source to the slip-rings via graphite brushes. In another method, the exciter 'stator' is mounted onto the main generator rotor shaft and rotates, while its 'rotor' is stationary. This produces a poly-phase AC output from the winding on its rotating element, which is rectified by a series of rotor-mounted diodes. This output of the diode assembly is a direct current connected to the winding directly without the need for a slip-ring. This is commonly referred to as a brushless excitation system. Lastly, static excitation is a process where poly phase external power, via an excitation transformer, is rectified utilising solid state devices to produce a DC excitation current. The produced current is supplied to the rotor via the slip-ring brush-gear assembly [28].

3.2.5   Generator rotor losses

Rotor losses are generated in the form of heat. Losses are due to electromagnetic and mechanical sources. Rotors experience primarily copper and frictional losses during operation. Copper losses are due to current flow and can be easily calculated. Frictional losses are constituted of bearing and windage losses. Bearing losses occur due to the friction between the rotating shaft and bearing housing. Windage losses occur during the interaction of the surrounding medium and the rotor body. The ineffective dissipation of the heat generated during these mechanisms can directly influence the thermal sensitivity of a rotor. Heat that is not distributed symmetrically can result in thermal instability. The manner in which these losses are monitored can aid in better understanding the mechanism of thermal instability as well as aid in trouble shooting once a rotor has failed TIT. Refer to section 4.3 for greater detail regarding rotor losses.

3.3   Generator rotor vibration

The basic design of a generator rotor is discussed in the previous section. The analysis of rotor vibration characteristics is an invaluable tool for the detection of rotor operational anomalies or breakdown. The vibration behaviour of a rotor is largely influenced by these design considerations.

A vibration can be described as oscillations about an equilibrium point, which are characterised by an amplitude and frequency. Vibration magnitude can be determined by either measuring the shaft or bearing oscillation. Vibration is measured in terms of displacement and expressed in micro meters peak to peak. Vibration can be measured by a number of instruments – displacement transducer, velocity transducer or acceleration transducer. Vibration behaviour is generally captured using a Bode Plot to plot the phase and magnitude [29]. Acceptable generator rotor vibration limits during operation are specified by the manufacturer based on design constraints. High vibrations can lead to machine shutdown or component damage. Generator rotors can experience two kinds of vibration: one caused by mechanical effects and the other by electrical effects.

3.3.1   Mechanically induced imbalance

The initial sources of rotor mechanical vibration are physical dissymmetries when manufactured, resulting in a varying mass distribution around the geometric axis. Generator rotors are generally balanced in a high-speed balancing facility after manufacture or a major overhaul. The dissymmetries that the rotor may possess due to the manufacturing/overhaul process are offset balanced during this process [30].

Mechanical unbalance vibrations are not dependant on excitation and will not vary with excitation levels. However, the magnitude may vary with rotor angular speed. A number of conditions can lead to generator rotor mechanical imbalance: mass loss/redistribution, misalignment, rubs, oil whirl and shaft cracks [31].

3.3.1.1 Mass loss/redistribution

An unbalanced condition occurs when the centre of mass of the rotor does not coincide with its centre of rotation. Mass loss can be confined to the following areas: balance weights, cooling fan blades, locking components and coupling bolts/nuts.

Thermally shrunk-on components such as fan hubs, couplings, slip-rings and CRRs can move or reseat during operation. CRRs are the most highly stressed component on the generator rotor, experiencing high hoop stresses. A loose or cracked CRR that moves causes a continuously changing unbalance.

A mass redistribution, on the other hand, involves the migration of non-fastened rotor components. For example, the windings and insulation system may migrate under high centrifugal forces. The mass of the copper coils is sufficient to cause an imbalance with just a slight movement [32], [33].

3.3.1.2 Misalignment

Variations in alignment of the generator rotor coupling in relation to the turbine coupling may result in external forces being applied to the rotor shaft. This can affect the rotor rigidity and the overall system-dynamic response. Two types of misalignment can be experienced between the generator rotor and turbine rotor couplings, namely angular misalignment and parallel misalignment, as illustrated in Figure 3.4 (below). Angular misalignment occurs when the mating faces of the coupling are not perpendicular to the central axes of both rotors. Parallel misalignment occurs when the central axes of both rotors are parallel to each other but offset. Severe misalignment can cause bearings and seals to deteriorate and, more seriously, to transfer enough force to the rotor resulting in a bend or crack. Vibrations can be exacerbated by bearing supports that are incorrectly shimmed and fastened [34].
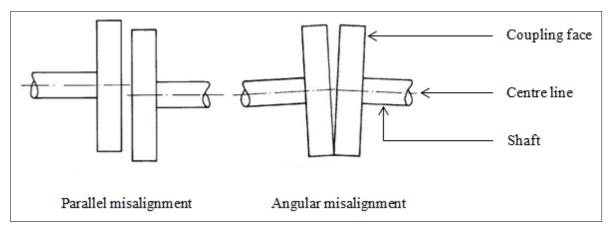
Figure 3.4: Generator rotor coupling parallel and angular misalignment

3.3.1.3 Rub

Rotor rub is an uncommon occurrence on large turbo-generators as a small number of components may rub during operation. A lack of clearances could cause contact between the cooling fans and shroud, the seals and shaft, and the rotor and stator. It is, however, highly unlikely for the rotor to rub against the stator due to the large air-gap. The most common rub that can take place is a hydrogen seal rub. Contact between the hydrogen seal or oil seal and the shaft influences the stiffness of the rotor. A higher stiffness of the rotor shaft causes the resonant frequency to increase. This condition will result in a change in vibration magnitude and phase angle [35], [36].

3.3.1.4 Oil whirl

A generator rotor can experience a fluid-induced instability, commonly referred to as oil whirl or whip. This is a natural occurrence created when a cylinder rotates within a cylinder in the presence of a fluid, that is, the rotor shaft within a curved bearing using lubricating oil. The distance between the journal and bearing centres is referred to as the eccentricity. The likelihood of an oil whirl being experienced is governed by the eccentricity ratio, defined by dividing the eccentricity by the radial clearance between the journal and bearing. A low eccentricity ratio favours the development of a fluid instability. Oil whirl can only develop in one supporting bearing at a time and can be easily detected. Varying the oil temperature or supply pressure may help to reduce the instability. The key to avoiding oil whirl/whip is to ensure a high eccentricity ratio [37].

3.3.1.5 Shaft cracks

Generator shafts subject to high levels of stress can experience crack propagation. Common areas affected are CRRs, rotor slot top teeth and dovetails. Cracking can create differences in rotor shaft stiffness, resulting in uneven flexure of the rotor as it operates [32].

3.3.2   Electrically induced unbalance

Electrically induced unbalance is typically manifested by the thermal behaviour of the rotor. As the rotor is excited by an increasing current, the copper winding will rise in temperature. The increasing temperature naturally causes the copper to expand within the slots and overhang area, but not in proportion to the expansion of the steel rotor forging, as the coefficient of expansion of copper is nearly twice that of steel. The expanding copper will exert axial forces on the other components of the rotor slot contents, body wedges, blocking and CRR assembly. The heat generated within the winding will also be conducted through the steel body and dissipated by the cooling medium. If this heat transfer process continues symmetrically along the body of the rotor, a thermal unbalance will not be experienced. However, if the heat transfer process or coil forces occur asymmetrically, an unbalance will be experienced, resulting in the bowing of the rotor body. The severity of the thermal bow will determine the amplitude of the vibration experienced at the bearings [38].

A thermal unbalance is characterised by a relationship between vibration and excitation. An increase in excitation results in an increase in vibration magnitude. Detailed causes of thermal imbalance are outlined in Section 3.4.4.

3.3.3 Identifying causes of vibration

Identifying the causes of vibration takes thorough knowledge of the machine's behaviour during operation. Table 3.1 (below) summarises the vibrational response for the conditions discussed in Section 3.3 [39]. The values reflected apply to bearing vibrations.

3.3.4 Generator rotor vibration evaluation

Vibration monitoring and evaluation forms a critical aspect of rotor condition assessment during operation and testing. Vibration analysis was primarily utilised to evaluate the functionality of the bearing system where high vibrations indicated bearing failure. Vibration analysis has however evolved into a sophisticated method over recent years. Contemporary vibration assessment techniques can aid in the identification of numerous mechanical and electrical sources of vibration. There is however no accepted standard on vibration limits. There exist many guides to assist operators to determine what is suitable for their particular machine. Some adopt ISO 7919-2 covering steam driven turbo-generators in excess of 50MW [40]. ISO 7919-4 encompasses the field of gas turbines [41]. The IRD Mechanalysis Vibration Severity Chart can also be consulted and sets down guidelines for vibrational limits [42]. Vibration analysis is a complex field that relies on the knowledge of machine design elements as well as operational behaviour which will not form part of the scope of this study.

Table 3.1: Vibrational response summary of generator rotor unbalance conditions

Cause of Vibration	Amplitude	Frequency	Phase
Mass loss/redistribution	Proportional to unbalance; largest in radial direction	1 x rpm	Single reference mark
Misalignment	50% or more radial vibration; large in axial direction	1 x rpm commonly 2 or 3 x rpm possible	Single, double and triple reference mark
Rub	-	0 to 50% of 1 x, 1x, higher harmonics	Erratic
Oil whirl	May change rapidly	50 to 50% or 1 x rpm	Unsteady
Shaft cracks	Variable during transients	1, 2 x rpm	Change in 1 x phase can occur
Thermal unbalance	Disappears when power is turned off	1 x rpm or 1 or 2 x line frequency	Single or rotating double mark

The mechanical causes of vibration have a regular and fixed pattern, facilitating the identification of the root cause. A well-established condition-monitoring system would be able to identify these causes through pre-programmed detection algorithms. The physical cause of the mechanical imbalance is also easily identifiable, for example, a misalignment may be detected by the condition monitoring equipment; the couplings can be easily checked for misalignment, while a cracked shaft can undergo non-destructive testing to locate the crack.

Generator rotors are predisposed to thermal sensitivity owing to their complex design, material composition and operating requirements, as discussed in Section 1.3. Manufacturing/refurbishment techniques introduce component variation which cause most rotors to exhibit some level of thermal sensitivity and may require attention according to the degree of sensitivity. Thermally induced vibration in generator rotors is by far the most difficult to diagnose and treat. The symptoms may be a bowed shaft and a vibration signature linked to the excitation current, but the possible underlying causes are numerous. Difficulty arises when physically determining the cause of the thermal imbalance without excitation, making mechanically dynamic or electrical causes impossible to diagnose. A thorough inspection and methodical strip down of the rotor in search of anomalies will require the rotor to be removed from the stator. Since the exact conditions that cause the thermal unbalance are not acting on the rotor, physically identifying the anomaly becomes near impossible. This phenomenon is commonly referred to as a Thermal Instability/Sensitivity. Conventional balancing techniques are not suited to detect and correct such problems [43]. The experiences discussed in Chapter 2 and the sources of vibration discussed in Section 1.3 make it clear that this phenomenon calls for detailed evaluation and understanding.

3.4   Rotor thermal sensitivity

Generator rotor thermal sensitivity can be classified into two categories, linear or non-linear vibration.

3.4.1   Linear vibration

A linear condition is where the vibration of the rotor is proportional to the excitation current level. The graph depicted in Figure 3.5 (below) illustrates the typical behaviour of a rotor experiencing a reversible thermal sensitivity. When the current is increased the vibration level increases – from point A to D. When the current level decreases, the vibration level correspondingly decreases from point D to G.
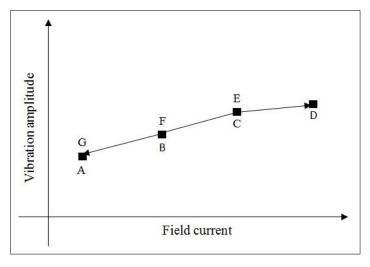
Figure 3.5: Generator rotor experiencing linear vibration behaviour

3.4.2 Non-linear vibration

A non-linear rotor vibration condition is not proportional to the excitation current. The graph depicted in Figure 3.6 (below) illustrates that the vibration increases with current from points A to D but does not decrease with a reduction in current from points D to G. This type of thermal sensitivity is generally very severe and could lead to disassembly or rewind [44].
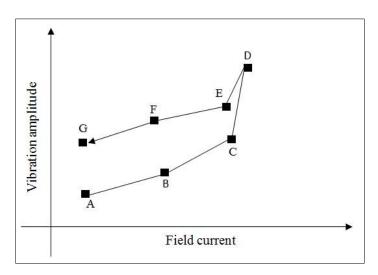
Figure 3.6: Generator rotor experiencing non-linear vibration behaviour

3.4.3 Causes of linear and non-linear vibration

There exist a number of possible causes of thermal linear and non-linear vibration, as shown in Table 3.2 (below) [6].

Table 3.2: Causes of thermal sensitivity linear and non-linear vibration

Linear Vibration	Non-Linear Vibration
Copper coils adhering to the slot liners	Differences in coefficients of friction – copper coil surfaces, inter-turn insulation, slot liners, overhang insulation, blocking surfaces
Inter-turn shorts	Wedge fit
Asymmetric overhang blocking	Wedge movement
Asymmetric heat distribution	Wedge yield
Uneven paint thicknesses	Overlapping inter-turn insulation
Shifted slot liners or inter-turn insulation	Overlapping overhang insulation
Operating close to vibration critical	Copper coils adhering to slot liners
Blocking fit	Uneven winding
	End block movement
	Broken turns
	Coil movement

The numerous causes of thermal sensitivity are complex and vary from design to design. It has been found that even subtle influences can create a thermal imbalance. For example, a rotor is cleaned differently on either end; this causes a difference in emissivity in the rotor surface finish resulting in a thermal unbalance during operation [45]. Rotor thermal sensitivity may be influenced by individual causes or a number of causes acting collectively to create a difficult fault-finding scenario. For example, in one instance, a unit exhibited unexplained high vibration levels during loading. Several theories were considered, including unstable foundation, misalignment, shorted turns and a cracked shaft. After much effort, it emerged during strip down that insulation blocks were not within tolerances, causing the top copper bar to deform during operation. After considering the rotor condition, it was deemed necessary to rewind [46]. A number of the major causes of thermal sensitivity are discussed in more detail in the next section. This will assist in understanding the complex interactions between components in the generator that cause thermal sensitivity problems.

3.4.4   Common causes of generator rotor thermal instability

The most common causes of thermal sensitivity are shorted turns, coil movement, blocked ventilation slots or inadequate cooling, non-uniform windings, distance blocking variations, ill-fitted body wedges and tight rotor slots.

3.4.4.1 Shorted turns

One of the most common failure mechanisms of a generator rotor is inter-turn shorts. In 2003, it was estimated that over 50% of installed generators in the United States ran with shorted turns. Shorted turns occur when there is a breakdown in the insulation between turns [47]. This can lead to

asymmetrical heating of the rotor body. Of particular significance are coils that are adjacent to rotor poles (smaller coils); imbalances in adjacent coils are more likely to cause a thermal bend. Inter-turn faults cause a reduction in the active coils of the generator rotor. A pole that has a number of shorted turns will operate at a lower resistance as compared to the opposite pole. This condition will have an effect on the thermal losses (I^2R) of each pole; the lower resistance pole will operate at a lower temperature, while the opposite pole with a higher resistance will operate at a higher temperature. This effect will cause a thermal gradient along the rotor body resulting in a bow of the shaft and increased vibration, as illustrated in Figure 3.7 (below) [48]. A short in Pole A will result in the illustrated bow pattern. Hence current excitation will have an effect on the vibration levels.
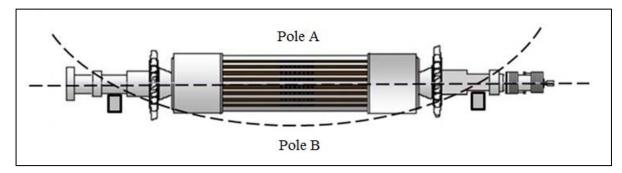
Figure 3.7: Generator rotor body thermal bow due to shorted turns

Shorted turns are generally easy to detect before commissioning by performing either a RSO Test, as described in Chapter 2 Section 2.4.2, or during a Stray Flux Test in a balancing facility [49]. If a shorted-turn is experienced during operation, it can still be detected with a stray flux probe, and a load adjustment can be made to enable smooth operation.

3.4.4.2 Coil movement

During the heating cycle, coils may move to one side of the rotor, creating a ratcheting effect that leads to imbalance [45].

3.4.4.3 Blocked ventilation slots or inadequate cooling

Restrictions in cooling can severely affect the thermal balance of the rotor. Certain rotor designs are cooled by the winding being in direct contact with the cooling medium, as described in Section 3.2.3. The introduction of foreign material (contamination) can block vent ducts. Vent ducts can also be blocked if inter-turn insulation migrates within the rotor slot. This results in an uneven temperature distribution along the length of the rotor. Localised heating in excess of 250 °C has been reported as a result of partial blockage [50]. An imbalance is experienced similar to that of an inter-turn short.

3.4.4.4 Non-uniform winding

If a rotor is not wound uniformly from pole to pole with the same insulation dimensions and assembly of materials, differences in frictional forces may arise, leading to a restriction in expansion

of the copper coils. This may occur within the rotor slots or under the CRR. The asymmetrical expansion causes a varying force distribution on the rotor body, resulting in a bowing condition. A copper turn may also expand radially to a greater degree than other coils. A small displacement in the radial geometry of the rotor can result in a large unbalanced force (F), which is expressed as:

$$F = mrw^2 \tag{3.1}$$

where m is the mass, r is the radius and w is the angular velocity of the rotor. It can be further seen that the unbalanced force is directly proportional to the radius of the rotor, making larger units more susceptible to a non-uniform winding. This can affect rotors that have been in operation for a long period and have experienced insulation breakdown, as well as newly assembled rotors that have been non-uniformly wound. This condition is best prevented by making sure that the rotor is wound to exact specifications and tolerances to maintain uniformity throughout the winding, as shown in Figure 3.8 (below).
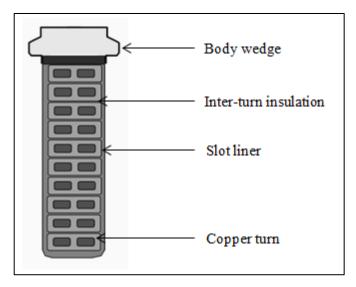
Figure 3. 8: Schematic of a uniformly wound rotor slot with coils, insulation and wedge

3.4.4.5 Blocking

Blocking used within the overhangs of the rotor must be spaced and fitted appropriately to ensure uniform expansion of the coils without restriction. Incorrectly fitted blocking can result in an uneven force distribution under the CRRs when the winding expands. The asymmetrical forces transfer through the CRRs and end disc, resulting in the rotor body bowing. A typical blocking arrangement is shown in Figure 3.9 (below).
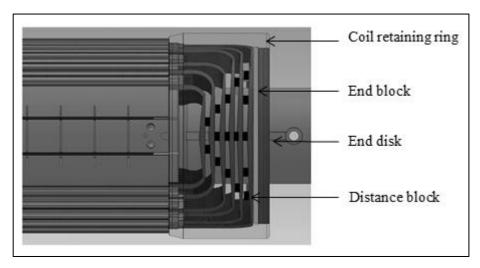
Figure 3. 9: Typical blocking arrangement of a generator rotor overhang

3.4.4.6 Wedge fit

A rotor can suddenly experience thermal sensitivity following a partial re-wedge. Wedges may be replaced owing to damage or improvements in design. Ill-fitting rotor body wedges that may be too loose or too tight create an uneven interference fit throughout the slot length. This can lead to the restriction of movement of copper coils in the axial and radial direction. Wedges with non-uniform tolerances at dimension A and B of Figure 3.10 (below) will result in the insulation material and top copper turn being squeezed into these gaps, creating a deformation that binds the copper in place. This prevents expansion and contraction [51].
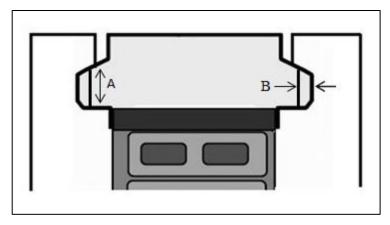
Figure 3.10: Thermal sensitivity rotor body wedge fit considerations

3.4.4.7 Tight slots

Rewound rotors may sometimes experience tight slots when the original copper is being reused, but this is not necessarily an exclusive relationship. After years of usage, the original copper may no longer be symmetrical and flat. Coils that have been bound within rotor slots due to friction cannot expand freely and begin to exert a force on the steel body. It has been reported that rotor coils can expand in length up to 40% more than the steel body [50]. Design clearances are then compromised, creating excessive radial forces within the slots, which in turn bring about thermal bowing of the

rotor. For example, in Figure 3.11 (below), pole A may experience a tight slot, whereas pole B remains unrestricted, resulting in the illustrated bow pattern when current is increased.
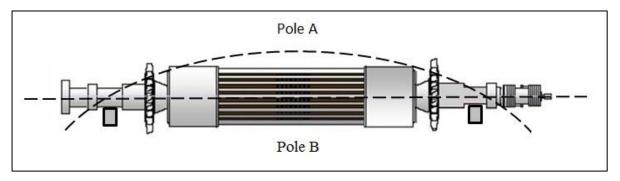
Figure 3.11: Thermal bow due to tight rotor body slots

3.5   Methods to detect thermal sensitivity/instability

Determining whether a rotor is thermally sensitive is relatively straightforward, as the relationship between the current and vibration levels is sufficiently indicative. However, the methodology used to monitor this relationship is pertinent. The ability to create the specific operating conditions for the rotor to exhibit a latent thermal sensitivity problem is important. Three methods of TIT exist. The first test is an online test performed after the rotor has been commissioned. The remaining two tests occur within a balancing facility capable of performing either a Friction Thermal Instability Test or a Current Thermal Instability Test. Facilities that can perform a CTIT can also generally perform a FTIT as well, but not necessarily vice-versa.

It should be noted that there is no international standard for the testing methodology or acceptance criteria for vibration limits when performing TIT. The methodologies that frame these tests remain undisclosed, as they form part of the intellectual property of the OEM /utility/repairer that performs the test [4]. The matter is further compounded by the large capital investment required to construct a balancing facility capable of performing TIT. This results in the subject matter not being widely published either, which makes testing and interpretation the prerogative of the OEM/utility/repairer. Interpretation and test methodology determine whether a rotor is fit for service or not. This can have significant consequences in terms of warranties and profitability when the rotor is refurbished/overhauled. As a final factory acceptance test may result in a rotor failing due to thermal sensitivity, the magnitude of consequences for the client or the OEM/utility/repairer cannot be underestimated. In the following section, the different types of thermal sensitivity testing will be discussed.

3.5.1   Online thermal instability testing

The following online TIT method is outlined in [52]. This is an OEM methodology with which a number of other references concur [53]. Initially, the rotor is tested for inter-turn shorts, as discussed in Section 3.4.4.1. The next step is to distinguish between the effects of real power and reactive

power loading, as vibration change arising from real power loading is indicative of bearing alignment shifts during operation. A three-phase diagnostic test is reported, as per Figure 3.12 (below).

The initial step is to supply the rotor with a constant current while varying the megawatt loading on the generator from 15% to 60%. This corresponds to points 1 through 4 in Figure 3.12 (below). Comprehensive vibration, voltage, current and temperature readings should be taken throughout this process. Any alarming parameters should be monitored.

The second step is to apply a constant real power load of about 60% to 80% of rated power, followed by raising the field current to the maximum rated value. Each test level should be maintained until steady state operation is reached. This corresponds to points 5 through 8 in Figure 3.12 (below). If thermal vibrations are experienced before the maximum rated current is applied, the process should be repeated until the current level associated with an acceptable vibration level is reached. A thermally sensitive field will exhibit a significant change in vibration or phase, while the field current is increased at constant real power loading. At this time [9] suggests that the field current be reversed to be able to detect coil movement (Section 3.4.4.2).

The final step is to decrease the current from the maximum level to the initial starting value. This corresponds to points 9 through 12 in Figure 3.12 (below). If the vibration and phase correspond to the initially measured values, the thermal vibration is classified as linear. Commonly, this sort of vibration can be solved with a compromise balance mass. If, however, the vibration level remains high and does not return to the originally measured values, the vibration is considered to be non-linear and will require a detailed investigation.

If a thermal sensitivity problem is detected while performing this test, a number of scenarios can unfold. The thermal sensitivity may be within vibration limits and the rotor fit for operation. However, if undesirable levels of vibration are experienced, a compromise balance mass may be required. The rotor will have to be decommissioned for this to take place. If a compromise balance mass does not solve the problem, the rotor will have to be returned to a repair facility to be evaluated. This method of testing may be the best to detect a thermal sensitivity issue, as it is done under operating conditions, but the time lost and capital spent to commission and decommission the unit makes it an undesirable option as a final proving test.
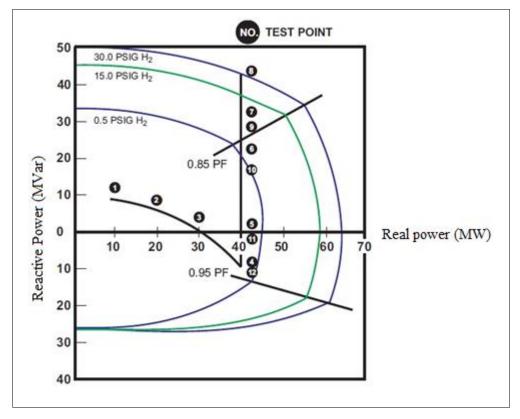
Figure 3.12: Machine capability diagram outlining rotor thermal sensitivity test procedure for online testing [5]

3.5.2 Current thermal instability test

CTIT is a specialised test requiring a balancing facility able to inject current into the rotor as well as having the required facilities to deal with the electrical field created. Very little is known about this test methodology. In [4], some details are shared regarding this type of test as performed by an OEM, which describes the procedure as a patented solution. Also referred to as a 'heat run test', current is injected into the rotor at rated speed. Temperature, pedestal and shaft vibrations are monitored and recorded throughout the test. The rotor is initially taken to rated speed, thereafter current is applied in increments until the targeted stabilized mean winding temperature (MWT) is reached. A three-phase process is then followed, as depicted in Figure 3.13 (below). Step one is the heating phase until the MWT is reached, corresponding to time t_1. Thereafter, the MWT is maintained until time t_2. This is referred to as the stabilisation phase. The final phase is the cooling phase that lasts till t_3. During this phase, the current is turned off while being cooled at rated speed. No further detail is shared with regard to temperature value limits as these are critical to the test and may be considered proprietary information.
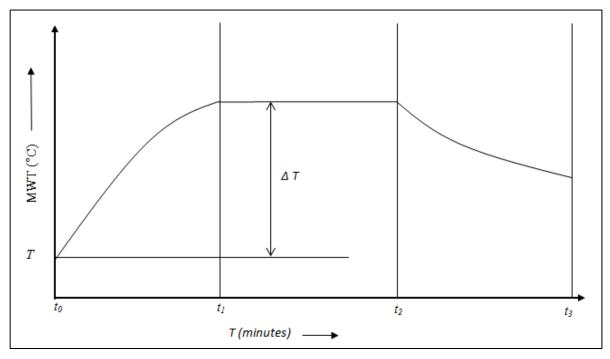
Figure 3.13: Graph depicting an OEM process for thermal sensitivity testing via CTIT

3.5.3   Friction thermal instability test

Reference material regarding FTIT is scarce. Chapter 2 Section 2.6 establishes that the test is a prominent methodology used globally to perform TIT. Local utility experience regarding this test involves the rotor being operated at rated speed where the frictional (windage) interaction between the rotor surface and surrounding air cause the rotor to heat. Rapid or controlled heating is not possible when using this method. Vibration and temperature values are monitored at all times. This test can be performed in any balancing facility as no specialised equipment is necessary. This is one of the probable reasons why it is has been found to be such a popular methodology. During this test, temperatures reached are typically the ambient temperature plus 55 °C to 75 °C [54].

A variation on the FTIT method is mentioned briefly in [4]. This process involves the blowing of heated air into the rotor winding enclosed within a 'heat box' at rated speed. This methodology would rely on both friction and an external heat source. It has, however, been found that similarly to FTIT, a significant temperature rise in the rotor winding cannot be achieved in a short period of time.

3.5.4   Suitability of testing methodologies

The current knowledge base regarding TIT raises the following key questions:

- Is a simulated approach being performed in a balancing facility suitable for thermal sensitivity testing?
- What procedure should be followed to perform the testing, CTIT or FTIT?
- What acceptance criteria should be used?

Currently, the available information does not allow for conclusive answers to the above questions. It has already been stated that online thermal instability testing is the technique that best suits the detection of latent rotor thermal instability as it offers true steady-state operation conditions. Online thermal instability testing can, however, also be destructive, resulting in increased vibrations after test completion [53]. On-line thermal instability testing does not reassure the utility that a repaired/overhauled generator rotor is fit for service prior to commissioning. Any remedial action necessary comes at a high expense of decommissioning, fault finding, repair and retesting. This methodology is thus not suited for the testing of repaired/overhauled rotors but is best suited to vibration problems experienced during the rotor's operational lifetime.

It falls to CTIT and FTIT to determine reliably whether a rotor has a thermal sensitivity problem prior to the rotor being dispatched to site and commissioned. These tests are performed at the repairer's facility where any remedial action can be performed in house and retested conveniently at a lower expense. Figure 3.14 (below) illustrates a typical testing scenario used by an OEM/utility when performing CTIT within a balancing facility. A rigorous testing process is followed with multiple thermal balances, frequent electrical testing and inspections. The process is concluded with a final thermal balance performed on-line after the rotor has been commissioned [55].

Once again the difficulty arises as to which method would be best suited to detect a thermal sensitivity problem. The answer to this question is not obvious, as the research related to these areas of study is either proprietary information or has not been explored as yet. The first step into trying to answer any of the above questions would be to determine the differences between CTIT and FTIT. The presented research focuses on determining the difference between CTIT and FTIT as testing models. As mentioned previously, as final proving techniques, these testing modes can adversely affect the manufacturer/repairer as well as the operator. The following sections present some background history of thermal sensitivity as well as previously conducted research.

3.6   Solutions to rotor thermal sensitivity/instability

A number of novel ideas have been proposed over the years to deal with rotor thermal sensitivity. The best form of prevention is in the design of a generator rotor. A rotor should be designed to minimise potential thermal sensitivity. Factors that contribute to design improvements are frictional coefficients between components, rotor slots, rotor wedges, cooling and rotor length. A compromise balance has already been mentioned in the section above, and is achieved by adjusting the rotor cold balance condition at rated speed so as to influence the balance behaviour under operating conditions. This method is suited to slight thermal vibrations that are linear in nature.

The concept of thermal balancing of generator rotors is proposed in [56]. This process involves the insertion of an obstruction into the rotor axial ventilation ducts. The rotor vibration is monitored as

the temperature changes in order to determine where the obstruction should be inserted. The vibration data are captured on a polar plot, and the direction of the thermal vector is found to be the same as that of a static weight added to the warmer side of the rotor body.

Install into balancing facility

Rotor inspection

Thermal balancing at critical speed

Electrical testing

Return to assembly shop

Electrical testing

Thermal balancing at critical speed

Confirm vibration signature

Electrical Testing

Perform inspections

Ship to site

Electrical testing

Commision rotor

Thermal balance at critical speed online

Commence commercial operation

Figure 3.14: Process flow diagram for the thermal balancing of a generator rotor

Consequently, the obstruction will correspond to the location of the weight. However, the magnitude of the correction is determined by a process of trial and error. Once the location and number of ventilation slots to be blocked are determined, blocking strips are inserted into the slots through the generator air-gap. Silicone rubber plugs have also been used for the same purpose [57]. This has been found to be a difficult and time-consuming process. In essence, this method modifies the rotor's cooling arrangement to compensate for the thermal imbalance. The benefit of this method is that it can be performed in situ. However, the feasibility of this method has yet to be determined, as it has not been found to be an adopted technique. Different rotor designs may not allow access to the ventilation slots without removing the CRR. The method also results in the introduction of a foreign body within the rotor that may become dislodged and cause a malfunction during operation [58].

An online automatic rebalancing technique utilising mounted heater elements is proposed by [59]. In order to be able to thermally balance a rotor, dedicated heater elements are mounted on the circumference of the rotor and are actively controlled to maintain thermal balance. A control system is used to automatically adjust the heating element temperatures in real time to maintain thermal balance. This is, however, not the first time this method has been proposed, as General Electric patented a similar system in 1964 [60]. This method possesses a number of risks, including the introduction of foreign material, and has not been proved as a viable solution to thermal instability.

3.7 Historical overview of thermal sensitivity/instability

It was initially discovered that a rotor can experience a thermal imbalance attributable to the production of high vibrations by the asymmetrical heating or cooling of the rotor (an example of the earliest reports was published in 1947 by a manufacturer in [56]). This development incited further research into the causes of thermal imbalance as well as efforts to mitigate the effects experienced. A number of factors including tolerances and dimensions of materials, cooling, contamination and paint thickness were found to contribute to thermal imbalances. Sensitivity to these factors increased with rotor size, as this problem was not evident in smaller units [57]. Further research uncovered that electrical effects caused by rotor winding inter-turn shorts can lead to thermal sensitivity [61]. In the 1960s, OEMs began to recognise the problem and proposed patented solutions to detect and solve thermal sensitivity failures. These included online automatic thermal balancing and the introduction of an in-house 'heatrun' at rated speed [4], [60].

By the 1980s, generator rotors had gradually increased in size and rating. OEMs had started to recognise the importance of design considerations in relation to thermal sensitivity as well as introducing a thermal balancing procedure as part of their factory acceptance criteria [62]. Mainstream recognition was given to the phenomena of thermal sensitivity in the 1990s, with notable works such as [45], [52]. Reasons were given for the behaviour of rotors that experience thermal sensitivity as well as industrial experiences. A procedure for on-line thermal sensitivity testing was outlined for the first time. Recognition was given to thermal sensitivity, with the inclusion of a section on rotor vibration in an international standard [31].

In the 2000s, thermal sensitivity testing was being adopted by a number of utilities, making it no longer exclusive to OEMs. During this period, many behavioural anomalies were found in relation to thermal sensitivity as well as means of combating the problem. There was a unique case where a rotor exhibited both linear and non-linear vibration [63], [64]. Figure 3.15 (below) illustrates a timeline of the milestones of developments in the area of rotor thermal sensitivity. During this period, the testing methodology presented for thermal sensitivity within the factory balancing facility was not accounted for. A methodology for on-line testing was presented in [52], but insufficient detail was presented for a 'heatrun' test mentioned in [4] (owing to proprietary information) as well

as a thermal balancing test in [55]. The suitability of these in-house testing methodologies to detect latent thermal sensitivity mechanisms is not apparent at present.
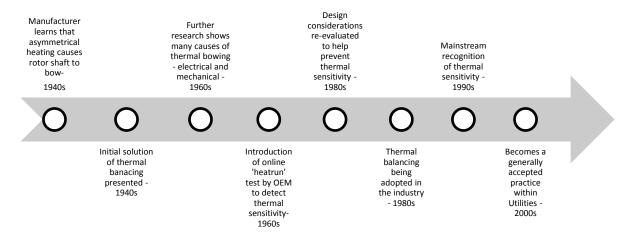
Figure 3.15: Basic timeline of the understanding and detection of thermal sensitivity

3.8 Conclusion

In this chapter, the intricacies of generator rotor construction are presented. This information assists the reader to understand how these complexities can make a turbo-generator rotor susceptible to thermal sensitivity. Furthermore, the theory surrounding TIT is evaluated and its shortcomings exposed.

The different components that form the structure of the generator rotor are reviewed: rotor forging, shaft, winding and exciter assembly. Modern generator rotors have grown in size and complexity over the years as the demand for energy increases. This development has resulted in varying designs that experience unique problems when all the different components come together to form the rotor assembly, with the expectation of homogenous operation. This chapter presents an overview of the vibration behaviour related to this unique design covering both mechanical and thermally induced vibrations.

A framework for methods used to perform TIT is also presented, providing a systematic approach to how TIT is performed. Three methods are reviewed: online thermal instability testing, CTIT and FTIT. These testing methodologies are seen as the most critical final proving mechanisms to ensure that a rotor is fit for service. Neither the methodology for these tests (especially CTIT and FTIT) nor which test is best suited for detecting latent thermal instability problems could be ascertained. Practices related to these testing methodologies can pose a major risk to utilities and OEMS in regard to financial losses and component reliability, especially since no international standard exists. Thus, it would seem that these practices and methodologies are preferred because they form part of patented solutions that do not belong to the general knowledge base.

Chapter 4 | Development of a model to evaluate TIT techniques

4.1 Introduction

The phenomenon of generator rotor thermal sensitivity was initially observed during the early 1900s. The scope of research and advancement in this field has subsequently ranged from strategies to reduce failures associated with thermal sensitivity to design improvements to reduce potential thermal sensitivity. Although TIT models have been offered during this period, no clear description is available to account for numerous aspects of this phenomenon. These shortcomings are particularly evident in in-house factory acceptance testing, in which the differentiation between FTIT and CTIT is unclear. Thermal Instability Testing is a technique accepted by many OEMs and utilities, but the testing framework adopted is regarded as a patented solution. The uncertainty surrounding in-house TIT methods is further compounded by the absence of an international standard. The performance of TIT is significant from both a reliability and fault-finding perspective. Previous works have shown that detecting thermal sensitivity issues prior to despatching generator rotors for commercial operation is essential. In-house testing also facilitates a quicker fault-finding process and subsequent re-test to verify any remedial action. However, an adequate framework to determine the differences between FTIT and CTIT has not yet been proposed.

This chapter aims to address the aforementioned shortcomings, specifically with regards to the in-house TIT methodologies widely used by many utilities, OEMs and repairers globally. This is achieved by developing a direct thermal mapping method capable of highlighting the differences between FTIT and CTIT. Details of the experimental setup are presented. The capability of the experimental setup to produce detailed heat maps of the rotor surface is validated. A number of testing scenarios are proposed to evaluate TIT and assist with fault finding.

4.2 The importance of differentiating between FTIT and CTIT

A limited amount of work has been conducted over the years, as described in Section 3.7. A definitive understanding of in-house TIT methods does not exist. The deficiency can be overcome by directly evaluating the manner in which CTIT and FTIT function as tools for thermal sensitivity detection. It can, however, be assumed that in terms of engineering principles, the test methodologies differ fundamentally, as CTIT uses current as an excitation method, while FTIT relies on friction/windage. The fact that a generator rotor operates under current excitation could suggest that this would be a preferred method to detect latent thermal unbalances. These inferences would be considered assumptions, needing to be tested and proven.

Therefore, a methodology to assist in differentiating between the two techniques is imperative. The method should assist with determining the detailed thermal distribution of the entire surface of a turbo-generator rotor and account for the practical aspects of the rotor assembly and manufacture,

not just the ideal design condition. Furthermore, the possibility of utilising the test methodology as a fault-finding tool needs to be investigated.

4.3 Thermal analysis of generator rotors undergoing TIT

The detection of rotor thermal sensitivity does not rely on any thermal characteristics measured during testing but rather on vibration monitoring. A thermal bow associated with thermal sensitivity is detected via vibration data. However, data analysis seldom helps in locating the problem area. Solutions to the problem generally involve a compromise balance for minor imbalances or a full strip down for fault detection and repair for a major imbalance. Very little attention is given to the thermal characteristics of the rotor during testing. Rotor winding temperature may be determined using the following formula:

$$T_{HOT} = \left\{ \left(\frac{R_{HOT}}{R_{COLD}} \right) (234.5 + T_{COLD}) \right\} - 234.5$$

(4.1)

where R_{HOT} is the winding resistance at the testing point, R_{COLD} is the winding resistance at the reference temperature, T_{COLD} is the reference temperature value, and 234.5 is the thermal conductivity of copper. In solving this equation, it is necessary to be aware of sources of uncertainty. Uncertainty can be categorised as either epistemic or aleatory [65]. Aleatoric uncertainty is characterised by the lack of predictability or intrinsic randomness of a phenomenon; epistemic uncertainty is characterised by a deficit of knowledge. This approach requires that resistance and physical temperature measurements be known at a specific current and voltage level to obtain a reference value. Subsequent temperature rises can be calculated by utilising the rotor resistance measurement. The resistance measurement needs to be accurate and can be significantly affected by inaccuracies and errors in voltage and current readings [66]. This form of temperature monitoring is relatively basic, as it does not account for hot spots within the winding but rather the average rotor winding temperature. Furthermore, this method does not indicate the temperature of the rotor's other extremities such as the shaft, CRRs, or rotor surface. This would be valuable information [67]. The uneven thermal profiles of all of these components can lead to thermal instability. This drawback undermines the reliability of this model as a means to determine rotor thermal characteristics. It best serves to indicate average temperature while performing TIT. Accurately determining the thermal characteristics of the entire generator rotor body would be invaluable in determining the differences between FTIT and CTIT through a practical method that is not influenced by epistemic uncertainty. The main thermal parameters that govern the heat transfer processes during TIT will be discussed in the next section.

4.4 Thermal parameters governing TIT

Heat can be transferred by conduction, convection or radiation. The transfer of heat between the particles of a medium is referred to as conduction and applies mostly to solid bodies. Heat transfer within fluids and gases is known as convection. Radiation is the measure of photons that an object emits, which is determined by the emissivity, surface area and temperature of the object. The effects of radiation in an electrical machine are minimal and are therefore considered negligible [68]. Most thermal aspects of a machine can be accounted for by conduction and convection. Furthermore, contact resistance between the different materials of the generator rotor can lead to thermal variations that need to be accounted for.

4.4.1 Conduction

The discipline of conduction heat transfer was mathematically outlined by JB Fourier in an 1822 publication. The observation of one-dimensional heat flow in a rod gave rise to Fourier's Law of Conduction which stated "the time rate of heat transfer through a material is proportional to the negative gradient in the temperature and to the area [69]." The one-dimensional conduction equation is given by

$$q_x{''} = \frac{q_x}{A} = -k\frac{dT}{dx}$$

(4.2)

where $q_x{''}$ is the rate of heat flux, q_x is the heat rate, A is the cross-section area of the object, k is the thermal conductivity and T is the temperature [70]. Heat flows from an area of higher temperature to one of lower temperature, so a negative sign is used in the equation. The equation can also apply to a three-dimensional vector quantity $T(x,y,z)$.

$$q{''} = k\nabla T = -k\left(i\frac{\partial T}{\partial x} + j\frac{\partial T}{\partial y} + k\frac{\partial T}{\partial z}\right)$$

(4.3)

Furthermore, the heat transfer equation can be derived in the Cartesian coordinate system.

$$\frac{\partial}{\partial x}\left(k\frac{\partial T}{\partial x}\right) + \frac{\partial}{\partial y}\left(k\frac{\partial T}{\partial y}\right) + \frac{\partial}{\partial z}\left(k\frac{\partial T}{\partial z}\right) + \dot{q} = \rho c\frac{\partial T}{\partial t}$$

(4.4)

where $\dot{q}$ is the volumetric rate of heat generation, ρ is the density and c is the specific heat of a medium. To enhance the thermal analysis of electrical machinery owing to their geometry specificity, the heat transfer equation can be further represented in the cylindrical coordinate system.

$$\frac{1}{r}\frac{\partial}{\partial r}\left(kr\frac{\partial T}{\partial r}\right) + \frac{1}{r^2}\frac{\partial}{\partial \emptyset}\left(k\frac{\partial T}{\partial \emptyset}\right) + \frac{\partial}{\partial z}\left(k\frac{\partial T}{\partial z}\right) + \dot{q} = \rho c_p \frac{\partial T}{\partial t}$$

(4.5)

The heat transfer equation defines the conduction characteristics of a generator rotor undergoing FTIT or CTIT. The following section will outline the convection mechanism of heat transfer.

4.4.2 Convection

Convective heat transfer occurs when a moving fluid and a solid surface interact at a dissimilar temperature. Convection heat transfer can be either natural or forced. Forced convention occurs when the fluid flow is induced by an external mechanism e.g. the fan arrangement of the generator rotor body (see Section 3.2.2.). Natural convection, also referred to as buoyancy-induced flow, relies on a natural process to create heat flow i.e. lower density (hotter) elements rise as high density (colder) elements flow downwards under the influence of gravity, creating a natural fluid flow. The convection heat transfer equation is stated as

$$q_{conv} = hA(\Delta T) = hA(T_s - T_\infty)$$

(4.6)

where h is the convection heat transfer coefficient, A is the surface area, T_s is the surface temperature and T_∞ is the fluid temperature. The value of h is dependent on velocity; a higher velocity means a higher heat transfer coefficient value. Therefore, the value of h in forced convection exceeds that of natural convection.

The ratio of convection to conduction is defined as the Nusselt number, which is a dimensionless value.

$$Nu = \frac{q_{conv}}{q_{cond}}$$

(4.7)

where q_{conv} is the convection heat transfer and q_{cond} is the conduction heat transfer. A high-value Nusselt number indicates that convection heat transfer exceeds that of conduction. The convection heat transfer coefficient can thus be calculated by

$$h = \frac{Nuk}{L}$$

(4.8)

Where k is the fluid conduction coefficient and L is the length. In the next section, forced convection will be discussed, as this is the conventional cooling method of large turbo-generators.

4.4.3   Forced convection

Forced convection fluid flow within the air gap of a generator rotor can be classified as laminar, turbulent or a combination of both, i.e. vortex. Factors affecting the type of fluid flow are: flow velocity, rotor surface geometry, air gap width and type of fluid. The air gap is essentially situated between two cylinders, i.e. the rotor body and the stator bore or rotor body and balancing tunnel during TIT. Therefore, the flow characteristic between these cylinders can be defined for the Taylor number (T_a), calculated as

$$T_a = R_e \sqrt{\frac{L_g}{r_r}}$$

(4.9)

where R_e is the Reynolds number, L_g is the length of the airgap and r_r is the rotor radius [71]. The Nusselt number is calculated as follows depending on the value of T_a.

$$Nu = 2.2$$
(4.10)

If T_a is less than 41, the above equation applies, characterising laminar flow. When T_a is greater than a 100, turbulent flow will be experienced and is

$$Nu = 0.23 T_a^{0.63} Pr^{0.27}$$
(4.11)

where Pr is the Prandl number. A combination flow or vortex flow is when the value is between 41 and a hundred, defined in equation 4.12.

$$Nu = 0.386 T_a^{0.5} Pr^{0.27}$$
(4.12)

Forced convection is the favoured method of cooling in large turbo-generators. The method is efficient and allows for the construction of higher rated units that operate at lower temperatures.

4.4.4   Contact resistance

Turbo-generators are constructed of numerous materials, as described in Section 3.2. The contact or interface between these materials can significantly affect the thermal distribution of the rotor. An appreciable temperature drop is experienced at a material interface point. This is dependent on the surface roughness/finish of the materials. At interface points that are peaks, good contact is made, while poor contact is made at valleys. The gaps created are generally filled by gas or fluid, depending on the manufacturing process or operation. The contact resistance created is difficult to analyse as conduction, convection and radiation heat transfer occur at the interface. Contact

resistance is a function of surface roughness, contact pressure, type of matter within the air-gap, material properties and air-gap temperature. Furthermore, the resistance value can be decreased by improving the surface finish, increasing the contact pressure and inserting a better thermal conductor within the air-gap [72].

The complex construction of the generator rotor gives rise to a number of areas of contact resistance e.g. coils and insulating material, steel shaft and insulating material, shrunk-on components, wedges and body, to name a few. The varied and complex interactions of the different materials make calculating the contact resistances within a generator rotor rather difficult [73].

4.5   Turbo-generator rotor losses

The symptom for losses in an electric machine is the generation of heat, an understanding of which is essential in determining thermal performance. The generated losses can be of electromagnetic or mechanical origin. The main sources of losses during turbo-generator TIT are copper and frictional losses.

Copper losses in the turbo-generator are easily determined. The current source (I) of the rotor is DC in nature and passes through a copper conductor of resistance (R). The copper loss (P_c) is calculated using equation 4.13.

$$P_c = I^2 R \tag{4.13}$$

Frictional losses originate from two sources: bearing losses and windage losses. Both of these components are dependent on rotational speed. Bearing losses occur due to the friction between the rotating shaft and bearing housing. These losses are sensitive to type of lubrication fluid, bearing type and loading. Bearing loss (P_b) can be calculated using:

$$P_b = 0.5 \omega k_{fr} F d_b \tag{4.14}$$

where k_{fr} is the bearing coefficient of friction, F is the bearing dynamic load and d_b is the bearing inner diameter.

Windage losses occur during the interaction of the rotor body and the surrounding air medium (air is the medium surrounding the rotor during TIT). The velocity of the fluid flow of the air in the balancing tunnel is the same as the rotor velocity, except for the layer of air on the rotor surface, which is stationary. This condition results in a drag torque being created, leading to frictional losses. Windage loss (P_w) can be calculated using:

$$P_w = \frac{1}{32} k_s C_M \pi \rho_a \omega^3 d^2 L \tag{4.15}$$

where k_s is the surface roughness/finish coefficient, C_M is the torque coefficient, ρ_a is the density of air, d is the rotor outside diameter and L is the length [74].

4.6   TIT analysis approaches

The previous section covers basic theory regarding heat transfer. As an initial step, taking into account the distinctive design of the generator rotor, thermal analysis can be conducted using modern methods such as a lumped-parameter thermal network (LPTN) or numerical methods such as finite-element analysis (FEA) or computational fluid dynamics (CFD) [75]. The suitability of these analytic techniques will be evaluated in this section.

4.6.1   Lumped-parameter thermal network

LPTN analysis or thermal resistance network analysis is the most conventional analytical approach to estimate the temperature rise of electric machines [76]. The fundamental theory is that thermal systems are analogous to electrical circuits. This relationship indicates that the defining criteria for one system can be used to describe another, i.e. circuit theory concepts apply to an equivalent thermal network. The derivations of the following equations can be achieved by solving the one-dimension heat transfer equation. The thermal resistance (R_{t-x}) through a plain layer is

$$R_{t-x} = \frac{\Delta T}{q_x} = \frac{L}{kA} \tag{4.16}$$

where L is the plain layer thickness, k is the conduction coefficient and A is the cross-sectional area. The radial thermal resistance through a cylindrical shell (R_{t-r}) is

$$R_{t-r} = \frac{ln\left(\frac{r_2}{r_1}\right)}{2\pi L k} \tag{4.17}$$

where r_2 is the outer radius, r_1 the inner radius and L the axial length. The axial thermal resistance through a cylindrical shell (R_{t-a}) is

$$T_{t-a} = \frac{L}{\pi k (r_2^2 - r_1^2)} \tag{4.18}$$

This method can be broadly divided into two sections of computation, according to the source, heat-transfer and flow-network analysis [75]. Heat transfer analysis accounts for the thermal aspects,

while flow-network analysis accounts for the fluid dynamics aspects of the electrical network. The equivalences between common quantities are shown in Table 4.1 (below).

Table 4.1: Quantity equivalences for lumped-parameter thermal model

Thermal Quantities	Electrical Quantities
Temperature (℃)	Voltage (V)
Heat (Q)	Current (I)
Heat flux (q)	Current density (J)
Thermal resistance (R_{th})	Resistance (R)
Thermal resistivity (ρ_{th})	Resistivity (ρ)
Thermal capacitance (C_{th})	Capacitance (C)
Thermal conductance (G_{th})	Conductance (G)
Thermal conductivity (λ)	Conductivity (σ)

LPTN analysis has become prominent as a result of the work outlined in [77] related to totally enclosed fan-cooled electrical machines. The prevalence of this estimating method is due to the quick solution times it provides, requiring reduced computational effort. Furthermore, knowledge of electrical principles makes accessing and understanding the solving framework straightforward. The determination of thermal resistances, however, can be challenging and requires a great effort on the part of the user [78]. In the last decade, substantial innovation has taken place to improve LPTN methods and better account for the thermal parameters that are challenging to estimate [73], [79]-[84]. In recent years, the technique has been widely used, although analysis associated with large turbo-generators is not prevalent [73], [85] - [91]. As with all methods of analysis, a detailed knowledge of machine characteristics is essential to enable accurate analysis: inaccuracies in dimensional data, operating specifications and material thermal properties will result in unreliable results. Complex geometries are difficult to analyse using LPTN analysis e.g. stator windings and the rotor [92].

4.6.2   Numerical method – FEA and CFD

FEA and CFD are the two prominent numerical methods used to analyse heat transfer of electrical machines, providing a high degree of accuracy as compared to LPTN. However, these methods require significant computational effort, especially when intricate component geometries or non-homogeneous components are analysed.

FEA is a complex method defined by a system of partial differential equations [93], [94]. As with LPTN, detailed knowledge of the component being analysed is required to ensure that correct heat conduction information is utilised. Intricate models can be labour and time intensive to set up and configure. The most crucial limitation of FEA in regard to turbo-generator analysis is that it is incapable of analysing cooling flow [95].

CFD is capable of analysing heat transfer as well as dynamic fluid flow. These capabilities make CDF a very powerful tool to evaluate both 2-D and 3-D models. Similar to FEA, CFD is defined by a system of partial differential equations referred to as the conservation equations. Mastering CFD requires specialised skills and knowledge of the CFD modelling software package. Accuracy can only be assured by improved modelling techniques where consideration is given to defining accurate boundary conditions, defining interface gaps, building precise geometries and utilising accurate machine specifications. The high computational processing power required by CFD creates long lead times to complete solutions. Setting up the framework for the solution is also time consuming and in some instances may take up to several months [96].

4.6.3   Modelling methodology consideration

In this section, LPTN, FEA and CFD will be evaluated to achieve the objectives outlined in Section 4.2. All the analytical methods considered are dependent on input data for accurate results. The immediate challenge, from the perspective of a utility/non-OEM repairer, would be acquiring the information necessary to undertake the analysis. Information regarding design geometries and machine parameters is impossible to acquire from turbo-generator OEMs. If intellectual property is shared, the repercussions will compromise the OEM's ability to be competitive, innovative and profitable within the power generation industry.

Assuming readily available data, all of the analysis methods are well suited to the design evaluation of the thermal performance of a generator rotor, based on ideal parameters. Turbo-generator rotors are designed to produce a uniform thermal distribution along the rotor body, but in reality this is not the case [4]. The difficulty arises when specific tolerances and assembly differences develop during the repair or winding process of the rotor that cannot be accounted for by the design. Years of operation and maintenance alters the rotor components and tolerances from the initial design specifications. If these parameters could be determined, the resources required to perform simulations for every rotor design undergoing TIT would not be feasible. Hence, a practicable method that takes into account all the parameter variations is required to determine the thermal performance of the rotor.

Furthermore, assuming that all the design variations could be modelled, LPTN will not be considered due to its limitations in regard to complex geometries and accuracy. FEA has been successfully utilised in the past for the analysis of heat flow in synchronous machines [97], [98]. Of particular interest is an analysis by [99] related to shorted turns, thermal unbalances and manufacturing non-conformities of a turbo-generator rotor. The complexity of the rotor, however, led to extensive discretisation of the model at the expense of accuracy. Furthermore, the inability of

FEA to analyse fluid flow makes it an unsuitable method, as turbo-generator rotors rely on fluid flow for the cooling circuit.

CFD is well suited to the intended application, but the high computational processing power required to model a 3-D turbo-generator rotor at steady state renders the method practically and financially unfeasible [100]. Discretisation of the model can be considered to reduce the processing power required [97], [101]. However, simplification of the rotor model would lead to a loss of detail. For example, take the modelling of a turbo-generator rotor cooling circuit. Generator rotor winding designs vary considerably depending on the OEM. The cooling medium is in direct contact with the winding to facilitate the transfer of heat effectively and uniformly. To be able to model this process, a detailed understanding of the cooling design is necessary. The flow of the cooling medium is dependent on operational speed, rotor surface wedge configuration, rotor geometry and the cooling design. These complexities make the modelling process difficult and lead to a number of assumptions being made to reduce the detail of the model. Consequently, simulation accuracy will be inadequate and may not indicate the true thermal performance of the rotor. Furthermore, changes, errors or problems during refurbishment cannot be accounted for by CFD or FEA.

In most scenarios where any type of modelling takes place, the completed solution needs to be verified. During the verification process, empirical data is required to calibrate analytical models to ensure accuracy [75]. An approach to directly map the thermal signature of a turbo-generator rotor is a feasible option. A practical method is required to be able to incorporate all design inconstancies and produce a true representation of the actual physical thermal signature of the methods utilised to detect thermal sensitivity. This approach will negate the need to perform any modelling process.

4.7   Formulation of a physical testing method

The previous section shows that modern thermal analysis techniques are unsuitable for the purpose of producing an accurate thermal analysis of the different types of TIT methods. A direct mapping method to physically determine the thermal distribution of a turbo-generator rotor body is presented in this section. This is achieved by devising an experimental setup capable of thermally mapping the rotor. This experimental technique will help to improve on associated shortcomings posed by contemporary testing methodologies, namely FTIT and CTIT.

4.7.1   Use of infrared sensors

Section 4.3 discusses the deficiencies of contemporary methods of thermal measurement. These shortcomings must be overcome to facilitate accurate temperature measurement of the experimental setup. Rotor telemetry systems have been devised to monitor rotor ground faults and temperature measurement; the technology has improved significantly within the past decade. Temperatures are monitored by installing resistance temperature detectors (RTDs) within the rotor winding slots and

under the CRRs. The connections are wired to an antenna mounted on the rotor body. The antenna transmits the digitised temperature values to a data acquisition unit external to the generator [102]. This method is dependent on the number of RTDs installed for accurate measurement of the thermal distribution of the rotor. Hot spot detection may still be a challenge depending on the RTD layout. Furthermore, the method requires significant modifications to the rotor insulation system to facilitate the installation of the RTDs and routing of the connections, which will involve substantial rotor disassembly. The invasive nature of the process would lead to further design variations that could affect rotor operation and thermal performance. Therefore, this method of temperature detection is ruled out for the experimental setup.

The widespread use of infrared thermography within the electrical industry has been commonplace for a number of years [103] – [105]. This non-contact, non-invasive method produces reliable and accurate results for fault finding and trouble shooting. Temperature measurements are made possible by detecting the radiant flux of an object; a temperature output is calculated through a calibration algorithm. Also referred to as a radiation thermometer, many varieties are available on the market today, from thermal imaging cameras to singular probes. Devices are able to measure a wide variety of temperature ranges and can operate at high speeds, making this approach an ideal choice for the proposed experimental setup [106].

4.7.2   Heat map

The preferred method of data capture is in the form of a matrix of temperature values corresponding to the physical mapping of the surface of the generator rotor. The method must transform these temperature measurements and physical coordinates into a 2-D heat map. Simply put, the direct thermal mapping method must present the 3-D temperature data (of the rotor surface) as a 2-D heat map. A heat map consists of a number of rectangular rows and columns that represent data values against a colour scale. This is a widely used method to display large matrices within many different fields such as natural sciences and biological science [107], [108]. Ultimately, the experimental setup required to map the temperature distribution of the rotor must be able to output data that can lead to the information being displayed as a heat map for easy interpretation to determine the differences between FTIT and CTIT.

4.7.3   Experimental setup

The use of a full scale turbo-generator rotor for the test setup is not feasible, as the availability of crucial generating and testing plant is reserved for commercial operation. Critical spares such as a large rotor cannot be made available for testing. The use of a balancing facility also comes at a great cost and associated operational risk. Thus, the experimental test setup is based on an appropriately scaled model for analysis.

4.7.3.1 Scaled 600 MW mini-rotor

A mini-rotor rated at 20 kVA designed to mimic a 600 MW generator rotor is used for analysis, as TIT is most prevalent in larger units. The rotor is similar to a 600 MW rotor in the following aspects:

- •   Two-pole 3000 rpm, 50 Hz
- •   Distributed and concentric field windings
- •   Damper bars
- •   Shaft mounted slip-rings
- •   Insulated bearings
- •   Mono-block milled shaft with slots

Table 4.2 (below) summarises the constructional details of both the mini-rotor as well as a typical 600 MW generator rotor [109].

Table 4.2: Comparison of specifications of the mini-gen rotor and 600MW Turbo-generator rotor

Parameter	Mini-rotor	600 MW Generator rotor
Rotor slots	32	32
Damper bars	48	48
Rotor diameter	178.5 mm	1165 mm
Shaft length (journal centres)	885 mm	10990 mm
Shaft diameter	67 mm	530 mm

The mini-rotor is tested to diagnose any latent problems that may affect its operation and create inaccuracies in results obtained. An insulation resistance and an RSO test were conducted, and the mini-rotor was found to be in a serviceable condition. Refer to Appendix A for results of the test.

4.7.3.2 Scaling of local balancing facility

To reasonably reproduce conditions under which a conventional 600 MW rotor undergoes TIT, the experimental setup is scaled according to the local utility balancing facility. The scaling ratio is based on the length of the rotors. From Table 4.2, the shaft lengths are 885 mm and 10990 mm respectively; the mini-rotor is down-scaled approximately to the ratio 2:25. Thus, the enclosure is down-scaled to the same ratio. The enclosure scaling configuration is summarised in Table 4.3 (below).

Table 4.3: Scaling ratio of the mini-gen rotor and 600MW Turbo-generator rotor

	Balancing facility dimensions	Scaling ratio	Enclosure dimensions
Length (mm)	25748	2:25	2060
Width (mm)	7840	2:25	627
Height (mm)	7840	2:25	627

From Table 4.3, a 3-D model of the intended experimental setup is initially developed, as shown in Figure 4.1 (below). The enclosure is constructed out of 12 mm fibre board and insulated with a number of layers of styrofoam similar to the insulative properties of a full-scale balancing facility. At the drive end of the rotor, a face seal is constructed around the bearing housing to enable the shaft to rotate without any loss of air volume/heat within the enclosure. Rubber seals are also utilised at the base of the enclosure. The rotor is driven by an induction motor rated at 3000 rpm. The different aspects of the experimental setup construction are discussed in more detail in the following sections. Refer to Appendix B for the physical layout of the experimental setup.
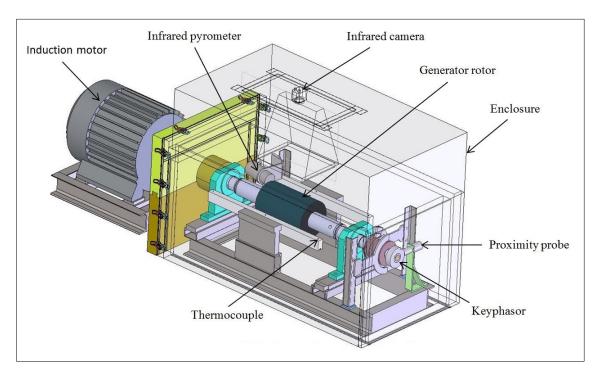

Figure 4. 1: Schematic of scaled experimental configuration used for rotor thermal mapping

4.7.3.3 Direct mapping with high-speed, high-resolution IR camera

The experimental setup utilises a high-speed, high-resolution (382x288 pixels) 80 Hz infrared (IR) camera capable of capturing the surface data of the rotor, illustrated in Figure 4.2 (below). The spectral range of the camera is rated at 7.5 µm to 13 µm. The long wavelength range of the camera increases temperature accuracy and minimises atmospheric absorption. Furthermore, the IR camera is capable of discerning, in great detail, differences in temperature across large or small temperature scales. Refer to Appendix C for specifications of the IR Camera utilised. A viewing window is not utilised but rather an inspection aperture, as large discrepancies in temperature readings can result. Sources have reported errors in readings of up to 40% [110] – [112]. The camera lens mounts into the aperture via a rubber seal that prevents air/heat loss and enables accurate measurement.

Figure 4.2: Optris Pi450 compact high-speed, high-resolution IR Camera

In essence, an IR camera detects radiation emitted from a body to determine the temperature. This is referred to as the emissivity of the material. Emissivity values range from 0 to 1. The higher the emissivity of the material, the greater the accuracy of the temperature measurement. A black body is referred to as a radiator as it radiates the maximum energy possible throughout the spectrum; an ideal radiator has an emissivity of 1. Therefore, the rotor body is painted with matt black paint to improve the accuracy of the data captured by creating a measurement surface with a higher emissivity [106].

4.7.3.4 Direct winding temperature measurement

The difficulties associated with determining the winding temperature of a generator rotor have already been mentioned. In brief, the measurement of an accurate average winding temperature depends on the capacity of the measuring instrumentation used as well as the method in which the voltage and current can be measured via the slip-rings without any interference. It should be highlighted that hot spot detection is not possible using this methodology [113].
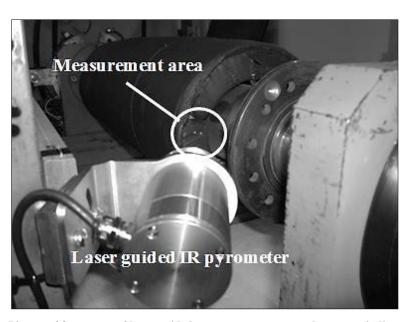

Figure 4.3: Picture of focus area of laser-guided pyrometer to capture the rotor winding temperature

These difficulties are overcome by capturing the winding temperature with a laser-guided IR pyrometer and painting the copper windings black to improve accuracy, as illustrated in Figure 4.3 (above). Hot spot detection is accomplished by the IR camera thermal map. The use of a laser-guided pyrometer is significant as the area of analysis can be focused on with precision. The spectral range of the IR pyrometer is 7.5 μm to 13 μm with a high optical resolution of 75:1 and 9 ms response time. The error margin of the measurement is approximately within 1%. The speed and accuracy of this device suits the intended purpose of the experimental setup. The comparison of the winding temperature as well as the surface temperature will provide some insight into how heat diffuses from the windings. Furthermore, it will provide an indication of the internal temperature of the rotor. Refer to Appendix D for specifications of the laser-guided IR pyrometer.

4.7.3.5 Rotor revolution tracking

A keyphasor probe is utilised to determine the angular position of the mini-rotor. This is achieved with the aid of a fixed collar with a machined notch and a proximity probe. An output is received when the notch passes the proximity probe and indicates when one revolution has passed. Thanks to the once per-revolution event tracking, it will be possible to determine when a map of the entire rotor surface has been completed. This event further facilitates a point of reference that enables a fixed start and end point for the capturing of mapping data allowing for easy comparison of results obtained during different testing scenarios. This arrangement is illustrated in Figure 4.4 (below).
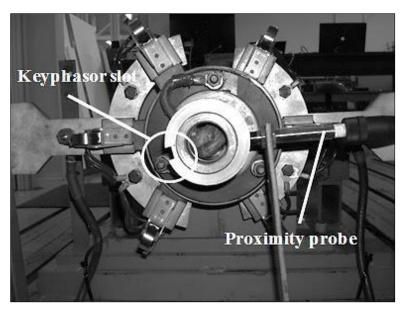

Figure 4.4: Picture of keyphasor and proximity probe arrangement to determine once per revolution event

4.7.3.6 Ambient and enclosure temperature monitoring

A number of thermocouples monitor the ambient temperature as well as the temperature within the enclosure. Thermocouples are positioned on either side of the mini-rotor with pairs of thermocouples near the slip-ring, the centre of the body, and the drive end. A thermocouple is situated externally to determine the ambient temperature.

The fully commissioned experimental setup is illustrated in Figure 4.5 (below). Figure 4.6 (below) details the internal layout when the enclosure is removed.
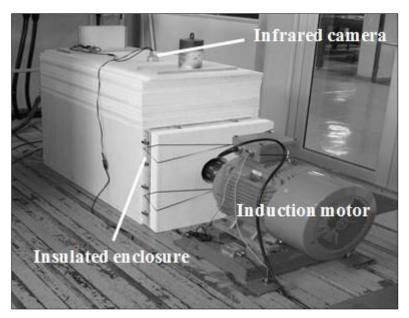

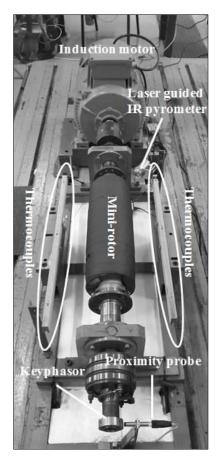**Figure 4.5: Picture of fully assembled and commissioned experimental setup**

Figure 4.6: Picture of internal layout of the experimental setup with the enclosure removed

4.7.4 Data capturing

Data acquisition is facilitated in two streams. The data from the IR camera and proximity probe interface is captured via a data-acquisition unit linked to a computer utilising proprietary software from the IR camera manufacturer known as Optris PI Connect [114]. The winding, ambient, and enclosure temperatures are captured via a separate unit linked to a computer. All data is time stamped to facilitate data synchronisation. An overview of the experimental layout and data acquisition is shown in Figure 4.7 (below).
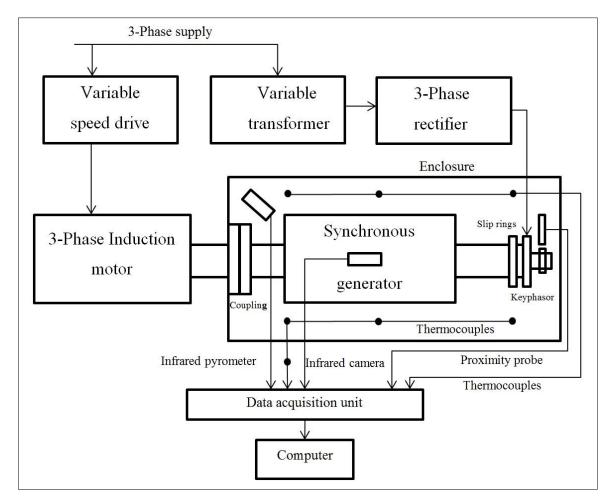

Figure 4.7: Experimental layout with associated instrumentation to capture the thermal profile of the mini-rotor

4.7.5 Generating a thermal map of the rotor

The initial step in constructing the heat map is to define the IR camera resolution pixel size that will correspond to the physical portion of the rotor to be measured. The distance of the IR camera from the test object (mini-rotor) determines the size of the measurement pixel and therefore the map resolution. The further away the IR camera is from the test object, the larger the pixel size. The pixel size is also dependant on the optical lens fitted to the IR Camera.

For the experimental setup, a wide angle lens (62° x 49°) is used to enable full coverage of the mini-rotor body while maintaining the smallest pixel size possible without compromising the capture of

significant details. The mini-rotor body is 500 mm in length with a diameter of 180 mm. The field of view of the camera is adjusted to be able to monitor the entire rotor body. This is accomplished by using the proprietary IR camera field of view calculation tool, illustrated in Figure 4.8 (below). A distance of 440 mm away from the rotor body is calculated to be the optimum field of view by virtue of yielding the following dimensions: the width or horizontal field of view (HFOV) is 527 mm, the height or vertical field of view (VFOV) is 396 mm and the diagonal or diagonal field of view (DFOV) is 659 mm. The instantaneous field of view (IFOV) is the geometric dimension of each pixel and is calculated to be 1.38 mm. For optimum measurement results, a 3x3 pixel measurement block known as the MFOV, or recommended smallest measured object size, is suggested by the source [114]. The MFOV is characterised by a group of pixels surrounding a central pixel.
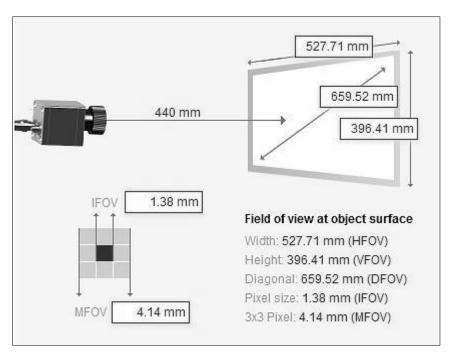

Figure 4.8: Field of view calculator used to determine camera pixel sample size for mini-rotor

The IR camera is rated at 80 Hz i.e. the ability to capture 80 samples per second. The highest sampling accuracy to map the surface of the rotor is accomplished by operating the rotor at 1 Hz i.e. 80 samples of the rotor body are taken during one revolution. Sampling of the IR camera in actuality is measured to be 77 Hz for the experimental setup. From the determined sampling rate, the optimum measurement pixel configuration is calculated as illustrated in Figure 4.9 (below). The rotor circumference is 565.5 mm: dividing this value by the sampling rate will produce the required pixel configuration size to map the rotor surface in the radial direction – 7.34 mm. The IFOV is 1.38 mm, thus the number of pixels required in the radial direction is calculated by dividing 7.34 mm by 1.38 mm, yielding 5.31 pixels. Given that only whole pixels are utilised for measurement, 0.31 pixels corresponding to 0.44 mm of the rotor body will not be measured. This will result in approximately 94% of the rotor body being mapped in the radial direction. The optimum number of pixels is the radial direction is thus 5 pixels.

In the axial direction, the optimal pixel number is chosen as 3, based on achieving a final pixel configuration closest to the optimum of 3x3. Thus, this final pixel configuration is a measuring cluster of 3x5 pixels. This hybrid cluster conforms to the 3x3 optimum measuring configuration as two central pixels are surrounded by adjacent pixels.

The number of clusters required to map the rotor surface is calculated at approximately 120 (500 mm divided by 4.14 mm). The area not covered in the axial direction is measured to be 0.78 mm which is considered as negligible as the rotor body covering has an overhang which is larger than the winding i.e. the configuration is able to map the winding in its entirety, as it is smaller than that rotor body length.

Figure 4.10 (below) illustrates the array used to generate the heat map. The output of the array is a matrix of temperature values that correspond to the rotor body. The data is processed and heat map generation is performed using Matlab. A high-resolution heat map is generated containing a matrix of 120x77 temperature values.
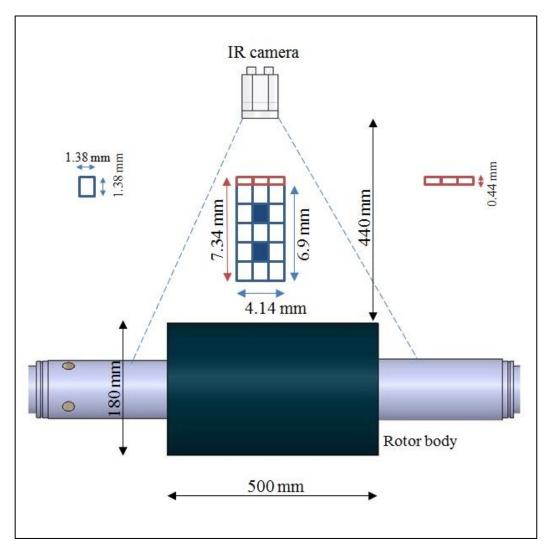

Figure 4.9: Heat map sampling pixel arrangement base on the field of view of the infrared camera
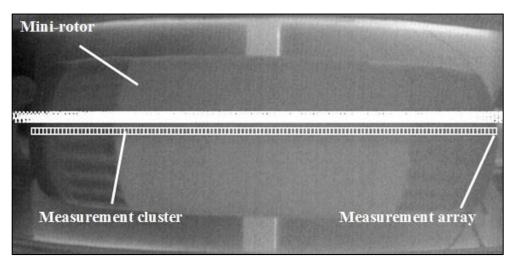
Figure 4.10: Pixel cluster measurement array used to capture the thermal profile of the mini-rotor surface

4.8 Verification of experimental setup for TIT method analysis

A method to practically map the surface of a mini-rotor directly is presented. This method is able to take into consideration the non-uniformities of the mini-rotor construction as opposed to just the idealised design. The salient requirement of the experimental setup is to be able to detail the thermal distribution of the mini-rotor. This is facilitated by the use of a heat map containing temperature values that represent the physical thermal map of the rotor surface. The heat map will facilitate the practical evaluation of the two different methods of TIT. Furthermore, the heat map can be interpreted to assist in fault finding. By defining a methodology to scan an array of pixels on the rotor surface and utilising this data to form a matrix of temperature values, it is possible to create a heat map. A sample of a heat map created using the experimental setup is illustrated in Figure 4.11 (below).

The experimental setup is unable to determine the heat distribution within the rotor. This, however, is not the aim of the experimental setup and is not significant owing to the nature of heat diffusion within the rotor body. Heat is diffused from the coils, which are the heat source, to the surroundings. The surface covering of the rotor (fibre glass banding) is in close contact with coils, making heat diffusion easily detectible. The direct monitoring of the winding temperature, however, will give some indication as to the internal temperature of the rotor. To all intents and purposes, surface monitoring will practically and adequately determine the thermal distribution of the rotor. Furthermore, the 6% non-coverage error margin in the radial direction is found to be acceptable, as this does not represent a significant loss of area to prevent the accurate mapping of the rotor surface. The experimental setup is thus verified for the purpose of thermal mapping of the mini-rotor body surface.

The challenges associated with the down scaled experimental setup are discussed in this section. During operation the cooling medium utilised is pressurised hydrogen. It is less dense than air

resulting in less windage and ventilation losses. Hydrogen gas also possesses greater efficiency at cooling the rotor having a higher thermal conductivity and surface heat transfer coefficient than that of air. TIT however is performed the world over in the absence of hydrogen. The cooling medium utilised is air and there are a number of reasons to support this practice but the primary reason being safety. During conventional TIT the slip-ring brush-gear assembly is housed within the testing facility in its entirety while during operation the assembly is housed outside the generator casing. This is done to prevent the ignition of hydrogen within the casing resulting in a catastrophic explosion and failure. This however does not make TIT testing in air invalid, the result being that the rotor will heat at a faster rate due to increased windage and decreased rotor surface heat transfer. This will have very little effect on the thermal behaviour of the rotor.

Deep groove ball bearings are utilised in the experimental setup while half-moon white metal bearings are used in operation as well as in a conventional balancing facility. The thermal behaviour of these bearings differ as the ball bearing does not take advantage of jacking oil that is able to cool and lubricate the white metal bearings more efficiently creating less friction. TIT vibration analysis is largely dependent on bearing pedestal vibrations. The type of pedestal and bearing affect the measured output vibration. The vibration signature measured on a ball bearing and a half moon bearing will differ significantly making a comparison difficult. Furthermore, during operation the rotor is coupled to the turbine shaft which affects the stiffness of the rotor thereby changing the vibrational characteristics.

The scaling factor utilised is based on the length of the local utility balancing facility as well as that of a 600 MW generator rotor. The length was used as it is the only constant that can be maintained in the scaling process. The mini-rotor diameter was influenced by the machine rating which determined the size of the armature required thus the form factor of the body, which did not scale proportionately to the diameter of the full scale rotor. The rotor body slots were machined according to this specification. The mini-rotor shaft diameter was determined in accordance to the rotor body and to facilitate an appropriate bearing system. Lastly, the scaling of the experimental rotor resulted in a shortened shaft of less mass and reduced rotor body diameter. This significantly increased the stiffness of the rotor as compared to a full scale rotor. The increased rotor stiffness results in a very stable rotor where a thermal bend will be improbable. This coupled with the bearing configuration produces a poor environment for vibrational analysis. The abovementioned variances are not considered critical, as the thermal behaviour of the rotor will not be affected to such an extent that the rotor thermal performance will not be adequately portrayed during testing.
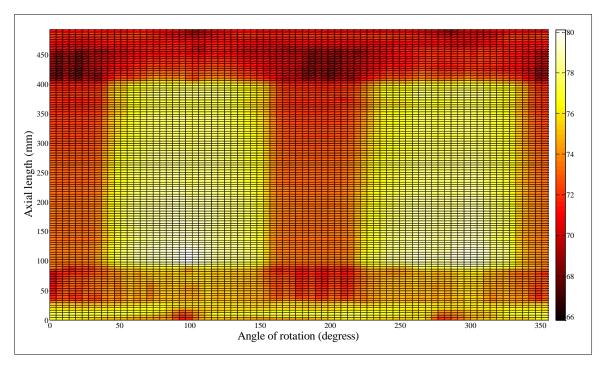
Figure 4.11: Sample of a generated high resolution heat map utilising the direct mapping method

4.9   Conclusion

In this chapter, thermal parameters that govern the heating behaviour of the rotor are defined. An extensive investigation into analytical as well as numerical methods to evaluate the different types of TIT is presented. LPTN methods are found to be best suited to quick and uncomplicated component analysis. Although FEA is well suited to complex geometries, it is unable to model fluid flow, which is imperative for the rotor cooling circuit. The complexities of CFD and the high analytical processing resources needed render this technique impractical. Furthermore, analytical and numerical techniques rely on accurate input data based on design specifications that may be proprietary information. These analysis techniques are also unable to cater for design variations in the final constructed component but rather rely on the ideal design details as input parameters. Therefore, modern analysis techniques are found to be unsuitable for the evaluation of TIT.

A method to directly map the surface of a synchronous generator is presented. This is a practical approach, able to map the temperature profile of the rotor surface, accounting for all rotor design variations that may exist. The experimental setup is scaled according to the local balancing facility and is built, commissioned and validated to produce an accurate heat map of the rotor surface. Test scenarios are devised in the next chapter to evaluate CTIT, FTIT and the possibility of using the model to aid in fault detection.

Chapter 5 | TIT experimental results and analysis

5.1 Introduction

Chapter 2 highlights a local utility's experience of a high rotor failure rate whilst undergoing TIT. This leads to the evaluation of the suitability of the test methodologies used to conduct TIT. It emerges that two TIT methodologies are utilised by utilities internationally, namely FTIT and CTIT, without preference. Additionally, it appears that there is neither preference for nor any well-established grounds for selection of a particular method. Chapter 3 discusses how the unique design of the turbo-generator rotor makes it susceptible to thermally induced vibrations. Different methods used to perform TIT are evaluated for online and in-house testing. The methodologies utilised for in-house testing, which are of particular interest, are difficult to evaluate owing to the lack of associated information, as these form part of patented testing solutions offered by OEMs and service providers. Chapter 4 presents a framework to enable the thermal mapping of a generator rotor. The experimental setup is constructed and verified to thermally map the surface of a mini-rotor as well as to acquire a direct temperature measurement of the winding. Therefore, evaluation of the two types of testing methodologies is made possible through detailed analysis of the thermal behaviour of the mini-rotor under test conditions.

The experimental results obtained from performing the FTIT and CTIT are presented in this chapter. Quantitative and qualitative analysis of the results from direct thermal mapping of the rotor under each test condition is carried out for the purposes of evaluation. Deficiencies of contemporary TIT modes are ascertained. Additionally, the fault detection capability of the direct thermal mapping method is presented.

5.2 Overview of testing scenarios

Different testing methodologies are considered to enable the effective utilisation of the experimental setup to evaluate the different aspects related to TIT. Three principle aspects are investigated:

- Mapping the rotor under the effects of friction to evaluate FTIT.
- Mapping the rotor under current excitation to evaluate CTIT.
- Fault finding capability of the mapping method.

FTIT is expected to take substantially longer to perform, as the primary source of heat generation is via the frictional interaction between the rotor surface and the surrounding air volume. Mapping of the rotor surface was performed at regular intervals to capture the thermal performance of the rotor. The winding temperature as well as the enclosure temperature were monitored.

CTIT was evaluated by injecting current into the mini-rotor winding at different levels. The current levels were maintained for a period of time, while thermal mapping was carried out at frequent intervals. The winding temperature as well as enclosure temperature was monitored.

The fault-finding capability of the thermal mapping method was assessed by introducing a fault condition on the mini-rotor and thereafter attempting to identify and locate the fault area.

5.3   Thermal map interpretation and physical orientation

The physical representation of the thermal map presented in future sections is illustrated in Figure 5.1 (below). All conventions were observed when viewing the rotor from the non-drive end. The thermal map orientation is of the rotor body with the non-drive end associated with the x-axis. The rotors' angle of rotation is in the clockwise direction. The y-axis is associated with the length of the rotor.
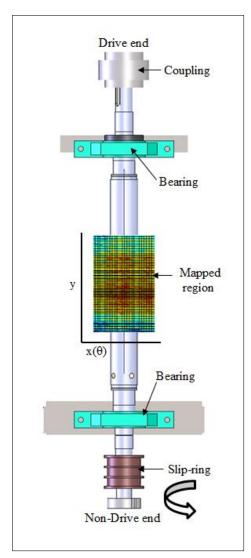

Figure 5.1: Schematic explaining thermal map display orientation showing x and y axes

5.3.1   Scenario 1: FTIT

FTIT was performed under the influence of air friction/windage while the rotor was operated at 3000 rpm. The test was run for eight hours and readings were taken every 30 minutes. A time-based evaluation approach was followed owing to the nature of the heating mechanism. During the temperature mapping process, the rotor speed was decreased via controlling the speed of prime mover (induction machine). Rotational speed was decreased to 60 rpm with consideration of the maximum sampling rate of the camera. Upon completion, the rotor was run-up to 3000 rpm. During this process, surface mapping, winding temperature, enclosure temperature and ambient temperature were recorded.

The ambient temperature measured 20°C at a barometric pressure of 831.3 mbar at the time of testing and fluctuated to a small degree measuring 22°C at the conclusion of the rest. The average surface, enclosure and ambient temperatures are plotted in Figure 5.2 (below) for the eight-hour time duration. The average surface temperature, heating rate was observed to be higher for the first four hours of the test, being 7.3°C per hour. For the final four hours of the test, the average heating rate decreased to 2.55 °C per hour. This trend indicates that the rotor surface has reached thermal equilibrium and that the full spectrum of heating behaviour of the rotor was captured using the friction mechanism for the chosen time duration.
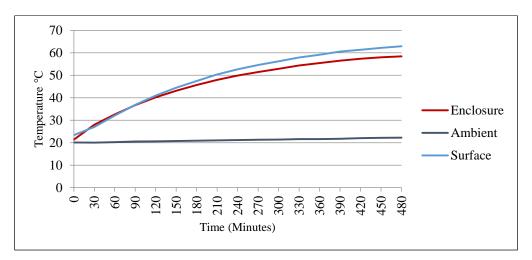

Figure 5.2: Plot of FTIT average surface temperature over the 480 minute test duration

Temperature recordings, at two-hour intervals, related to FTIT are presented in Figures 5.3 to 5.8 (below). For the entire sequence of temperature data captured (every 30 minutes), refer to Appendix E. Each figure consists of a thermal map of the surface of the rotor at a specific time interval with associated data i.e. average rotor surface temperature, average temperature distribution along the vertical and horizontal planes, and a histogram consisting of all bin values recorded during the entire test duration. All further temperature data presented in this chapter follow the same format.
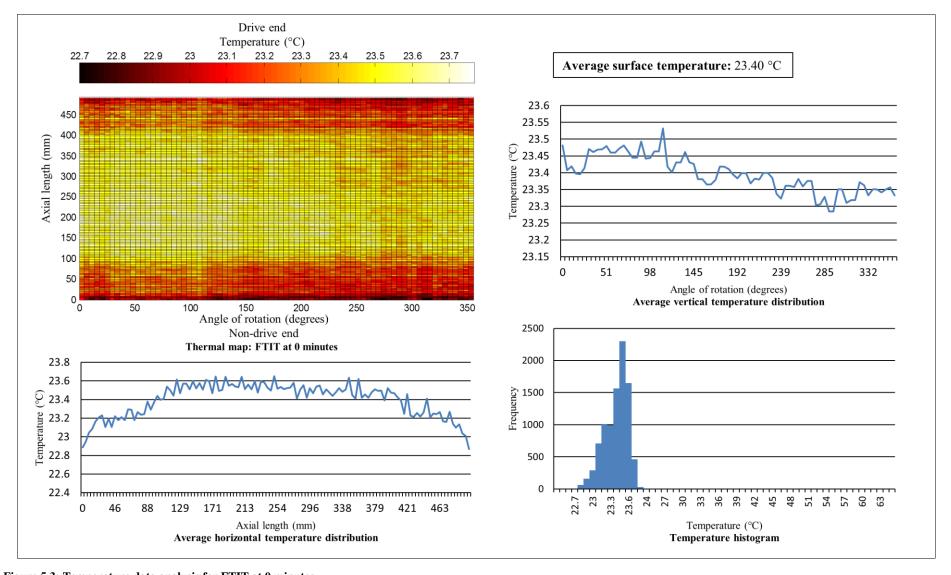
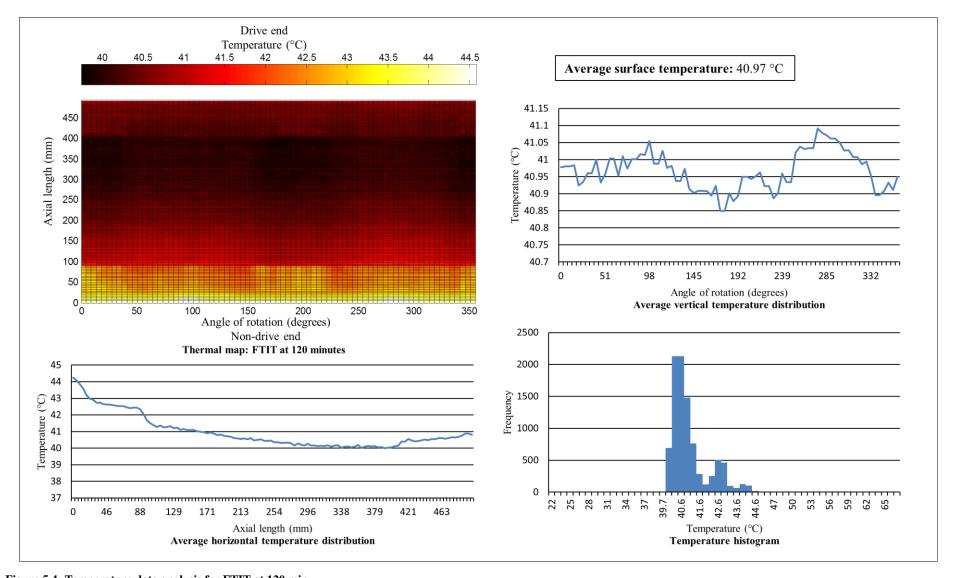**Figure 5.3: Temperature data analysis for FTIT at 0 minutes**

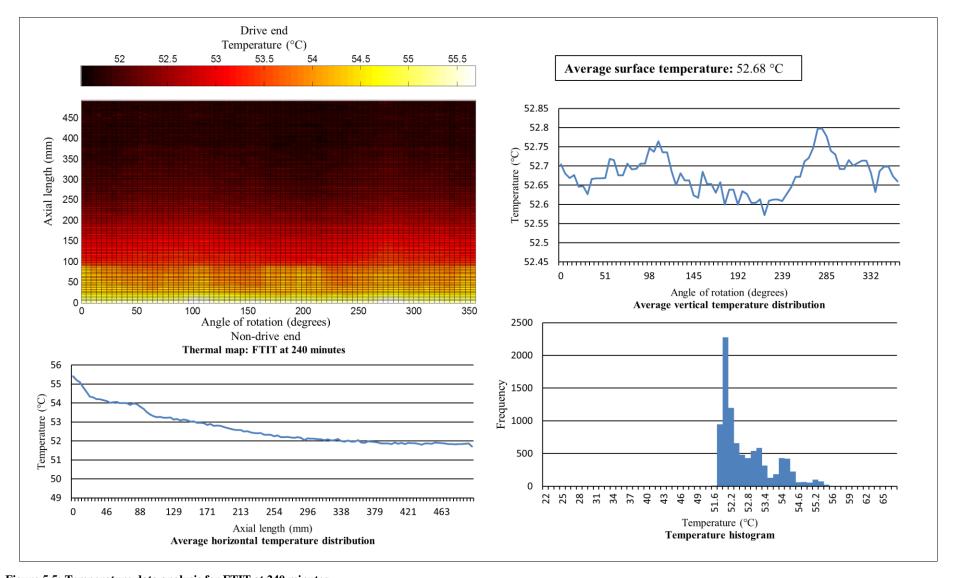**Figure 5.4: Temperature data analysis for FTIT at 120 min**

Figure 5.5: Temperature data analysis for FTIT at 240 minutes
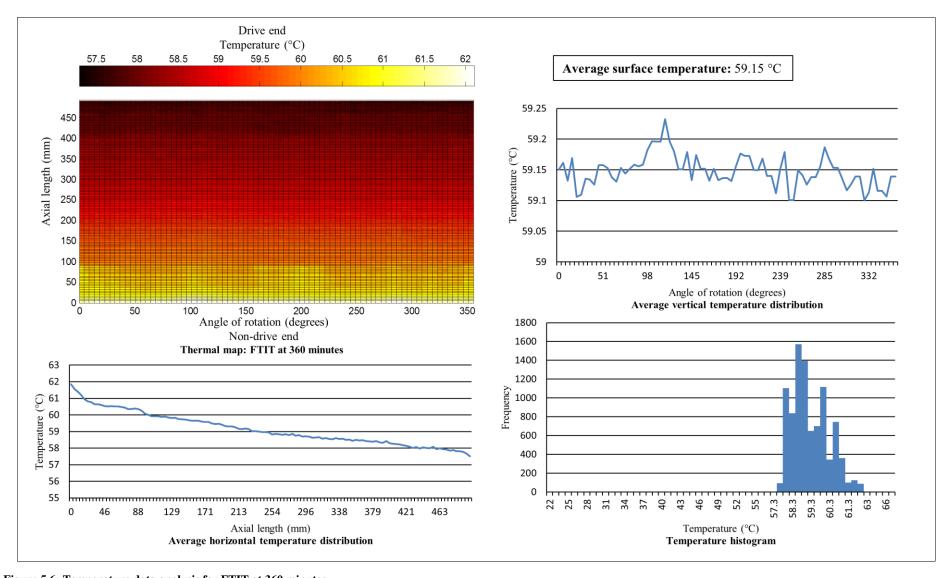
66

Figure 5.6: Temperature data analysis for FTIT at 360 minutes
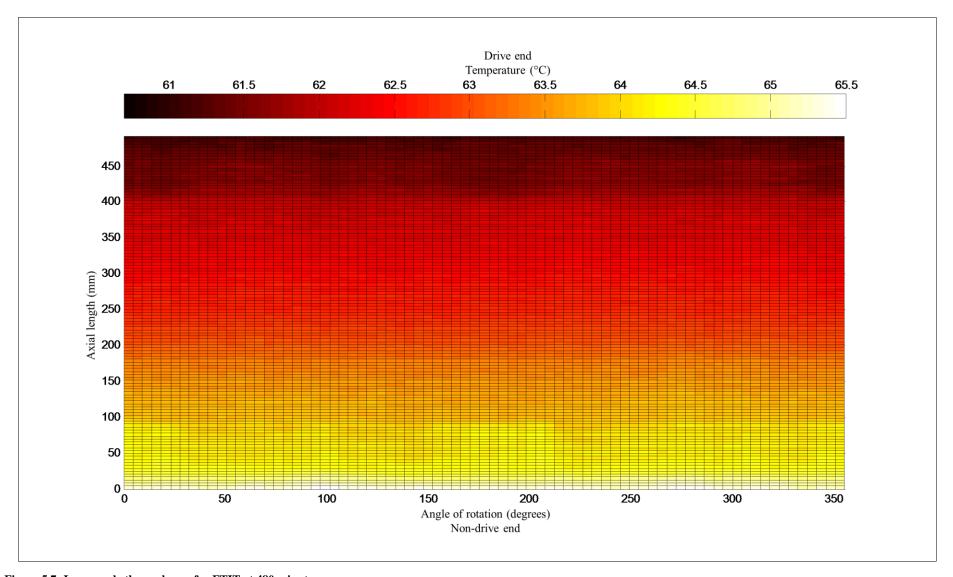
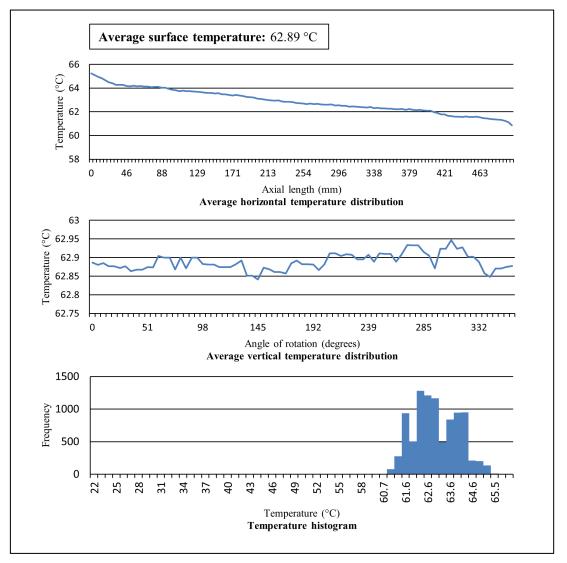**Figure 5.7: Large scale thermal map for FTIT at 480 minutes**

Figure 5.8: Temperature data analysis for FTIT at 480 minutes

Figure 5.3 (above) summarises the initial temperature distribution of the rotor surface prior to the commencement of the test, with an average surface temperature of 23.40 °C. The maximum average surface temperature achieved after eight hours was 62.89 °C. The surface temperature of the rotor does not follow a typical distribution. The histogram data for each testing interval captured is found to be positively skewed or skewed to the right. A trend is observed where the average horizontal temperature distribution showed that higher temperatures were experienced towards the non-drive end of the mini-rotor. The temperature gradient is clearly observed on the thermal maps and the trend is consistent throughout the test. A large-scale high-resolution thermal map is presented in Figure 5.7 (above) where the temperature distribution can be observed in detail. The drive-end of the mini-rotor was operated at a significantly lower temperature. The temperature difference between the drive and non-drive ends varied by up to 4°C throughout the testing procedure. This is significant, as even the slightest differences in temperature can lead to thermal sensitivity. The cause of this was suspected to be attributable either to bearing losses or rub at the non-drive end or heat generated by the slip-ring brush-gear interaction due to frictional losses. To determine the origin of the temperature gradient, the brush-gear assembly was removed and the test repeated.

69

The ambient temperature measured 21 °C at a barometric pressure of 841.3 mbar at the time of FTIT re-testing and fluctuated to a small degree measuring 22°C at the conclusion of the rest. The average surface, enclosure and ambient temperatures are plotted in Figure 5.9 (below) for the eight-hour time duration. The average surface temperature heating rate was observed to be higher for the first four hours of the test, being 3.0°C per hour. For the final four hours of the test, the average heating rate was 1.0°C per hour. This outcome differed drastically from the FTIT with the brush-gear fitted, where a higher heating rate was experienced, indicating that the brush-gear influenced the heating rate.

Temperature recordings, at two-hour intervals, related to FTIT with the brushes removed are presented in Figures 5.10 to 5.15 (below). For the entire sequence of temperature data captured (every 30 minutes), refer to Appendix F. Figure 5.10 (below) summarises the initial temperature distribution of the rotor surface prior to the commencement of the test: an average surface temperature of 23.2°C. The maximum average surface temperature achieved after eight hours was 39.4°C as compared to 62.8°C achieved in the previous testing scenario, indicating a drop of 23.4°C, quantifying the thermal influence of the brush-gear.
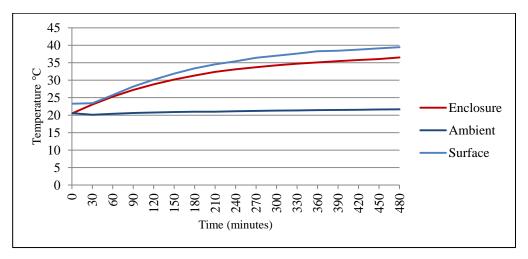

Figure 5. 9: Plot of FTIT average surface temperature over 480 minutes with brush-gear removed

The skewness of the histogram data plots were much closer to 0, i.e. a normal distribution of temperatures. No trend was observed where the average horizontal temperature distribution showed that higher temperatures were being experienced towards the non-drive end of the mini-rotor. A near-uniform temperature distribution could be clearly observed on the thermal maps, and the trend was consistent throughout the test. A large-scale high-resolution thermal map is presented in Figure 5.14 (below) where the temperature distribution can be observed in detail. The results obtained showed that the brush-gear slip-ring interaction introduced an additional thermal component that affected the rotor surface thermal distribution. The thermal losses experienced by the brush-gear slip-ring interaction were able to heat the rotor body to a significantly higher temperature at a higher thermal rate per hour. The gradient observed was proven to be due to this interaction.

Figure 5.10: Temperature data analysis for FTIT with brushes removed at 0 minutes

Figure 5.11: Temperature data analysis for FTIT with brushes removed at 120 minutes
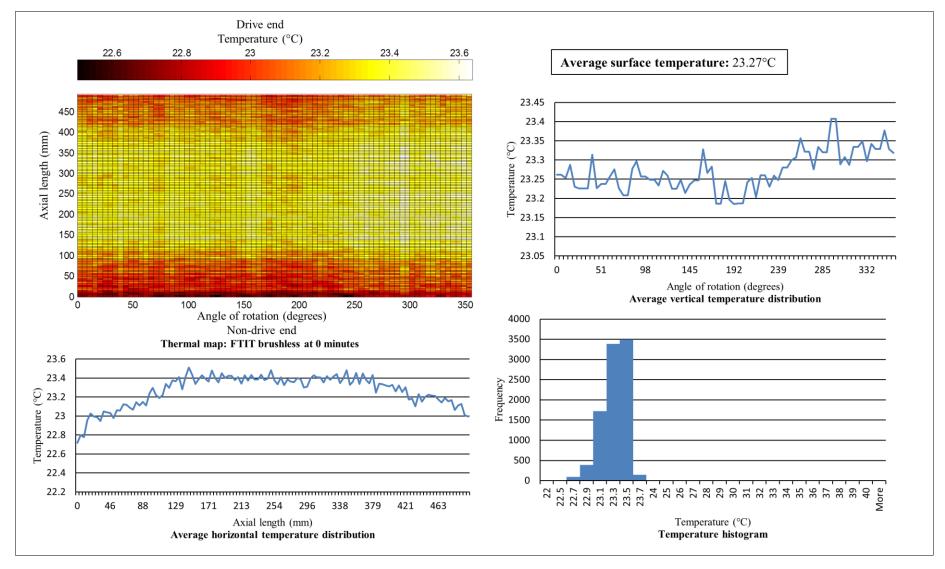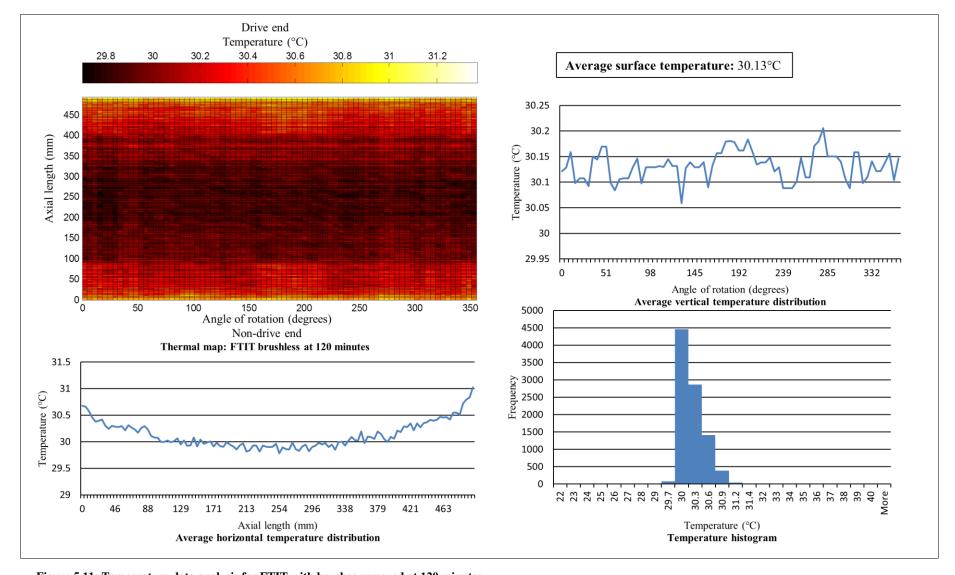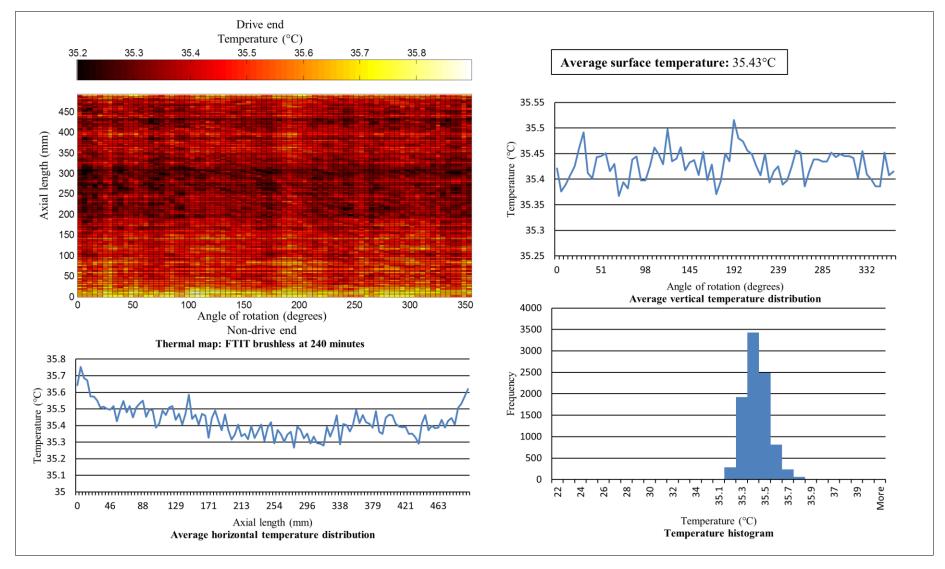
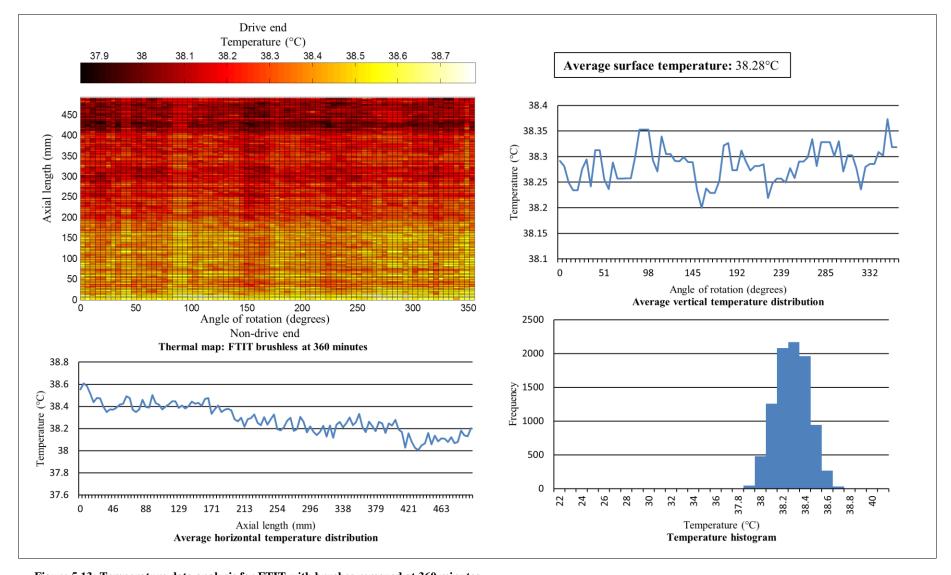**Figure 5.12: Temperature data analysis for FTIT with brushes removed at 240 minutes**

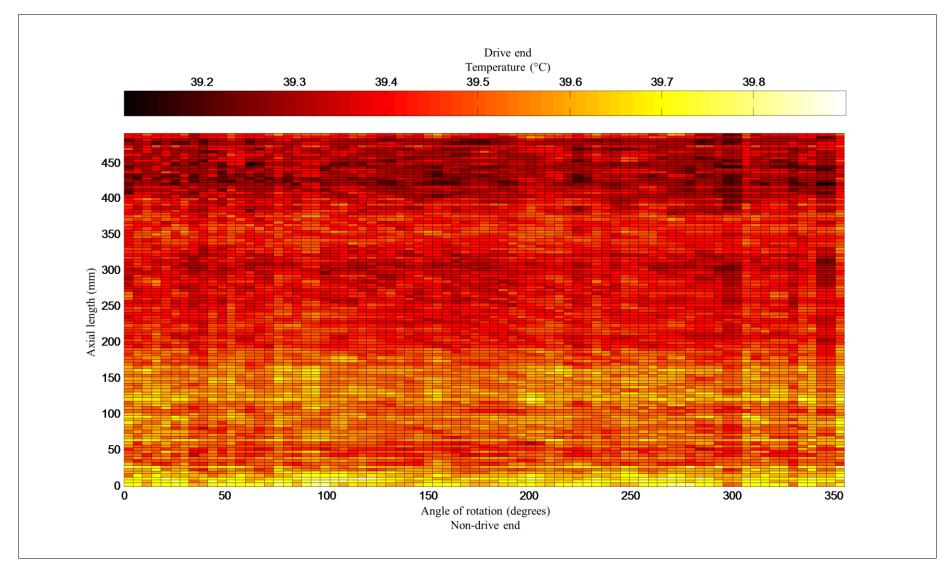**Figure 5.13: Temperature data analysis for FTIT with brushes removed at 360 minutes**

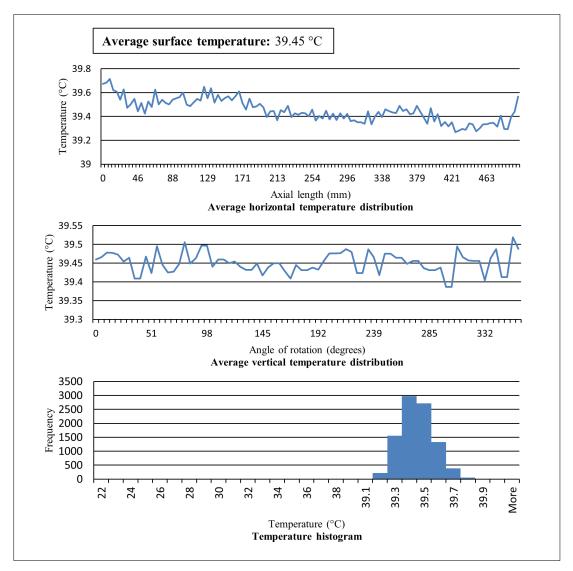**Figure 5.14: Large scale thermal map for FTIT at 480 minutes**

Figure 5.15: Temperature data analysis for FTIT with brushes removed at 480 minutes

This finding is of great significance, as during factory acceptance testing where FTIT is performed, the winding temperature is measured via the slip-ring connection. The phenomena experienced could negatively affect the outcome of the test by not proving to be a true reflection of the thermal performance of a rotor undergoing FTIT. By utilising the slip-ring assembly to determine the winding temperature an additional thermal component is introduced by the slip-ring brush-gear interaction influencing the rotor thermal distribution. This highlights a weakness in the current methodology surrounding TIT where this behaviour is not being taken into consideration. An asymmetrical distribution between the exciter and drive end of the rotor can result in the rotor being thermally sensitive which produces an inaccurate outcome of the test. Erroneous test outcomes can be expected using this methodology.

5.3.2   Scenario 2: CTIT

CTIT by definition requires the testing to be conducted utilising current injection. The mini-rotor was operated at 3000 rpm and excitation applied at different levels, as per conventional thermal

instability testing, as outlined in sections 3.5.1 and 3.5.2, based on the rating of the mini-rotor: 5 A, 10 A, 20 A and 35 A. A dwell time of one hour was observed at each current level, and mapping was performed every ten minutes. Sampling was carried out more frequently as opposed to FTIT, as heating of the rotor was anticipated to occur at a higher rate under current injection. Mapping and parameter recordings were obtained in the same manner as that of Scenario 1.

The ambient temperature measured 21°C at a barometric pressure of 838.9 mbar at the time of testing and fluctuated to a small degree measuring 20°C at the conclusion of the rest. The average surface, ambient and enclosure temperatures are plotted in Figure 5.16 (below) for the 210 minute duration. The average surface temperature heating rate varied based on the current level. A higher current level resulted in a higher surface temperature and an increased rate of temperature rise. This differs from FTIT (both scenarios), where surface temperature values stabilise as observed, whereas for CTIT, an equilibrium point is not reached, as a steady state operation is never achieved during this test method. The final temperature achieved for FTIT is influenced largely by the ambient temperature and component interactions, in which a state is reached where heat losses equal heat generated, i.e. equilibrium. The heating rate and achieved temperature can be controlled for CTIT as opposed to FTIT.
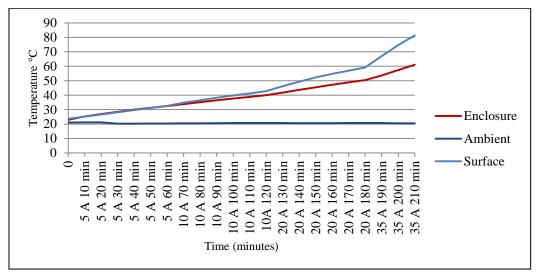
Figure 5.16: Plot of CTIT average surface temperature over the 210 minute test duration

Temperature recordings related to CTIT are presented in Figures 5.17 to 5.22 (below). For the entire sequence of temperature data captured (every 10 minutes), refer to Appendix G. Figure 5.17 (below) summarises the initial temperature distribution of the rotor surface prior to the commencement of the test: an average surface temperature of 23.7°C. The maximum average surface temperature achieved after three and a half hours was 81.2°C.

Figure 5.17: Temperature data analysis for CTIT at 0 A, 0 minutes

Figure 5.18: Temperature data analysis for CTIT at 5 A, 30 minutes

Figure 5.19: Temperature data analysis for CTIT at 10 A, 90 minutes

Figure 5.20: Temperature data analysis for CTIT at 20 A, 150 minutes
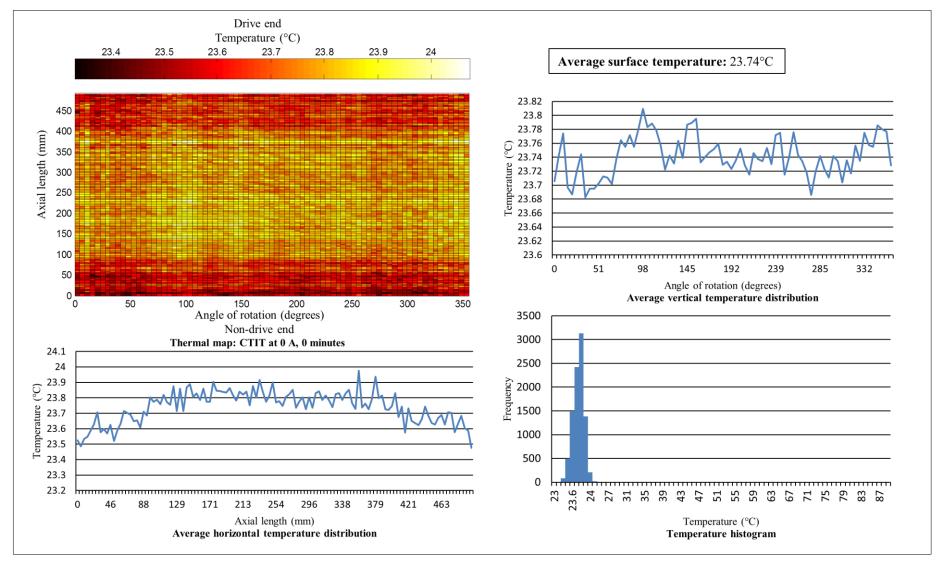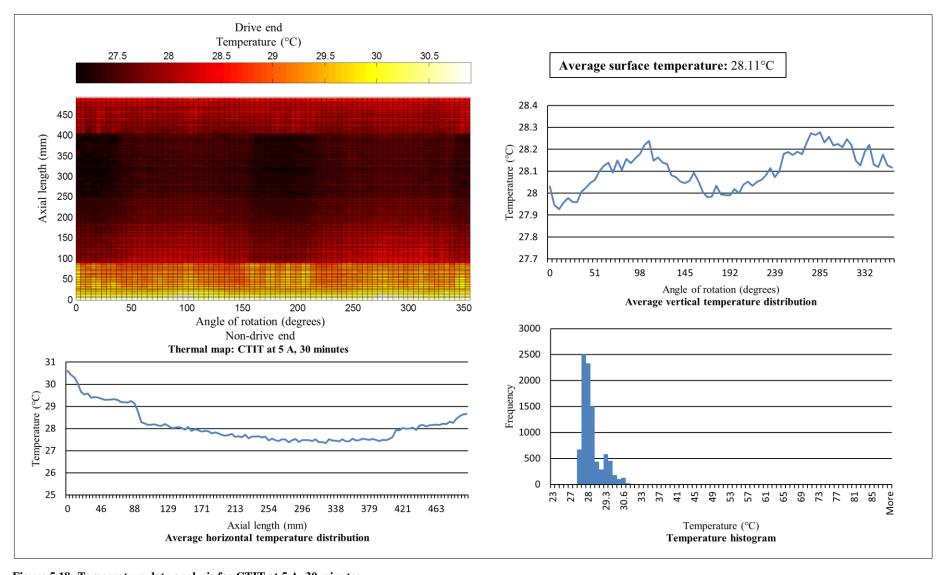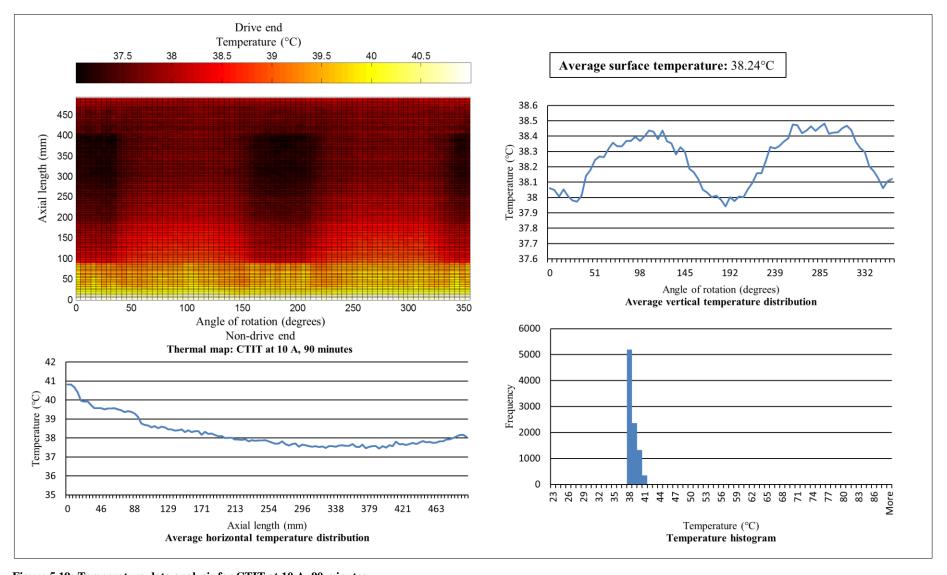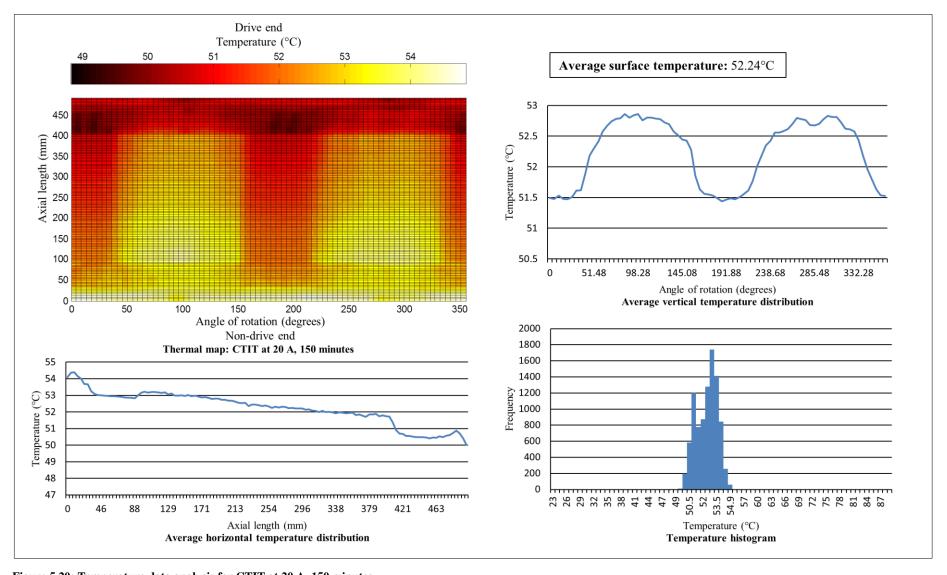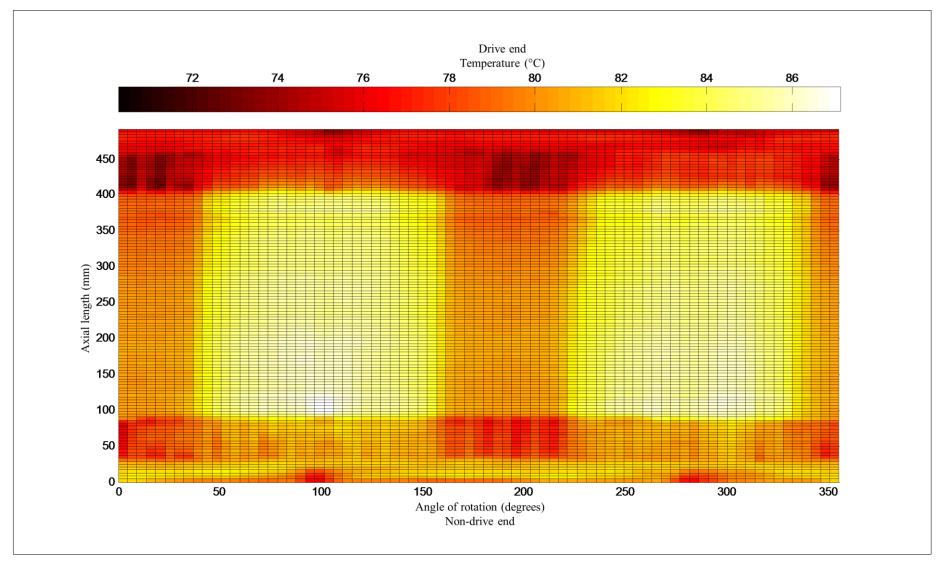
Figure 5.21: Large scale thermal map for CTIT at 35 A, 210 minutes

Average surface temperature: 81.29 °C

Average horizontal temperature distribution

Average vertical temperature distribution

Temperature histogram
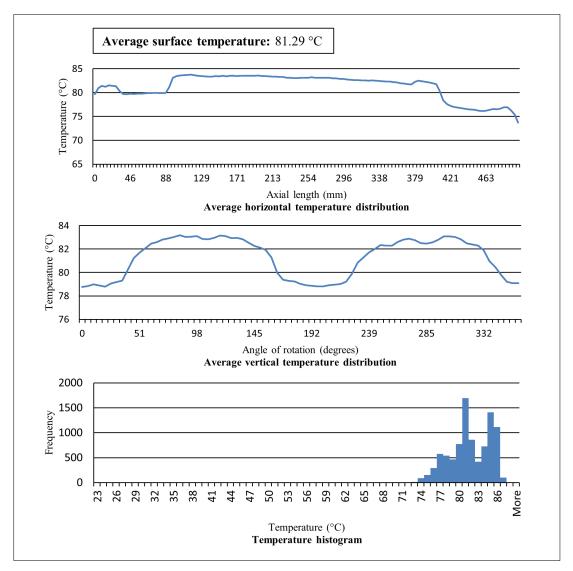
Figure 5.22: Temperature data analysis for CTIT at 35 A, 210 minutes

The histogram data for each testing interval captured was found to be positively skewed or skewed to the right for the first two and a half hours of the test. The trend changed to being negatively skewed or skewed to the left for the remaining duration of the test. A wide distribution of surface temperatures was observed. For example, at the completion of the test, the final data contained in Figure 5.22 (below) the surface temperature varied from a minimum of 70.2°C to a maximum of 87.2°C.

The effects of the collector assembly are also observed during CTIT, where the average horizontal temperature distribution shows that higher temperatures were experienced towards the non-drive end of the mini-rotor. The temperature gradient can be clearly observed on the thermal maps, and the trend is consistent until the application of higher current levels leading to higher temperatures than those of the collector assembly losses. Of particular interest is the average vertical temperature distribution, which exhibited a double peak in temperature distribution throughout the testing period.

A rectangular symmetrical area of a higher temperature could be observed on all the thermal maps throughout the test. These areas of high temperature were identified as the pole faces and associated coils. A large-scale high-resolution thermal map is presented in Figure 5.21 (above), where the temperature distribution can be observed in detail. The observations from the temperature maps are also correlated in the average vertical temperature distribution, as illustrated in Figure 5.22 (above). The higher temperatures of the poles can be clearly observed with a double-peaked horizontal distribution. The inter-pole areas are represented as the valleys of the distribution at lower temperatures. This observation differs greatly from that of FTIT. This is attributed to the manner in which heat is distributed, as the rotor winding is acting as the heat source. Because a rotor requires current during operation, it can be concluded that the thermal behaviour observed under CTIT is more representative of actual operating conditions.

5.4 Analysis of thermal sensitivity testing techniques

The presented experimental results for CTIT and FTIT show significant differences in the thermal behaviour of the mini-rotor during the different testing modes. Table 5.1 (below) summarises the experimental results obtained for FTIT, including and excluding the brush-gear effects, as well as for

Table 5.1: Statistical analysis summary of FTIT and CTIT testing scenarios

Time (min)	Current (A)	Mean (°C)	Median (°C)	Mode (°C)	Min (°C)	Max (°C)	Difference (°C)	Skewness	Kurtosis
Friction thermal instability testing									
0	0	23.40	23.4	23.5	22.70	23.80	1.10	-0.66	-0.12
30	0	27.01	26.8	26.4	25.90	30.00	4.10	1.33	1.26
60	0	32.05	31.8	31.3	30.70	35.60	4.90	1.37	1.27
90	0	36.82	36.5	36	35.60	40.60	5.00	1.39	1.34
120	0	40.97	40.60	40.20	39.70	44.60	4.90	1.42	1.24
150	0	44.47	44.00	43.80	43.30	48.00	4.70	1.32	0.87
180	0	47.44	46.70	46.70	46.20	50.90	4.70	1.23	0.60
210	0	50.38	49.90	49.60	49.30	53.70	4.40	1.15	0.38
240	0	52.68	52.30	51.90	51.60	55.70	4.10	1.08	0.26
270	0	54.57	54.20	53.70	53.30	57.40	4.10	0.90	-0.09
300	0	56.22	56.00	55.70	58.10	59.00	0.90	0.81	-0.17
330	0	57.90	57.60	56.80	56.30	60.70	4.40	0.71	-0.34
360	0	59.15	58.90	58.50	57.30	62.10	4.80	0.56	-0.47
390	0	60.55	60.30	59.80	58.60	63.50	4.90	0.51	-0.63
420	0	61.35	61.10	60.70	59.30	64.20	4.90	0.43	-0.63
450	0	62.20	62.00	61.70	60.00	65.00	5.00	0.28	-0.73
480	0	62.89	62.70	62.30	60.70	65.50	4.80	0.19	-0.77
Friction thermal instability testing excluding brush-gear									
0	0	23.27	23.30	23.40	22.5	23.7	1.20	-0.81	0.51
30	0	23.42	23.30	23.20	22.80	24.80	2.00	0.88	0.18
60	0	25.76	25.60	25.50	25.10	27.30	2.20	0.86	-0.01
90	0	28.20	28.10	28.00	27.60	29.60	2.00	0.99	0.48

Time (min)	Current (A)	Mean (°C)	Median (°C)	Mode (°C)	Min (°C)	Max (°C)	Difference (°C)	Skewness	Kurtosis
120	0	30.13	30.10	30.00	29.70	31.40	1.70	1.00	0.87
150	0	31.90	31.90	31.80	31.50	33.00	1.50	1.05	1.48
180	0	33.38	33.40	33.30	32.90	34.40	1.50	0.95	1.45
210	0	34.56	34.50	34.50	34.20	35.50	1.30	1.02	2.11
240	0	35.43	35.40	35.40	35.10	35.90	0.80	0.49	0.53
270	0	36.40	36.40	36.40	36.10	37.00	0.90	0.48	0.33
300	0	37.03	37.00	37.00	36.60	37.60	1.00	0.31	0.04
330	0	37.63	37.60	37.60	37.20	38.20	1.00	0.17	-0.26
360	0	38.28	38.30	38.30	37.80	38.80	1.00	0.02	-0.42
390	0	38.44	38.40	38.50	38.00	38.90	0.90	-0.27	-0.29
420	0	38.75	38.80	38.70	38.30	39.20	0.90	-0.16	-0.33
450	0	39.13	30.10	39.20	38.70	39.50	0.80	-0.30	-0.35
480	0	39.45	39.40	39.40	39.10	39.90	0.80	0.26	-0.09
Current thermal instability testing									
0	0	23.74	23.8	23.8	23.30	24.10	0.80	-0.28	-0.10
10	5	25.18	25.10	24.90	24.40	26.80	2.40	1.29	1.32
20	5	26.58	26.40	26.20	25.60	28.90	3.30	1.21	1.05
30	5	28.11	27.90	27.60	27.00	30.90	3.90	1.31	1.11
40	5	29.73	29.50	29.10	28.60	32.70	4.10	1.35	1.25
50	5	31.09	30.90	30.40	29.90	34.20	4.30	1.31	1.11
60	5	32.53	32.30	31.90	31.30	35.60	4.30	1.35	1.17
70	10	34.84	34.60	34.60	33.50	37.90	4.40	1.24	1.14
80	10	36.41	36.10	35.90	35.10	39.40	4.30	1.28	1.08
90	10	38.24	37.90	37.80	37.00	41.00	4.00	1.24	0.89
100	10	39.73	39.40	39.30	38.60	42.40	3.80	1.21	0.78
110	10	41.27	41.00	40.70	40.20	43.90	3.70	1.13	0.54
120	10	42.74	42.40	42.00	41.50	45.40	3.90	1.05	0.33
130	20	46.16	46.10	46.30	44.30	49.70	5.40	0.57	-0.08
140	20	49.32	49.40	49.70	46.60	52.40	5.80	0.14	-0.74
150	20	52.24	52.30	52.70	48.80	54.90	6.10	-0.26	-0.84
160	20	54.69	55.00	55.50	50.60	56.90	6.30	-0.58	-0.61
170	20	56.91	57.20	57.60	52.50	59.10	6.60	-0.73	-0.35
180	20	59.12	59.50	59.80	54.30	61.50	7.20	-0.87	-0.11
190	35	67.07	67.50	69.30	60.70	71.90	11.20	-0.20	-1.16
200	35	74.72	74.80	73.40	65.80	80.20	14.40	-0.25	-0.89
210	35	81.29	81.10	80.50	70.20	87.20	17.00	-0.37	-0.68

CTIT. The elements of the table comprise: time; current; mean surface temperature; median, mode, minimum (min) temperature of the rotor surface; maximum (max) temperature of the rotor surface; the difference between the min and max; histogram skewness; and kurtosis. The skewness indicates the asymmetry of the temperature distribution. A value of 0 indicates a symmetrical distribution. A positive value indicates skewness to the right and a negative value to the left. Kurtosis is a measure of the shape of the distribution i.e. the measure of the 'tailedness' of a distribution as compared to a

normal distribution. A normal distribution has a kurtosis of 0; high values indicate heavy tails or the presence of outliers, while lower values indicate light tails or the absence of outliers in a data set [115], [116]. The analysis of the results will be approached from two perspectives: quantitative and qualitative. The quantitative approach will focus on the statistical significance of the data, while the qualitative analysis will elaborate on how these outcomes affect the practical performance of TIT in the mainstream.

5.4.1 Quantitative analysis of TIT results

The distribution of the FTIT scenario indicates that the mean, median and mode are close to resembling a normal distribution, being equal. For example, at 180 minutes, the values are 47.44, 46.70 and 46.70; at 360 minutes the values are 59.15, 58.90 and 58.50. Upon further analysis of the initial four hours of FTIT, the distribution was skewed to the right, with positive kurtosis values indicating a leptokurtic distribution, i.e. a peaked distribution with outliers. This shift from a normal distribution indicates the heating phase of the mini-rotor surface during the test. The influences of the slip-ring brush-gear interaction, as observed within the thermal maps, contribute to this trend. As the effects of the slip-ring brush-gear interaction normalise during the concluding four hours of the test, the skewness of the distribution tends to become closer to a normal distribution (0), while the kurtosis becomes negative or platykurtic, indicating a flattening out of the distribution. Large differences of up to 5°C could be observed between the hottest and coolest part of the mini-rotor surface. From these observations, it can be inferred that this method of performing thermal sensitivity testing produces a slow, uncontrolled, uniform temperature distribution on the surface of the mini-rotor.

Once the brush-gear was removed, the resultant distributions indicated a uniform distribution, with the mean, median and mode being virtually identical throughout the testing period. A positive skewness was observed for a large duration of the test, later approaching 0 then proceeding to be slightly negatively skewed. The kurtosis values were close to zero, indicating a mesokurtic distribution, i.e. normality with no outliers. The effects of the removal of the brush-gear are quite significant, as this test did not reach the high temperatures experienced in scenario 1. Smaller differences could be observed between the hottest and coolest part of the mini-rotor rotor surface. A close to normal distribution of temperature along the surface of the mini-rotor can be expected for this mode of testing.

For the CTIT scenario, the mean, median and mode throughout the test are close to being equal or representing a normal distribution. As the test progressed and the current values increased, the skewness changed from being highly skewed to the right to approaching 0 and then proceeding to become highly skewed to the left. The kurtosis followed the same trend, initially being leptokurtic then mesokurtic and finally platykurtic. The kurtosis values indicate the presence of significant

outliers throughout the test. This behaviour can be attributed to the effect of a changing current source. Large differences of up to 17°C could be observed between the hottest and coolest part of the mini-rotor rotor surface. These observations show that as a heat source, the winding produces temperature profiles that are not homogenous throughout the mini-rotor surface. The non-homogenous (heterogenous) thermal nature of the rotor is due to the various materials constituting its construction; when excited, the materials undergo heat transfer at different rates. An overall higher mean temperature is achieved during CTIT as compared to the previous scenarios. The TIT data is summarised as a series of box plots in Figure 5.23 (below). FTIT shows a contracted distribution with the absence of significant outliers. A further contraction is observed once the brush-gear is removed, showing a normal distribution. CTIT, on the other hand, shows a large distribution of values with significant outliers.

A distinct difference in distribution patterns has been noted. A uniform distribution characterised the friction heating of the rotor. The evaluation of the distribution trend also highlights the effect of the slip-ring assembly during testing. The gradient created by the slip-ring brush-gear interaction was observable. The analysis disclosed that FTIT is characterised by a normal distribution that indicates a slow and uncontrolled process. On the other hand the distributions observed during CTIT were not uniform but started off as initially being leptokurtic then mesokurtic and finally platykurtic. This can be attributed to the changing current source. The differences in distributions indicate the dissimilarities between CTIT and FTIT. Where CTIT exhibits a number of outliers that are indicative of what may be the true thermal performance of a machine as opposed to FTIT which produces the ideal machine characteristic of a homogenous thermal distribution.
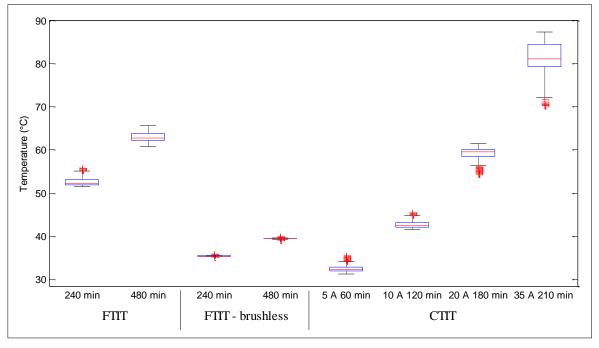

Figure 5.23: Pertinent box plots of thermal instability testing scenarios

5.4.2 Qualitative analysis of TIT results

These results indicate that the mode in which TIT is being performed globally requires a re-evaluation. The effects of the slip-ring brush-gear interaction for the friction scenario created an additional heating component, leading to asymmetries in the thermal distribution. A discernible thermal gradient was created, with the exciter end operating at a higher temperature. The effect of the collector assembly was quantified by executing the test with the brush-gear removed. During conventional FTIT, the winding temperature is determined by measuring the rotor winding resistance, as outlined in Chapter 4 Section 4.3. This can only be achieved via the collector assembly. The collector assembly has been found to be a major contributor to rotor heating as compared to friction alone. Furthermore, heating via friction was found to be slow, uniform and uncontrolled. If the heating rate was required to be increased to resemble the preferred online testing mode outlined in Chapter 3 Section 3.5.4, this would not be possible. FTIT is greatly influenced by ambient temperature and the interaction with the experimental setup. This influences at what point the equilibrium or maximum temperature is reached, which is significantly lower than that of CTIT. In essence, FTIT supports the assumption that a generator rotor, during operation, heats up uniformly and is able to provide that heating mechanism. This method, instead of evaluating the actual thermal behaviour of the rotor, is able to create the ideal heating conditions for rotor thermal behaviour. The FTIT scenario does not present the actual thermal behaviour of a rotor during operation and cannot be effectively used for generator rotor thermal sensitivity evaluation.

The results observed for CTIT differed in contrast to those for FTIT. The influence of the collector assembly was also apparent in the CTIT scenario but was immaterial, as CTIT depends on there being a pathway to inject current into the rotor. The temperature rise for CTIT is achieved via current injection: thus, the winding temperature initially rises and heat is dissipated from the winding outward. The composition of the rotor greatly affects the manner in which heat is distributed, i.e. the heat is distributed through the different materials at different rates. This is more representative of a rotor during operation. The manner in which the winding temperature is determined remains the same as per Chapter 4 Section 4.3. The winding temperature is ascertained utilising a numerical calculation reliant on accurately measuring the physical winding temperature, current, voltage and winding resistance at a reference instant. The subsequent temperature value can be calculated by utilising the rotor resistance measurement at any given time and current level. However, the winding is not physically exposed for the temperature measurement to be taken: thus, the rotor body temperature is sampled in several areas and then averaged on the assumption that the winding is at the same temperature. This is not a particularly sophisticated procedure to determine the winding temperature, especially for a test that requires a high degree of accuracy to evaluate thermal sensitivity.

This shortcoming is evident as the results for CTIT show a wide range of temperatures being experienced on the rotor surface during testing. To assume a normal distribution and then iterate temperature values for subsequent current levels introduces an inaccuracy of the actual temperature of the winding as well as the temperature distribution of the mini-rotor surface. Differences between the winding temperatures as compared to the mini-rotor average surface temperature are illustrated in Figure 5.24 (below). The winding temperature displayed was captured directly from the winding surface. The relationship between the average surface temperature and direct winding temperature support the narrative that current CTIT modes are not being conducted accurately. The winding and surface temperature can differ by up to 11°C. This is a phenomenon that is also prevalent for FTIT, as illustrated in Figure 5.25 (below).
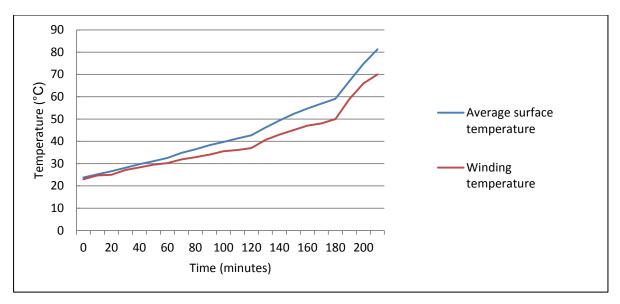
Figure 5.24: Direct winding and average mini-rotor surface temperature for CTIT
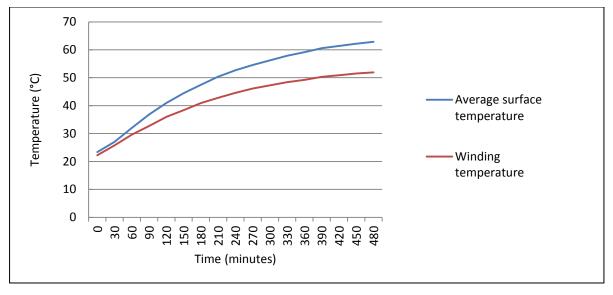
Figure 5. 25: Direct winding and average mini-rotor surface temperature for FTIT

89

The results observed for CTIT were indicative of the manner in which a rotor would behave during operation. Contemporary CTIT modes need to be augmented with the direct mapping method to ensure an accurate approach to thermal sensitivity testing. The analysis conducted strongly supports an augmented CTIT as a preferred method to test for rotor thermal sensitivity.

5.4.3   Scenario 3: Fault-finding capability

This final scenario is proposed for two principle reasons: first, the ability of the experimental setup to detect a fault condition; secondly, the use of the method to locate an area of concern on the rotor body, e.g. locating the slot where an anomaly is occurring, resulting in uneven heating. This will determine if the direct thermal mapping method can be an effective fault-finding tool once a thermal sensitivity problem is experienced and negate unnecessary expenses related to large turbo-generator rotor fault finding and disassembly.

An inter-turn short was induced between turns six and seven on coil eight of the A-pole of the mini-rotor with excitation applied at 20 A, as illustrated in Figure 5.26 (below). The rotor was then mapped after 30 seconds to determine whether the hot spot created was detected and if it can be successfully located. After 30 seconds, the thermal map was able to clearly identify an area exhibiting a higher temperature on the A-pole. The area is encircled in Figure 5.27 (below). The area of concern was located at approximately 100 radians on the diameter of the mini-rotor at the non-drive end. This is also correlated in Figure 5.28 (below) in the average horizontal distribution plot, where a slight peak is observed and outlined. This was then verified physically on the mini-rotor, which corresponded to the location of the induced inter-turn short. Furthermore, the fault condition was detected within 30 seconds of operation. The speed and accuracy of the experimental setup to detect and identify the location of the fault condition makes it suited to accurate faulting finding. The strength of this technique lies in its ability to detect faults that other condition assessment tests may not, as well as to quickly and efficiently aid in fault location. This result further indicates the need to modernise current TIT methods with the proposed augmented CTIT method.

5.5   Conclusion

In this chapter, the results obtained for the evaluation of FTIT and CTIT are presented. Thermal maps and associated data have been used to differentiate between FTIT and CTIT. The results conclusively depict appreciable differences between the testing methods. FTIT is found to embody a test method that assumes that a generator rotor experiences a uniform thermal distribution during operation. The distributions analysed were fairly uniform regardless of the effects of the collector assembly. The inability to control the rate at which the rotor was heated is also identified as a shortcoming, as this does not conform to real-life operation. FTIT therefore cannot be effectively used as a method to conduct rotor thermal sensitivity testing.

Figure 5.26: Inter-turn short induced between coils six and seven to evaluate fault analysis

On the other hand, CTIT illustrated an entirely different distribution where the pole faces of the rotor operating at higher temperature do not follow a uniform distribution. Injecting current at different levels into the rotor in a manner akin to the preferred method of online testing produced a constant rotor temperature shift. The thermal behaviour exhibited was congruent to that of a rotor under operating conditions.

Shortcomings identified related to the method in which the rotor temperature was evaluated during TIT. The calculation of the rotor winding temperature introduces inaccuracies, as the winding temperature does not match the surface temperature during the test. An augmented CTIT is proposed to improve the performance of TIT. Additionally, the ability of the direct thermal mapping method to identify areas of concern during TIT has been evaluated. The speed and accuracy of the method is significant in identifying and physically locating the area of concern.

The high-accuracy augmented CTIT method utilising direct thermal mapping makes it well suited to perform TIT. The ability of the method to closely mimic operating conditions as well as to aid in fault detection and location can considerably reduce the time taken to perform TIT as well as fault finding. Furthermore, these advances in TIT could potentially drastically reduce monetary losses associated with failed tests and fault finding, as well as overcoming problems associated with second-guessing results and methodologies.
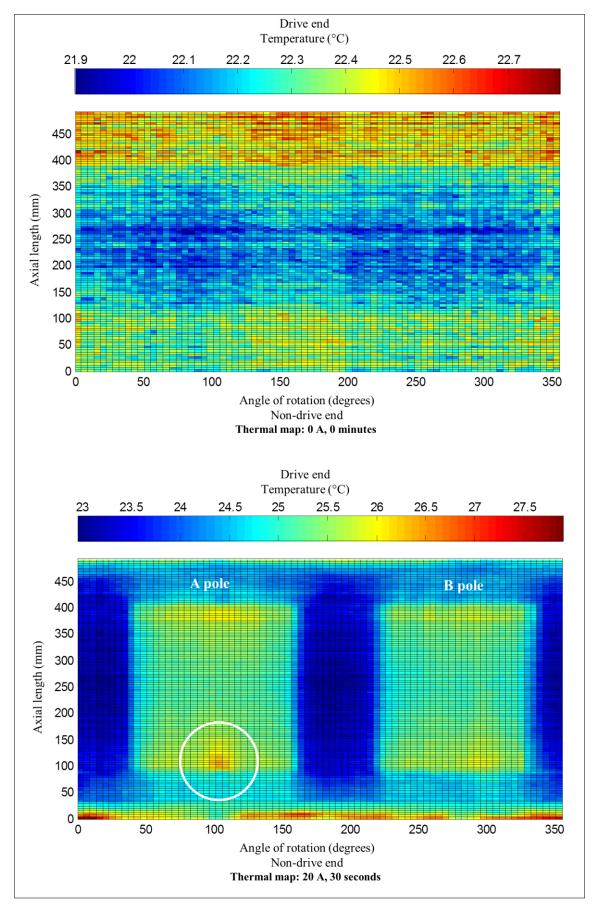
Figure 5.27: Thermal map of fault inducted condition clearly showing an area of high temperature
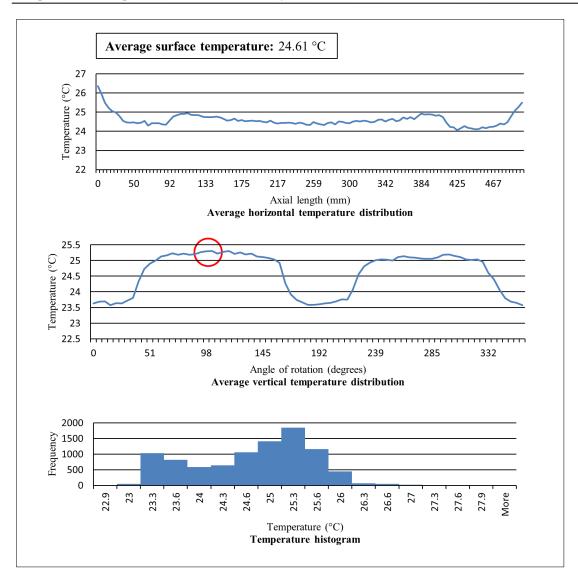
Figure 5.28: Temperature data analysis for fault finding: 30 seconds, 20 A

Chapter 6 | General Conclusions

6.1   Research overview

This chapter summarises the research undertaken by presenting an overview as well as conclusions reached. The principle objective of the research is to differentiate between two generator rotor thermal sensitivity testing techniques, i.e. FTIT and CTIT.

A review of the current state of the art regarding thermal sensitivity testing has revealed that the practice is utilised by many utilities, repairers and OEMs globally. Analysis of TIT-related testing at a local utility has highlighted a high failure rate of rotors over the past eight years. This occurrence has raised concerns into the efficacy of the mode in which TIT is being conducted. An insight into global trends regarding TIT has shown that no clear preference exists. Furthermore, the importance of a final proving test after the maintenance, repair, rewind or manufacture of large turbo-generator rotors to determine thermal sensitivity and hence suitability for service has been recognised. However, limitations in the understanding of the different testing processes exist. This has been exacerbated by the lack of an international standard, minimal knowledge within the public domain and differences in testing facilities and the small group of entities performing the test. The results of and manner in which the test is performed can have severe financial implications should a rotor fail thermal sensitivity testing. This undesirable result can lead to the entity performing the test changing testing parameters or acceptance criteria to limit financial losses, at the expense of rotor reliability.

The principle objectives of the research are outlined in Chapter 1 with an ultimate goal to determine the best suited mode for TIT. In the response to these objectives the following summary is offered:

- An experimental framework was designed, developed and tested based on a scale model of a 600 MW turbo-generator rotor. The mini-rotor mirrored the major characteristics of a large 600 MW turbo-generator rotor in the following aspects: two pole; 50 Hz; concentric flat bar field windings; damper bars; shaft mounted slip-rings; insulated bearings; and a slot milled mono-block steel forging. The testing enclosure was also scaled based on the mini-rotor dimensions and that of a local balancing and testing facility. The accurate scaling of the experimental setup provided an adequate platform to determine the thermal behaviour of the mini-rotor within reasonable tolerances to make conclusions that can relate to large turbo-generator rotors.

- Infrared technology was utilised to capture the thermal behaviour of the surface of the mini-rotor as well as to determine the temperature of the winding. A direct thermal mapping method was devised. A sampling array was developed to measure in detail the thermal

profile of the mini-rotor surface. A laser-guided pyrometer was utilised to directly acquire the winding temperature. The direct thermal mapping data was then found to be best represented as a temperature map. A high resolution temperature map of the mini-rotor surface with a 120x77 measuring point resolution was constructed and presented during different test conditions.

- The definitive results obtained from the direct thermal mapping method enabled a quantitative and qualitative analysis of FTIT and CTIT. Factors that affected the testing scenarios were uncovered. The results revealed that the rotor thermal behaviour is significantly different. This enables/aides in identifying a preferred technique for TIT: CTIT.

- The major shortcomings of both testing methodologies were identified. Of prominence was the manner in which the temperature information is captured during conventional TIT. The temperature profiles of the rotor surface as compared to the rotor winding were found to be different, which nullified conventional thermal monitoring. The direct thermal mapping technique can be utilised to improve TIT and ensure accurate thermal mapping and measurements.

- The direct thermal mapping method was evaluated for the purpose of rotor fault finding and trouble shooting. The method was able to identify an induced inter-turn short within 30 seconds of operation. With the aid of the temperature map, it was further possible to locate the fault area.

- An experimental framework was designed, implemented and validated to enable the analysis of the thermal profile of the surface of a rotor and winding. CTIT was identified as the method best suited to the purposes of thermal instability testing. The method can, however, be improved with the introduction of the direct thermal mapping method, which has potential applications in the domain of rotor fault finding.

6.2 Conclusions and significance of research

The fundamental differences between FTIT and CTIT as techniques to identify generator rotor thermal sensitivity have been ascertained. The use of an accurately scaled experimental setup as well as the development of the direct thermal mapping technique aided in this undertaking. The outcomes are as follows:

- FTIT created a scenario that allowed the rotor to heat up at a steady rate, creating a uniform surface temperature distribution. This mode supports the assumption that a generator rotor heats up uniformly during operation. In other words, FTIT is able to create the ideal heating conditions for rotor thermal behaviour. This, however, does not

present a true reflection of the behaviour of a rotor during operation (current injection) as illustrated by CTIT. Furthermore, the heating rate for FTIT is uncontrolled, i.e. the friction mechanism determined the temperature rise and could not be controlled during the test.

- The losses experienced by the collector ring assembly introduced a thermal component that affected the thermal distribution of the rotor. The heat generated by this interaction considerably increased the temperature of the non-drive end of the rotor. A thermal gradient was introduced that skewed the thermal performance of the rotor. During FTIT, this mechanism was prevalent; the rotor was able to reach a much higher temperature with the brush-gear installed as compared to when it was removed. This influence was also experienced during CTIT during lower current levels but became less pronounced at higher current levels. The effects of the thermal component created by the collector ring assembly can result in a thermal sensitivity problem being manifested. The outcome can create false test results, as the collector ring assembly, during operation, is situated externally to the main rotor body that operates within the generator casing. By virtue of the brush-gear assembly being situated externally to the main rotor body, the effects may not be as pronounced.

- CTIT differed significantly in contrast to FTIT. The current injection resulted in a heterogeneous distribution of temperatures along the rotor surface as opposed to the homogenous distribution in FTIT. A noticeable symmetrical region of higher temperature was observed along the pole face region. Furthermore, the heating rate could be controlled via the change in current applied during the test.

- The manner in which the rotor winding temperature is calculated while performing contemporary FTIT and CTIT is one of the main shortcomings that are evident. The use of a sampled, averaged body temperature to determine the winding temperature is not indicative of the actual winding temperature. Results indicate that the rotor surface temperature and winding temperature differ considerably. The assumption that the rotor surface temperature and the winding temperature are equal is incorrect and should not be used as a basis to calculate the winding temperature during testing.

- The direct thermal mapping method is capable of accurate and timeous fault detection. An area of concern can be located with high accuracy, enabling easier fault detection. The accuracy offered by the method will improve the trouble shooting aspect of a failed test, which has been found to be difficult when utilising current methods. The direct

thermal mapping method will go a long way in saving time and cost associated with returning a rotor to service.

The results observed from CTIT were indicative of the manner in which a rotor would behave during operation. FTIT, on the other hand, does not accurately portray the thermal behaviour of a rotor during operation, which makes it an ineffective method for TIT. CTIT is the preferred technique to perform TIT, but considering the shortcomings of the contemporary methodology, an augmented methodology needs to be considered. This can be achieved by incorporating the direct thermal mapping method to ensure accurate thermal mapping and monitoring of the rotor. The findings indicate very clearly that the outcomes are applicable to larger turbo-generators in general. The outcome dispels the uncertainties in respect to what technique should be utilised for TIT. This does not only benefit service providers but also customers who can request that TIT be performed via CTIT to ensure reliability, resulting in considerable capital savings in the long run. Furthermore, this could lead to the power industry adopting CTIT as the foremost technique for the testing of turbo-generator rotor thermal sensitivity. This definitive result could aid in the establishment of an international standard for the testing procedure as well as interpretation and acceptance criteria that will govern and standardise the practice of TIT.

6.3 Further research

The completed research has presented a number of opportunities for furthering this particular field of study. The following aspects will contribute to the better understanding and utilisation of TIT.

6.3.1 Adopting an augmented approach to TIT

The shortcomings of contemporary methods of TIT have been highlighted in Chapter 5. The inability to accurately determine the rotor surface as well as the winding temperature profile produces unreliable testing results. The direct thermal mapping method is capable of accurately determining the thermal profile of the rotor surface. This capability can improve the manner in which contemporary TIT is performed. The method has been successfully proven on an accurately scaled experimental setup. Therefore it is recommended that the augmented TIT utilising the direct thermal mapping method be implemented at a large-scale balancing facility. Furthermore, a diverse number of turbo-generator rotors of different designs may be evaluated. The direct thermal mapping method can also be evaluated to assist in fault detection and trouble shooting of larger generator rotors. Additionally, the ability to detect a wider range of faults as compared to those presented in Chapter 5 (inter-turn short) can be evaluated.

6.3.2 Influence of the collector ring assembly on TIT

During the evaluation of FTIT in Chapter 5, it was observed that the rotor collector ring assembly losses affected the thermal distribution of the rotor. This was found to be true for both CTIT and FTIT. This was quantified by comparing the results of the thermal maps obtained with the brush-

gear present and absent during testing. The phenomenon needs to be further evaluated on a large-scale rotor within a balancing facility. During conventional testing, the collector assembly is always connected to the rotor. This is also true during periods where the collector ring is not being utilised, i.e. during the barring process used to straighten rotors prior to testing. This period can last for a number of hours where the effects of the collector assembly are not considered. This warrants further investigation.

References

[1]   *IEEE Guide for Operation and Maintenance of Turbine Generators*, IEEE Std 67-2005 (Revision of IEEE Std 67-1990), 2006.

[2]   *IEEE Recommended Practice for Monitoring and Instrumentation of Turbine Generators*, IEEE Std 1129-1992, 1992.

[3]   C. V. Maughan, "Impact of Generator Design on Component Deterioration Mechanisms," in *Iris Rotating Machines Conference*, Schenectady, NY, 2010.

[4]   B. Irwanto, L. Eckert, and T. Prothmann, "Thermal Unbalance Behaviour of Turbogenerator Rotors," in *Proceedings of the 9th IFToMM International Conference on Rotor Dynamics*, 2015, pp. 2231-2242.

[5]   R. J. Zawaoysky and W. M. Genovese, "Generator Rotor Thermal Sensitivity – Theory and Experience," GE Reference Library, GER-3809, 2001.

[6]   C. V. Maughan, "Generator reliability as influenced by engineering design parameters," in *Electrical Insulation Conference and Electrical Manufacturing & Coil Winding Conference*, 2001, pp. 159-179.

[7]   G. C. Stone, E. A. Boulter, I. Culbert, and H. Dhirani, "Electrical Insulation for Rotating Machines," in *Power Engineering*, M. E. El-Hawary, Ed. Piscataway, NJ: John Wiley & Sons, 2004, pp. 189-190.

[8]   I. Kerszenbaum, "Inspection of Large Synchronous Machines," Piscataway, NJ: IEEE Press, 1996, pp. 57-58.

[9]   G. Klempner and I. Kerszenbaum, "Operation and Maintenance of Large Turbo-Generators," Piscataway, NJ : John Wiley & Sons, 2004, pp. 457-458.

[10]   P. Tavner, L. Ran, J. Penman, and H. Sedding, "Condition Monitoring of Rotating Electrical Machines, " in *The Institution of Engineering and Technology*, Stevenage Herts, UK: The Institute of Engineering and Technology, 2008, pp. 52-53.

[11]   J. Stein, "Main generator rotor maintenance," EPRI, Palo Alto, CA, Rep. 1013458, 2006.

[12]   C. Gonzalez, "High Speed Balancing Specifications for Generators," Eskom Rotek Industries, Johannesburg, RSA, Rep. TWG-F-23, 2013.

[13]   G. Csaba. (2015, May 22). *Balancing Facility Information* [Online]. Availible e-mail: gabor.csaba@vgpower.com Message: Balancing Facility Information

[14]   B. Moore. (2015, May 20). *Balancing Facility Information* [Online]. Availuble e-mail: bmoore@national-electric-coil.com Message: Balancing Facility Information

[15]   M. Ohm. (2015, May 22). *Elliot at-speed* [Online]. Availible e-mail: mohm@elliott-turbo.com Message: Balancing Facility Information

[16]   D. J. Pierre. (2015, May 29). *PhD Study* [Online]. Availible e-mail: david.j.pierre@power.alstom.com Message: Balancing Facility Information

[17]   S. Plessie. (2015, May 25). *Balancing Facility Information* [Online]. Availible e-mail: simphiwe.plessie@siemens.com Message: Balancing Facility Information

[18]   D. Rennie. (2015, May 20). *Balancing Facility Information* [Online]. Availible e-mail: don.rennie@siemens.com Message: Balancing Facility Information

[19]   S. Robinson. (2015, June 26). *Siemens Balancing Facility Information* [Online]. Availible e-mail: scott.robinson@siemens.com Message: Balancing Facility Information

[20]   A. Thackray. (2015, June 8). *Balancing Facility Information* [Online]. Availible e-mail: Alex.Thackray@Brush.Eu Message: Balancing Facility Information

[21]   J. Cockerille. (2015, May 24). *Balancing Facility Information* [Online]. Availible e-mail: jamie.cockerill@au.abb.com Message: Balancing Facility Information

[22]   I. E. Agency, "How will global energy markets evolve to 2035?, " in *World Energy Outlook Factsheet*, Paris, FR, 2013.

[23]   M. Finkenrath, J. Smith, and D. Volk, "Analysis of the globally installed coal-fired power plant fleet," in *International Energy Agency CCS Retrofit*, Paris, FA, 2012.

[24]   N. Scenario, M. East, and P. Cedex, "World energy outlook 2014 factsheet," in *International Energy Agency factsheet,*Paris, FA, 2015.

[25]   M. G. Say, "Alternating Current Machines, " Harlow Essex, UK: Pitman publishing, 1976, pp. 366-369.

[26]   K. Sedlazeck, C. Richter, S. Strack, S. Lindholm, J. Pipkin, and F. Fu, "Type testing a 2000 MW turbogenerator," in *Electric Machines and Drives Conference,*2009, pp. 465-470.

[27]   C. V. Maughan, "Maintenance of Turbine-Driven Generators," Schenectady, NY: Maughan Engineering Consultants, 2008, pp. 2-26 – 2-31

[28]   G. Golden, "Steam Turbine Generator Auxiliary System Maintenance Guide -Volume 7," EPRI, Palo Alto, CA, Rep. 1021775, 2011.

[29]   V. Wowk, "Machinery vibration: measurement and analysis, " New York, USA: McGraw Hill Professional, 1991.

[30]   L. T. Rosenberg, "Eccentricity, Vibration, and Shaft Currents in Turbine Generators [includes discussion]," in *Transactions of the American Institute of Electrical Engineers. Part III: Power Apparatus and Systems,* vol. 74, 1955.

[31]   *IEEE Guide for Operation and Maintenance of Turbine Generators*, IEEE Std 67-1990, 1990.

[32]   R. Jackson, I. Roberts, R. Thurston, and J. Worsfold, "Generator rotor monitoring in the United Kingdom," CIGRE, Paris, FR, Rep. 1986, 1986.

[33]   A. Lifson and H. R. Simmons, "Vibration Monitoring of Turbomachinery," in *Proceedings of the 19th Turbomachinery Symposium,* Houston, USA, 1990, pp. 101-118.

[34]   R. B. McMillan, "Rotating machinery: practical solutions to unbalance and misalignment," Lilburn, GA: The Fairmont Press, 2004, pp. 97-107.

[35]   P. Pennacchi and A. Vania, "Analysis of the Shaft Thermal Bow Induced by Rotor-to-Stator Rubs," in *IASME Transactions,* vol. 1, pp. 193-198, 2004.

[36]   M. L. Adams, "Rotating machinery vibration: from analysis to troubleshooting," Boca Raton, FL: CRC Press, 2009, pp 371-378.

[37]   A. Muszynska, "Rotordynamics," Boca Raton, FL: CRC press, 2005, pp. 224-226.

[38]   M. B. Jevtic, L. Z. Radovanovic, and Z. Z. Adamovic, "Numerical and experimental aspects of thermally induced vibration in real rotors," in *Thermal Science,* vol. 15, pp. 545-558, 2011.

[39]   P. Kiameh, "Electrical Equipment Handbook: Troubleshooting and Maintenance, " McGraw Hill, New York, USA: 2003, pp. 23-12 – 23-15

[40]   *Mechanical vibration - Evaluation of machine vibration by measurements on rotating shafts - Part 2: Land-based steam turbines and generators in excess of 50 MW with normal operating speeds of 1 500 r/min, 1 800 r/min, 3 000 r/min and 3 600 r/mi*n, ISO 7919-2:2009, 2009.

[41]   *Mechanical Vibration of Non-reciprocating Machines - Measurements on Rotating Shafts and Evaluation Criteria. Part 4: Gas Turbine Sets with fluid-film bearings*, ISO 7919-4:2009, 2009.

[42]   *IRD Vibration Severity Chart*, IRD Mechanalysis Inc., 1975.

[43]   M. Gilstrap, "Evaluating rotor unbalance problems, " *Orbit Magazine,* 1981.

[44]   D. J. Petty, "Analysis of bearing vibration monitoring," in *Understanding your Condition Monitoring,* IEE Colloqium , 1999, pp. 401-411.

[45]   J. G. Paxton, "Turbine Generator Rotor Thermal Unbalance," in *EPRI Proceedings: Utility Motor and Generator Predicitve Maintenance and Refurbishment Conference,* Palo Alto, CA, pp. 112-116, 1994.

[46]   J. McDowell and P. Swan, "Identification of a unique vibration problem, " *Orbit Magazine*, 1992.

[47]   J. Albright and D. Albright, "Generator Field Winding Shorted Turns: Observed Conditions and Causes," in *EPRI International Conference*, 2003.

[48]   M. Šašić, B. Lloyd, and A. Elez, "Finite element analysis of turbine generator rotor winding shorted turns," in *Energy Conversion, IEEE Transactions,* vol. 27, pp. 930-937, 2012.

[49]   D. Albright, "Interturn short-circuit detector for turbine-generator rotor windings," in *Power Apparatus and Systems,* IEEE Transactions, pp. 478-483, 1971.

[50]   N. N. Misra and D. K. Sood, "Failure analysis of generator rotors - causes and preventions," *Cigre*, Paris, FR, 2006.

[51]   R. J. Zawoysky and K. C. Tornroos, "GE Generator Rotor Design, Operational Issues, and Refurbishment Options," GE Reference Library, GER-4212, 2001.

[52]   R. J. Zawaoysky and W. M. Genovese, "Generator Field Thermal Sensitivity - Therory and Experience," in *EPRI Proceedings: Utility Motor and Generator Predicitve Maintenance and Refurbishment Conference,*TR-104625, 1994, pp. 96-110.

[53]   Y. Yang and Q. Zhao, "Generator thermal sensitivity analysis with Support Vector Regression," in *American Control Conference*, 2010, pp. 944-949.

[54]   N.E. Coil, "Rotor Thermal Sensitivity Testing," National Electric Coil, Columbus Ohio, USA, 2015.

[55]   T. Kawurama and E. Shoyama, "Latest Technology for Turbine Generators," *Hitachi Review,* vol. 27, 1978, pp. 367-372.

[56]   W.F. King, "Thermal Balancing of Large Rotors,"in *Allis-Chalmers Electrical Review,* Second quator, 1947, pp 8-11.

[57]   C. Laffoon, A. Hagg, C. Janthey, and P. Heller, "Modern Practice in the Balancing of Large Turbine-Generator Rotors," in *American Institute of Electrical Engineers,* vol. 70, 1951, pp. 593-598.

[58]   A. Narain Singh, "Foreign Material Exclusion of Large Turbo Alternators," in *South African Universities Power Engineering Conference*, Cape Town, RSA, 2009.

[59]   M. Zumbach, G. Schweitzer, and K. Schoellhorn, "On-line thermal balancing technique for a large turbo-generator," in *Journal of Vibration and Acoustics,* vol. 114, 1992, pp. 60-66.

[60]   S. Neal, "Automatic balancing apparatus," U.S. Patent 3 149 502, September 22, 1964.

[61]   P. K. Hermann, R. Mahrt, and H. H. Doon, "Detecting and Locating Interturn Short Circuits on Turbine-Generator Rotors," in *IEEE Transactions on Power Apparatus and Systems,* vol. 82, 1963, pp. 686-698.

[62]   T. Hanada and M. Ohi, "556 MVA Turbine Generator for Matsushima Thermal Power Station of Electric Power Development Co.," *Hitachi Review,* vol. 31, 1982, pp. 101-106.

[63]   A. Febriyanto and H. T. Sandewan, "Rotor Thermal Sensitivity experience on 143.4 MVA hydrogen-cooled turbo generator with direct-cooled rotor design," in *Electrical Engineering and Informatics (ICEEI)*, 2011, pp. 1-6.

[64]   Z. Racic and J. Hidalgo, "The effect of applied high speed balancing method on flexible generator rotor response in operation," in *Proceedings of the ISCORMA-4,* Calgary, Canada, 2007.

[65]   A. Der Kiureghian and O. Ditlevsen, "Aleatory or epistemic? Does it matter?," in *Structural Safety,* vol. 31, 2009, pp. 105-112.

[66]   E. Smith, "Main Generator Rotor Maintenance - Lessons Learned," EPRI, Palo Alto, California, Rep. 1013458, 2006.

[67]   B. M. Weedy, "The determination of the transient temperature distribution in a turbo-alternator rotor by means of an analogue," in *Proceedings of the IEE - Part C: Monographs,* vol. 109, 1962, pp. 126-137.

[68]   T. Tomaskov, M. Svoboda, A. Shlykevich, and P. Trnka, "Increase the thermal conductivity of high voltage electrical insulation systems," in *Power Electronics and Applications (EPE'15 ECCE-Europe),* 2015, pp. 1-6.

[69]   J. Fourier, *Theorie analytique de la chaleur, par M. Fourier*: Chez Firmin Didot, père et fils, 1822.

[70]   D. A. Kaminski and M. K. Jensen, "Introduction to thermal and fluids engineering," New York, USA: Wiley, 2005.

[71]   G. Taylor, "Distribution of velocity and temperature between concentric rotating cylinders," in *Proceedings of the Royal Society of London A: Mathematical,* Physical and Engineering Sciences, 1935, pp. 494-512.

[72]   F. P. Incropera, D. P. DeWitt, T. L. Bergman, and A. S. Lavine, "Fundamentals of heat and mass transfer," New York, USA.: Wiley, 2007.

[73]   D. Staton, A. Boglietti, and A. Cavagnino, "Solving the More Difficult Aspects of Electric Motor Thermal Analysis in Small and Medium Size Industrial Induction Motors," in *IEEE Transactions on Energy Conversion,* vol. 20, 2005, pp. 620-628.

[74]   J. Pyrhönen, T. Jokinen, and V. Hrabovcova, "Design Process of Rotating Electrical Machines," West Sussex, UK: Johan Wiley and Sons, 2008, pp. 293-330.

[75]   A. Boglietti, A. Cavagnino, D. Staton, M. Shanel, M. Mueller, and C. Mejuto, "Evolution and modern approaches for thermal analysis of electrical machines," in *Industrial Electronics,* vol. 56, 2009, pp. 871-882.

[76]   D. Gerling and G. Dajaku, "Thermal calculation of systems with distributed heat generation," in *Thermal and Thermomechanical Phenomena in Electronics Systems,* 2006, pp. 652.

[77]   P. H. Mellor, D. Roberts, and D. R. Turner, "Lumped parameter thermal model for electrical machines of TEFC design," in *IEE Proceedings B - Electric Power Applications,* vol. 138, 1991, pp. 205-218.

[78]   W. Soong, "Thermal Analysis of Electrical Machines: Lumped-Circuit, FE Analysis and Testing," in *Power Engineering Briefing Note Series,* vol. 2, 2008, pp. 21-22.

[79]   A. Boglietti and A. Cavagnino, "Analysis of the Endwinding Cooling Effects in TEFC Induction Motors," in *IEEE Transactions on Industry Applications,* vol. 43, 2007, pp. 1214-1222.

[80]   A. Boglietti, A. Cavagnino, and D. Staton, "Determination of critical parameters in electrical machine thermal models," in *IEEE Industry Applications,* vol. 44, 2008, pp. 1150-1159.

[81]   A. Boglietti, A. Cavagnino, D. A. Staton, M. Popescu, C. Cossar, and M. I. McGilp, "End Space Heat Transfer Coefficient Determination for Different Induction Motor Enclosure Types," in *Industry Applications Society Annual Meeting,* 2008, pp. 1-8.

[82]   A. Boglietti, A. Cavagnino, M. Parvis, and A. Vallan, "Evaluation of radiation thermal resistances in industrial motors," in *IEEE International Conference on Electric Machines and Drives,* 2005, pp. 481-485.

[83]   A. Boglietti, A. Cavagnino, and D. A. Staton, "TEFC induction motors thermal models: a parameter sensitivity analysis," in *Industry Applications Conference,* vol 4, 2004, pp. 2469-2476.

[84]   A. Boglietti, A. Cavagnino, M. Popescu, and D. Staton, "Thermal Model and Analysis of Wound-Rotor Induction Machine," in *IEEE Transactions on Industry Applications,* vol. 49, , 2013, pp. 2078-2085.

[85]   M. J. Duran and J. Fernandez, "Lumped-parameter thermal model for induction machines," in *IEEE Transactions on Energy Conversion,* vol. 19, 2004, pp. 791-792.

[86]   D. Staton, M. Popescu, C. Cossar, M. McGilp, S. Omori, and T. Kurimoto, "Analytical thermal models for small induction motors," in *International Conference on Electrical Machines*, 2008, pp. 1-6.

[87]   S. K. Chowdhury and P. K. Baski, "A simple lumped parameter thermal model for electrical machine of TEFC design," in *Power Electronics, Drives and Energy Systems (PEDES)*, 2010, pp. 1-7.

[88]   D. Gerling and G. Dajaku, "Novel lumped-parameter thermal model for electrical systems," in *Power Electronics and Applications,* 2005.

[89]   J. Puranen and J. Pyrhonen, "Optimization of the loadability of an induction servomotor with a coupled electromagnetic-thermal model," in *International Symposium on Power Electronics, Electrical Drives, Automation and Motion,*2006, pp. 153-158.

[90]   O. Aglen and A. Andersson, "Thermal analysis of a high-speed generator," in *Industry Applications Conference,* 2003, pp. 547-554.

[91]   A. M. E.-. Refaie, N. C. Harris, T. M. Jahns, and K. M. Rahman, "Thermal analysis of multibarrier interior PM synchronous Machine using lumped parameter model," *IEEE Transactions on Energy Conversion,* vol. 19, 2004, pp. 303-309.

[92]   S. Nategh, "Thermal analysis and management of high-performance electrical machines," Doctoral Thesis, School of Electrical Engineering, KTH Royal Institute of Technology, Sweden, 2013.

[93]   S. J. Salon, "Finite element analysis of electrical machines," New York, USA: Springer Science+Business Media, 1995.

[94]   Y. K. R. Chin, E. Nordlund, and A. Staton, "Thermal analysis-Lumped-circuit model and finite element analysis," in *IPEC 2003: 6th International Power Engineering Conference*, 2003, pp. 952-957.

[95]   C. Mejuto, "Improved lumped parameter thermal modelling of synchronous generators," Doctoral Thesis, School of Electrical Engineering, The University of Edinburgh, England, 2010.

[96]   C. Lim, "Thermal Modelling of the Ventilation and Cooling inside Axial Flux Permanent Magnet Generators," Doctoral Thesis, school of Electrical Engineering, Durham University, England, 2010.

[97]   L. Yiping, Y. Wenhao, H. Jiade, L. Weili, and C. Pengfei, "Effect of insulation property and distribution of turbo generator rotor on temperature field," in *2008 World Automation Congress*, 2008, pp. 1-5.

[98]   C. Mejuto, M. Mueller, M. Shanel, A. Mebarki, and D. Staton, "Thermal modelling investigation of heat paths due to iron losses in synchronous machines," in *Power Electronics, Machines and Drives,* 2008, pp. 225-229.

[99]   A. F. Armor, "1981 Power Engineering Society Prize Paper Transient, Three-Dimensional, Finite-Element Analysis of Heat Flow in Turbine-Generator Rotors," in *IEEE Power Engineering Review,* 1981, pp. 11-23.

[100]   M. Mohammadi, H. Ansari, P. Bahemmat, and A. A. Kharamani, "Thermal analysis of the rotor of large air-cooled turbo generators," in *Thermal Power Plants (CTPP),* 2011, pp. 1-6.

[101]   F. Marignetti, V. D. Colli, and Y. Coia, "Design of Axial Flux PM Synchronous Machines Through 3-D Coupled Electromagnetic Thermal and Fluid-Dynamical Finite-Element Analysis," in *IEEE Transactions on Industrial Electronics,* vol. 55, 2008, pp. 3591-3601.

[102]   C. V. Maughan and J. M. Reschovsky, "Advances in motor and generator rotor health," in *International Symposium on Electrical Insulation (ISEI),* 2010, pp. 1-4.

[103]   T. Suesut, N. Nunak, T. Nunak, A. Rotrugsa, and Y. Tuppadung, "Emissivity measurements on material and equipment in electrical distribution system," in *Control, Automation and Systems (ICCAS),* 2011, pp. 1259-1263.

[104]   E. A. E. Jebaseeli and S. Paramasivam, "Real Time Temperature Measurement for the Thermal protection of Switched Reluctance Machine," in *International Journal of Engineering & Technology,* 2013, pp. 2983-2987.

[105]   C. Mejuto, M. Mueller, M. Shanel, A. Mebarki, M. Reekie, and D. Staton, "Improved synchronous machine thermal modelling," in *International Conference on Electrical Machine* , 2008, pp. 1-6.

[106]   D. P. DeWitt and G. D. Nutter, "Theory and practice of radiation thermometry," Wiley Online Library, 1988.

[107]   C. H. Chen, "Generalized association plots: Information visualization via iteratively generated correlation matrices," in S*tatistica Sinica,* vol. 12, 2002, pp. 7-30.

[108]   L. Wilkinson and M. Friendly, "The history of the cluster heat map," *The American Statistician,* vol. 63, 2009.

[109]   S. J. Hoffe, "Synchronous generator fault diagnosis using shaft signal measurements," Masters Dissertation, University of the Witwatersrand, School of Engineering and the Build Environment, Johannesburg, RSA, 2007.

[110]   T. Holliday and J. A. Kay, "Understanding infrared windows and their effects on infrared readings," in *Pulp and Paper Industry Technical Conference (PPIC),* 2013, pp. 26-33.

[111]   T. Holliday and J. A. Kay, "Understanding Infrared Windows and Their Effects on Infrared Readings," in *IEEE Transactions on Industry Applications,* vol. 50, 2014, pp. 2403-2409.

[112]   A. J. Holliday and J. Kay, "The use of infrared viewing systems in electrical control equipment," in *Pulp and Paper Industry Technical Conference,* 2005, pp. 291-295.

[113]   H. W. Kudlacik and D. M. Willyoung, "Local Rotor Winding Temperature Measurements for Large Turbine-Generator Fields," in *Transactions of the American Institute of Electrical Engineers. Part III: Power Apparatus and Systems,* vol. 81, 1962, pp. 687-693.

[114]   M. Epslon, "Operators manual thermoIMAGER TIM Connect, " MICRO-EPSILON MESSTECHNIK GmbH & Co. KG, Germany, 2016.

[115]   A. Field, "Discovering statistics using IBM SPSS statistics," London, UK: Sage, 2013.

[116]   R. M. Weiers, "Introduction to business statistics," Ohio, USA: Cengage Learning, 2010.

Appendix A | Mini-rotor condition assessment

An insulation resistance and an RSO Test were carried out on the mini-rotor to detect any latent defects that may influence the results acquired from the experimental setup. The rotor was found to be in a serviceable condition.

The insulation resistance was tested at 500 V yielding a value 581.8 MΩ. According to IEEE 43-2000 Recommended Practice for Testing Insulation Resistance of Rotating Machinery, this value is satisfactory and shows that the mini-rotor insulation system is not compromised.

The RSO results showed no indication of inter-turn shorts, as illustrated in Figure A.1 (below)
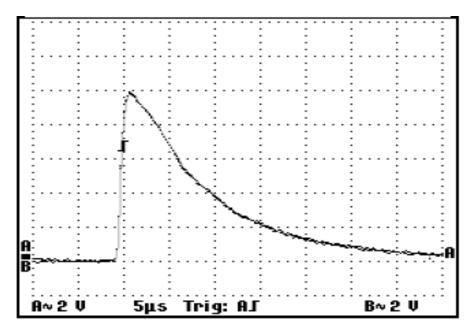
Figure A.1: RSO plot for mini-rotor

Appendix B | Experimental setup dimensions and layout
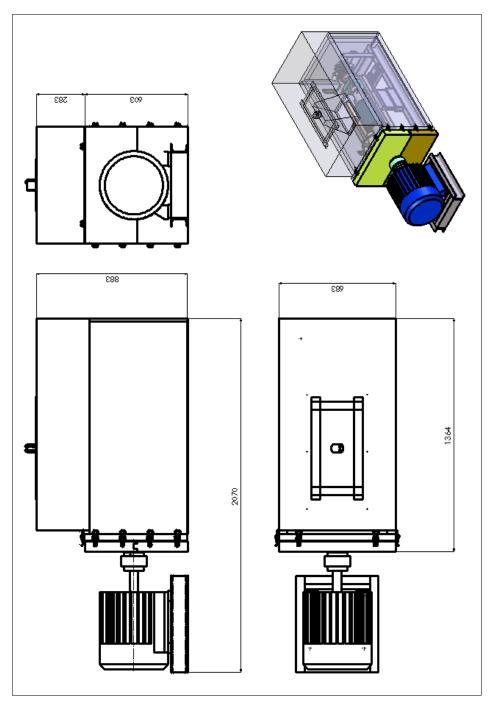
Figure B. 1: Experimental setup dimensions and layout
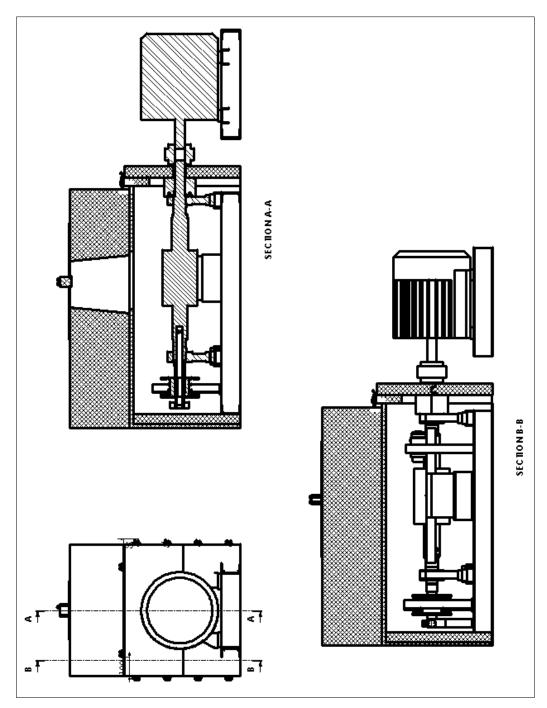
Figure B.2: Sectional views of experimental setup

Appendix C | Infrared camera - Optris PI400

C.1 Optris PI400 infrared camera datasheet

Base Model	PI160	PI200 / PI230	PI400 / PI450
Type	IR	BI-SPECTRAL	IR
Scope of supply	USB camera incl. 1 lens, USB cable (1 m), table tripod, PIF cable incl. terminal block (1 m), software package optris PI Connect, aluminium case	USB camera (BI-SPECTRAL) incl. 1 lens, USB cable (1 m), table tripod, focussing tool, PIF cable incl. terminal block (1 m), software package optris PI Connect, aluminium case	USB camera incl. 1 lens, USB cable (1 m), table tripod, PIF cable incl. terminal block (1 m), software package optris PI Connect, aluminium case
Detector	FPA, uncooled (25 µm x 25 µm)	FPA, uncooled (25 µm x 25 µm)	FPA, uncooled (25 µm x 25 µm)
Optical resolution	160 x 120 pixel	160 x 120 pixel	382 x 288 pixel
Spectral range	7.5 - 13 µm	7.5 - 13 µm	7.5 - 13 µm
Temperature ranges	-20°C...100°C, 0°C...250°C, 150°C...900°C, Option: 200°C...1500°C*	-20°C...100°C, 0°C...250°C, 150°C...900°C, Option: 200°C...1500°C*	-20°C...100°C, 0°C...250°C, 150°C...900°C, Option: 200°C...1500°C*
Frame rate	120 Hz	128 Hz***	80 Hz
Optics (FOV)	23° x 17° FOV / f = 10 mm or 6° x 5° FOV / f = 35.5 mm or 41° x 31° FOV / f = 5.7 mm or 72° x 52° FOV / f = 3.3 mm	23° x 17° FOV** / f = 10 mm or 6° x 5° FOV / f = 35.5 mm or 41° x 31° FOV** / f = 5.7 mm or 72° x 52° FOV / f = 3.3 mm	38° x 29° FOV / f = 15 mm or 62° x 49° FOV / f = 8 mm or 13° x 10° FOV / f = 41 mm
Thermal sensitivity (NETD)	0.08 K with 23° HFOV / F = 0.8 0.3 K with 6° HFOV / F = 1.6 0.1 K with 41° and 37° HFOV / F = 1	0.08 K with 23° HFOV / F = 0.8 0.3 K with 6° HFOV / F = 1.6 0.1 K with 41° and 72° HFOV / F = 1	0.08 K / 0.04 K with 38° HFOV / F = 0.8 0.08 K / 0.04 K with 62° HFOV / F = 0.8 0.1 K / 0.06 K with 13° HFOV / F = 1.0
Option for visual camera (only for BI-SPECTRAL camera)	-	Optical resolution: 640 x 480 Pixel Frame rate: 32 Hz*** Optics (FOV): 54° x 40°, PI230: 30° x 23°	-
Accuracy	±2°C or ±2%	±2°C or ±2%	±2°C or ±2%
PC interface	USB 2.0	USB 2.0	USB 2.0
Process interface (PIF)	0 - 10 V input, digital input, 0 - 10 V output	0 - 10 V input, digital input, 0 - 10 V output	0 - 10 V input, digital input, 0 - 10 V output
Ambient temperature (T_{Umg})	0°C...50°C	0°C...50°C	0°C...50°C / 0°C...70°C
Storage temperature	-40°C...70°C	-40°C...70°C	-40°C...70°C / -40°C...85°C
Relative humidity	20 - 80%, non-condensing	20 - 80%, non-condensing	20 - 80%, non-condensing
Enclusure (size / rating)	45 x 45 x 62 mm³ / IP 67 (NEMA 4)	45 x 45 x 62 mm³ / IP 67 (NEMA 4)	46 x 56 x 90 mm³ / IP 67 (NEMA 4)
Weight	195 g, incl. lens	215 g, incl. lens	320 g, incl. lens
Shock / vibration	25G, IEC 68-2-29 / 2G, IEC 68-2-6	25G, IEC 68-2-29 / 2G, IEC 68-2-6	25G, IEC 68-2-29 / 2G, IEC 68-2-6
Tripod mount	1/4-20 UNC	1/4-20 UNC	1/4-20 UNC
Power supply	USB powered	USB powered	USB powered

114

C.2 Calibration certificate

Kalibrierzertifikat

WKS 16010009

Calibration Certificate

Zertifikat-Nr.
Certificate No.

Gegenstand *Object*	**Infrarotkamera** *Infrared Imager*	Die Kalibrierung erfolgt durch Vergleich des Prüflings mit der Anzeige des Vergleichsgerätes, das durch den Deutschen Kalibrierdienst (DKD) bzw. der Physikalisch-Technischen Bundesanstalt (PTB) kalibriert wurde.
Typ *Type*	OPTPI400O80T900	
Serien-Nr. Kamera *Serial No. Camera*	15120040	
Serien-Nr. Optik *Serial No. Optics*	15120007	*The calibration is performed by comparison with standards which are calibrated by the Deutscher Kalibrierdienst (DKD) or Physikalisch-Technische Bundesanstalt (PTB).*

Vergleichsgeräte *Calibrated Standards*	**Serien-Nr.** *Serial No.*	**Kalibrierzeichen** *Calibration mark*	**Kalibrierdatum** *Calibration date*
OPTLS (8-14µm)	70101	73213 PTB 15	2015-06
OPTCTL2MHSF (1,6µm)	10067604	73327 PTB 14	2014-12
Exactus (0,9µm)	EXA2074	73123 PTB 14	2014-12

Die Kalibrierung der Temperaturquellen erfolgt nach ST-CAL[1)], die Kalibrierung des Gerätes nach CT-CAL[1)]. / *The calibration of the temperature sources fulfils ST-CAL[1)], the calibration of the product fulfils CT-CAL[1)].*

Messunsicherheit/*Measurement Uncertainty* ±0,25°C oder ±0,25% (der jeweils größere Wert gilt)
±0.25°C or ±0.25% (whichever is greater)

Die Messergebnisse sind nur zum Zeitpunkt der Kalibrierung gültig! Alle genannten Anzeigewerte bescheinigen eine Genauigkeit von 2% oder +/-2°C (der jeweils größere Wert gilt) unter diesen Bedingungen. / *Each of the named indicated values certifies an accuracy of 2% or +/-2°C (whichever is greater) under the conditions mentioned here.*

Raumtemperatur/*Ambient Temperature* 24,9°C Messfeld/*measuring field:* 5x5

Emissionsgrad/*Emissivity* 1,0 Position Messfeld/*position measuring field:* 191,144

Optris GmbH   Ferdinand-Buisson-Str. 14   D-13127 Berlin   Tel.: +49(0)30 500197-0
Fax: +49(0)30 500197-10   Email info@optris.de   Homepage www.optris.de

optris
infrared thermometers

Kalibrierzertifikat

Calibration Certificate

WKS 16010009
Zertifikat-Nr.
Certificate No.

Messergebnisse / *Results*

Temperaturpunkt / temperature point [°C]	Anzeigewert des Gerätes / indicated value of the unit [°C]	Blenden- durchmesser / aperture [mm]	Distanz/ distance [mm]	Temperatur- Bereich / temperature range [°C]	Mess- unsicherheit /uncertainty [°C]
24,9	25,9	50	100	-20…100	0,6
50,2	50,4	50	100	-20…100	0,6
100,2	100,2	50	100	-20…100	0,6
24,9	25,9	50	100	0…250	0,6
50,2	50,3	50	100	0…250	0,6
100,2	100,1	50	100	0…250	0,6
200	199,9	50	100	0…250	0,6
200	199,2	50	100	150…900	0,6
500	499,4	50	100	150…900	1,8

Das Gerät entspricht den Herstellerangaben.
This device meets the manufacturer's specifications.

Qualitätssicherung   **Datum:** 14.01.2016   **Prüfer:**
Quality Control   *Date:*   *Inspector:*

DIN ISO 9001:2008
(Registrier-Nr./ *Registration no.*: 068887 QM08)

[1] **Werksnorm/** *Factory standard*

Appendix D | Laser-guided pyrometer – Optris CT laser

D.1 Optris CT laser datasheet

optris® CTlaser LT

Precise non-contact temperature measurement with precise aiming from -50°C to 975°C

FEATURES

- Low and high temperature measurements of smallest spots up from 0.9 mm
- Double laser aiming marks real spot location and spot size at any distance
- Optics 75:1 with selectable focus
- CT laser F (fast) for scanning of fast moving low temperature objects up from 9 ms response time
- Usable up to 85°C ambient temperature without cooling and automatic laser switch off at 50°C
- Selectable analog outputs 0/4-20mA, 0-5/10V, thermocouple type K or J
- Optional plug in digital interfaces USB, RS232, RS485, CAN or Profibus DP

General Specifications

Environmental rating	IP 65 (NEMA-4)
Ambient temperature	-20°C to 85°C (sensing head, 50°C with laser ON) 0°C to 85°C (electronics)
Storage temperature	Sensing head: -40°C to 85°C Electronics: -40°C to 85°C
Relative humidity	10 - 95%, non condensing
Vibration (sensor)	IEC 68-2-6: 3 G, 11 - 200 Hz, any axis
Shock (sensor)	IEC 68-2-27: 50 G, 11 ms, any axis
Weight	Sensing head: 600 g Electronics: 420 g

Electrical Specifications

Outputs/analog	channel 1: 0/4 - 20 mA, 0 - 5/10 V, thermocouple J, K channel 2: sensing head temperature (-40°C to 85°C as 0 - 5 V or 0 - 10 V), alarm output
Alarm output	Open - collector (24 V / 50 mA)
Optional	relay: 2 x 60 V DC/42 V ACeff; 0.4 A; optically isolated
Outputs/digital (optional)	USB, RS232, RS485, CAN, Profibus DP, Ethernet
Output impedances	mA max. 500 Ω (with 5-36 V DC) mV min. 100 kΩ load impedance thermocouple 20 Ω
Inputs	programmable functional inputs for external emissivity adjustment, ambient temperature compensation, trigger (reset of hold functions)
Cable length	3 m (standard), 8 m, 15 m
Current draw	max. 160 mA
Power Supply	8-36 V DC
Laser 635 nm	1mW, ON/OFF via electronic box or software

Measurement Specifications

Temperature ranges (scalable via programming keys or software)	-50°C to 975°C
Spectral ranges	8-14 µm
Optical resolution (90% energy)	75:1 CTlaser 50:1 CTlaser F
Selectable focus (CTlaser)	CF1 (0.9mm@70 mm) CF2 (1.9 mm@150 mm) CF3 (2.75 mm@200mm) CF4 (5.9 mm@450 mm) SF (16 mm@1260 mm)
System accuracy[1] (at ambient temp. 23 ±5°C)	±1% or ±1°C[2,3] (CTlaser) ±1.5% or ±1.5°C[2,3] (CTlaser F)
Repeatability (at ambient temp. 23 ±5°C)	±0.5 % or ±0.5°C[1,2] (CTlaser) ±1 % or ±1°C[1,2] (CTlaser F)
Temperature resolution (NETD)	0.1°C / 0.5°C (with CTlaser F)
Response time (90% signal)[4]	9 ms (CTlaser F) 120 ms (CTlaser)
Emissivity/Gain (adjustable via programming keys or software)	0.100 - 1.100
Transmissivity/Gain (adjustable via programming keys or software)	0.100 - 1.100
Signal processing (parameter adjustable via programming keys or software, respectively)	peak hold, valley hold, average; extended hold function with threshold and hysteresis
Software	optris Compact Connect

1) different spotsizes for CTlaser F (D:S = 60:1)
2) whichever is greater
3) at object temperatures >0°C, ε =1
4) with dynamic adaption at low signal levels

D.2 Calibration certificate

+optris
infrared thermometers

Kalibrierzertifikat
Calibration Certificate

WKS CTL16011201
Zertifikat-Nr.
Calibration Certificate No

Gegenstand	Infrarotthermometer		Die Kalibrierung erfolgt durch Vergleich des
Object	*Infrared Thermometer*		Prüflings mit der Anzeige des Vergleichsgerätes,

Gegenstand   Infrarotthermometer
Object   *Infrared Thermometer*

Typ   OPTCTLLTSF
Type

Serien-Nr.   6015553
Serial No

Die Kalibrierung erfolgt durch Vergleich des
Prüflings mit der Anzeige des Vergleichsgerätes,
das durch den Deutschen Kalibrierdienst (DKD)
bzw. der Physikalisch-Technischen Bundesanstalt
(PTB) kalibriert wurde.
*The calibration is performed by comparison with
standards which are calibrated by the Deutscher
Kalibrierdienst (DKD) or Physikalisch-Technische
Bundesanstalt (PTB).*

Vergleichsgeräte				
Vergleichsgeräte	OPTLS (8-14µm)	SN 70101	73213 PTB 15	2015-06
Calibrated Standards	OPTCTL2MHSF (1,6µm)	SN 10067604	73327 PTB 14	2014-12
	Keithley 2700	SN 1035646	144969 D-K-19053-01-00	2014-11
	Exactus (0,9µm)	SN EXA2074	73123 PTB 14	2014-12

Die Kalibrierung der Temperaturquellen erfolgt nach ST-CAL, die Kalibrierung des Gerätes nach CTL-CAL.
The calibration of the temperature sources fulfils ST-CAL, the calibration of the product fulfils CTL-CAL.

Messunsicherheit / *Measurement Uncertainty*   1°C / ±1%

Raumtemperatur / *Ambient*   23°C (±5°C)

Luftfeuchte / *Humidity*   26%

Emissionsgrad Einstellung / *Emissivity Setting*   1.00

Messergebnisse / *Results*

Sollwert/*Reference* (°C)	Istwert/*Actual Value* (°C)	Abweichung/*Difference* (°C)
24,1	24,0	− 0,1
166,0	166,2	+0,2
500,0	500,0	0

Das Gerät entspricht den Herstellerangaben.
This device meets the manufacture specifications.

Qualitätssicherung   Datum: Prüfer:
Quality Control   *Date*   *Inspector*

DIN ISO 9001:2008   12.01.2016
(068887 QM08)

Optris GmbH   Ferdinand-Buisson-Str. 14   D-13127 Berlin   Tel.: +49(0)30 500197-0
Fax: +49(0)30 500197-10   Email info@optris.de   Homepage www.optris.de

Appendix E | FTIT temperature data analysis
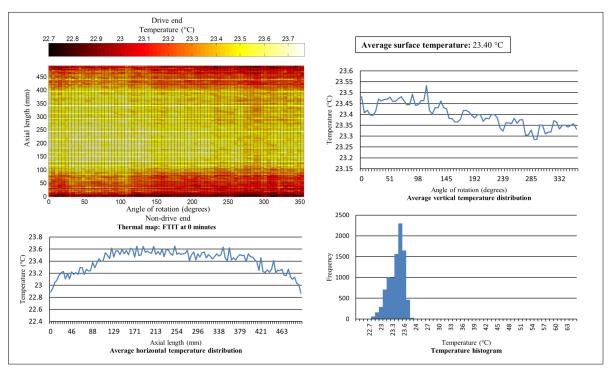
Figure E.1: Temperature data analysis for FTIT at 0 minutes
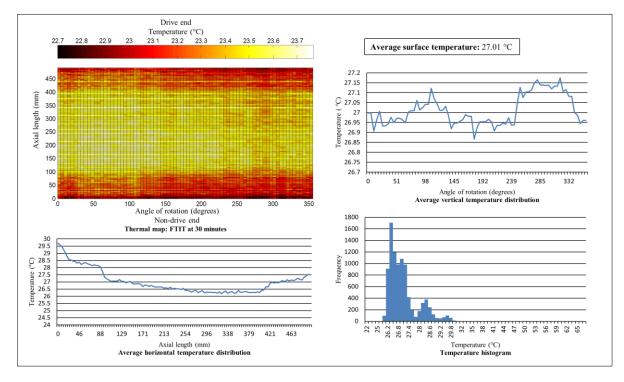
Figure E.2: Temperature data analysis for FTIT at 30 minutes
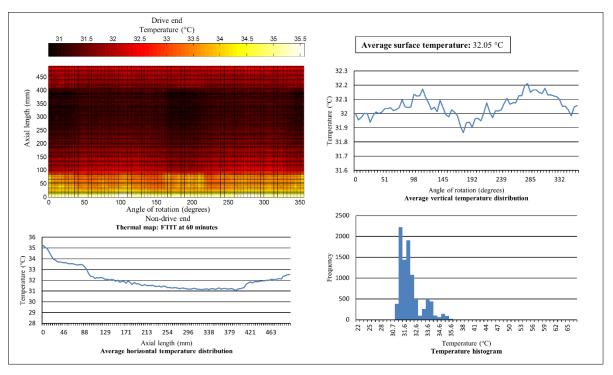
Figure E.3: Temperature data analysis for FTIT at 60 minutes
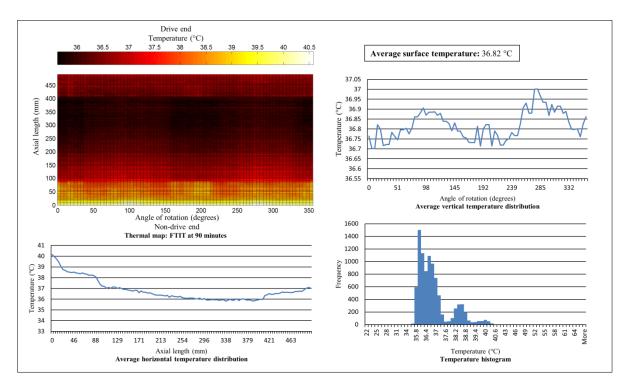
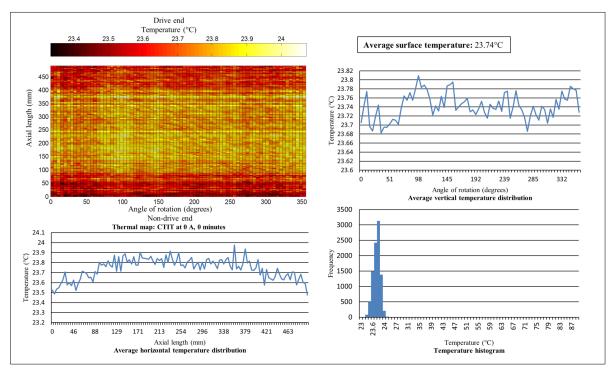**Figure E.4: Temperature data analysis for FTIT at 90 minutes**
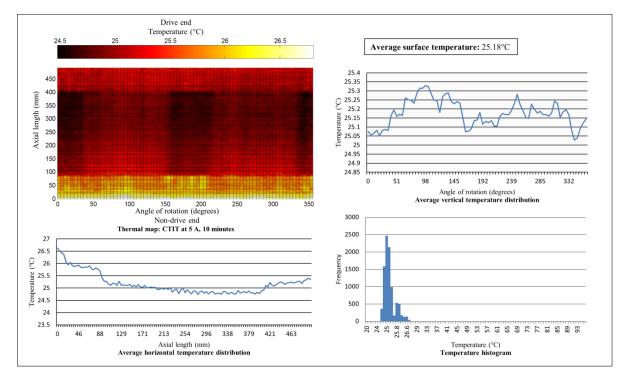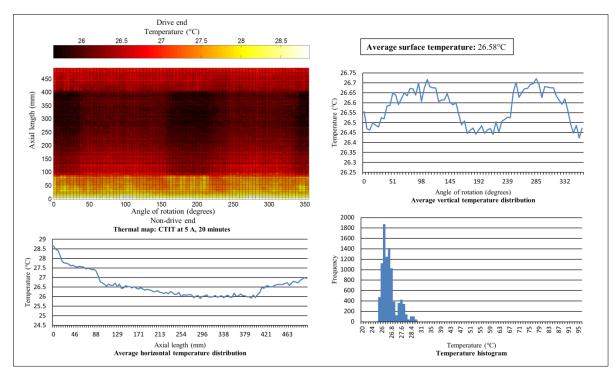
120
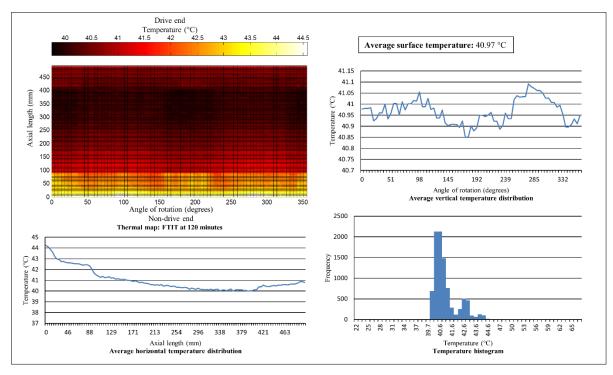
Figure E.5: Temperature data analysis for FTIT at 120 minutes
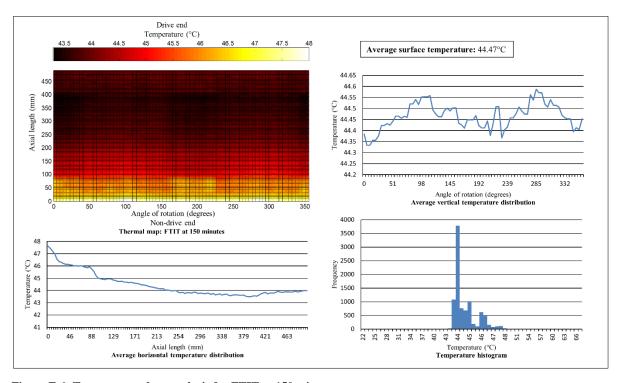
Figure E.6: Temperature data analysis for FTIT at 150 minutes
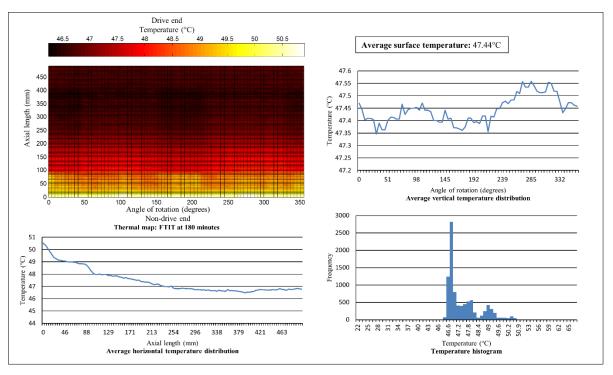
Figure E.7: Temperature data analysis for FTIT at 180 minutes
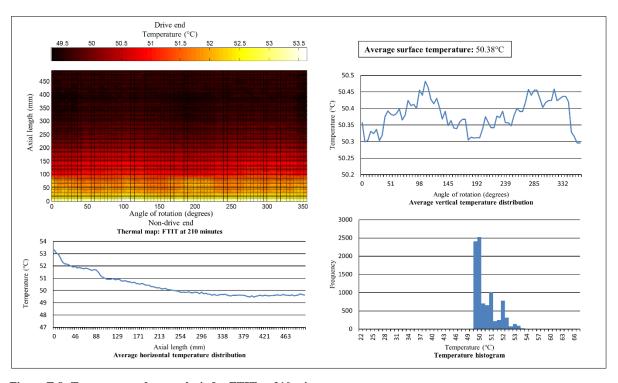
Figure E.8: Temperature data analysis for FTIT at 210 minutes
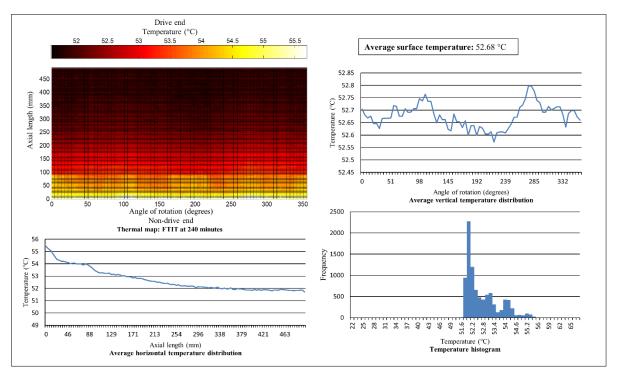
Figure E.9: Temperature data analysis for FTIT at 240 minutes
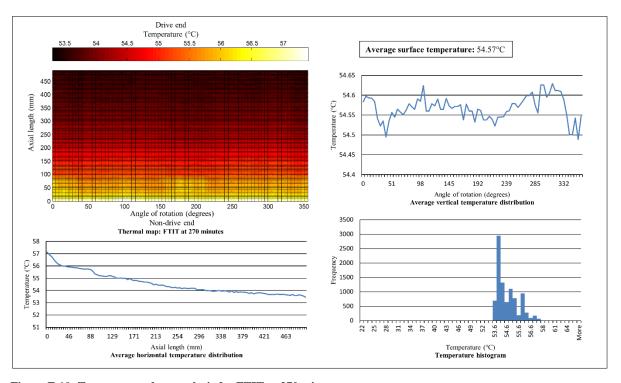
Figure E.10: Temperature data analysis for FTIT at 270 minutes
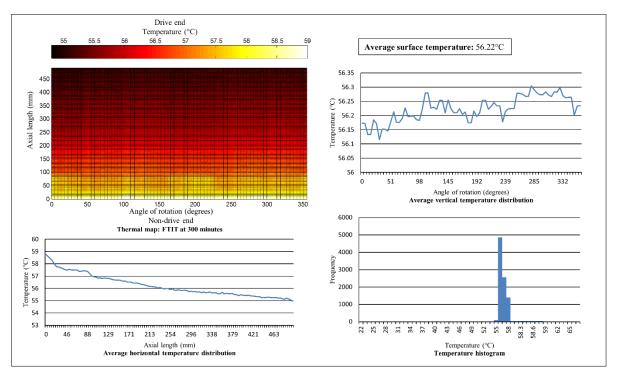
Figure E.11: Temperature data analysis for FTIT at 300 minutes
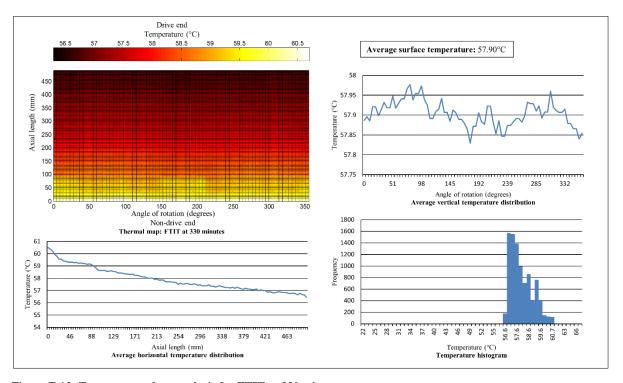
Figure E.12: Temperature data analysis for FTIT at 330 minutes
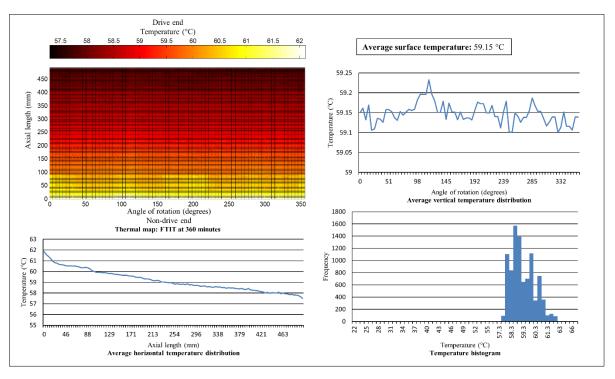
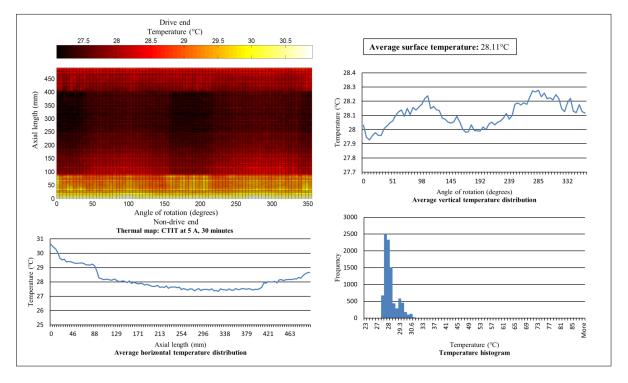**Figure E.13: Temperature data analysis for FTIT at 360 minutes**
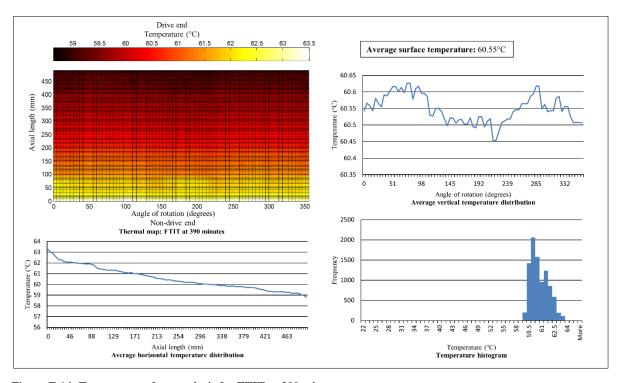
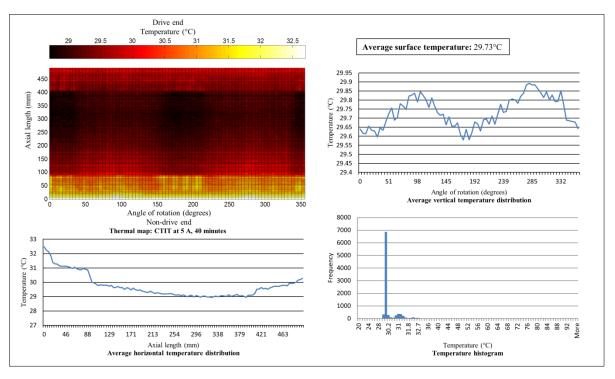**Figure E.14: Temperature data analysis for FTIT at 390 minutes**
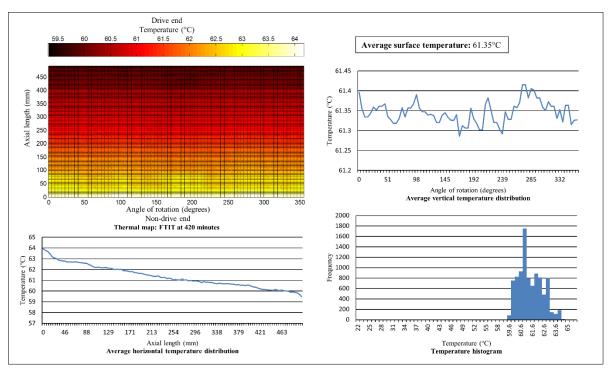
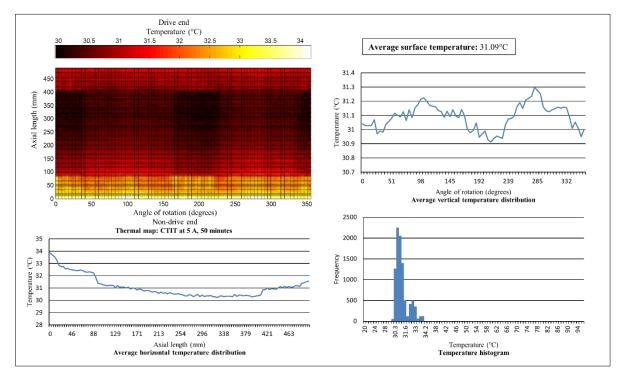**Figure E.15: Temperature data analysis for FTIT at 420 minutes**
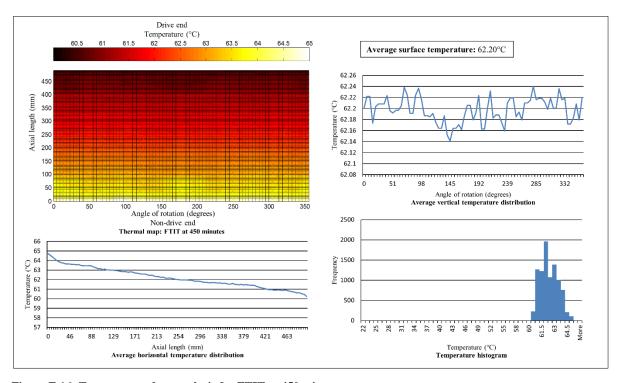
**Figure E.16: Temperature data analysis for FTIT at 450 minutes**
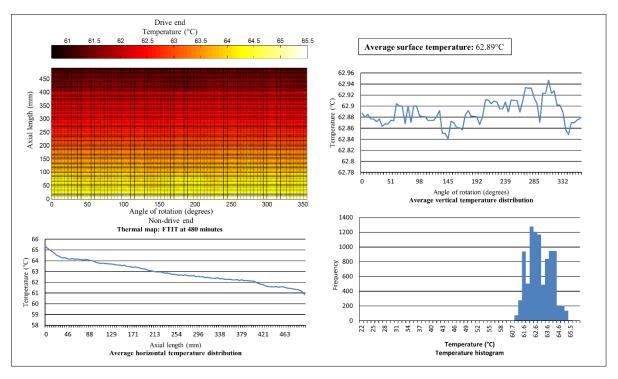
**Figure E.17: Temperature data analysis for FTIT at 480 minutes**

Appendix F | FTIT temperature data analysis with brushes removed
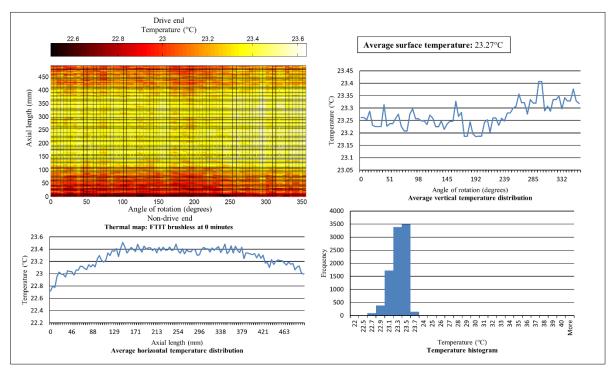
Figure F.1: Temperature data analysis for FTIT with brushes removed at 0 minutes
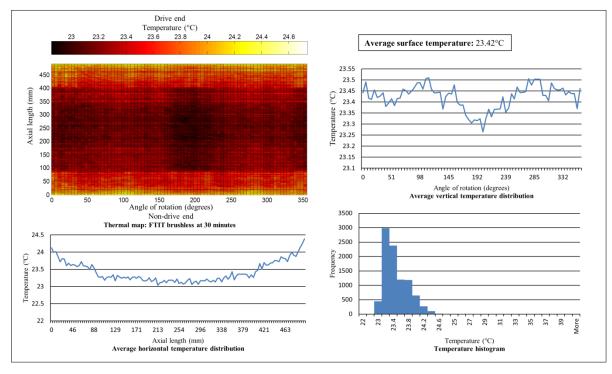
Figure F.2: Temperature data analysis for FTIT with brushes removed at 30 minutes

128
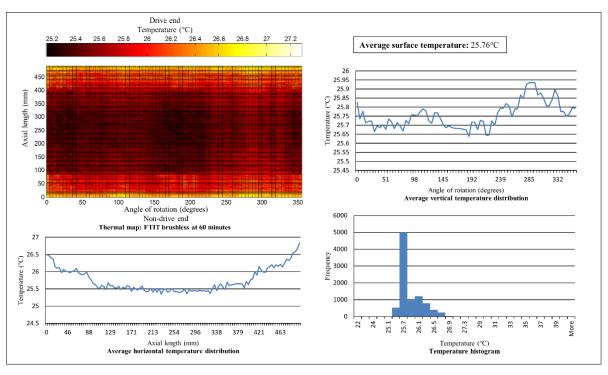
Figure F.3: Temperature data analysis for FTIT with brushes removed at 60 minutes
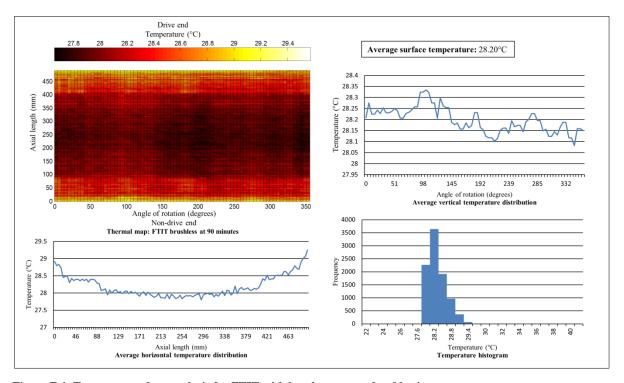
Figure F.4: Temperature data analysis for FTIT with brushes removed at 90 minutes
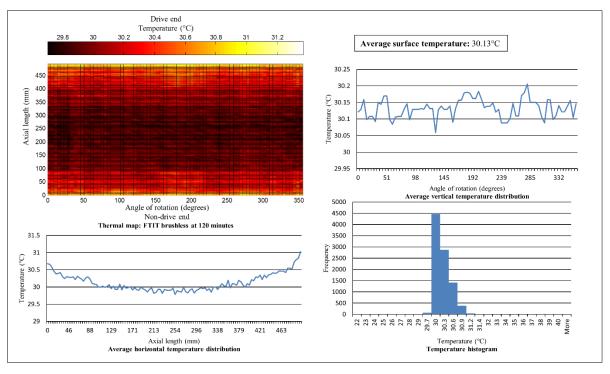
Figure F.5: Temperature data analysis for FTIT with brushes removed at 120 minutes
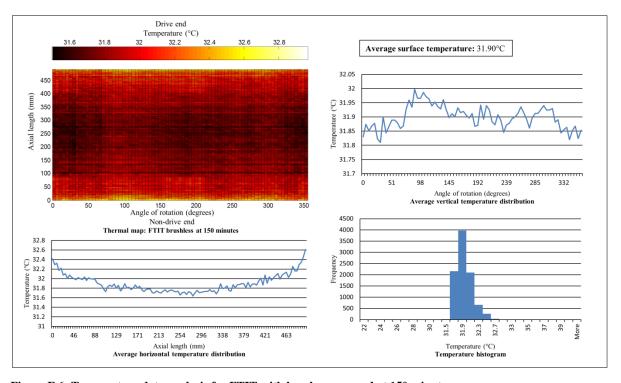
Figure F.6: Temperature data analysis for FTIT with brushes removed at 150 minutes
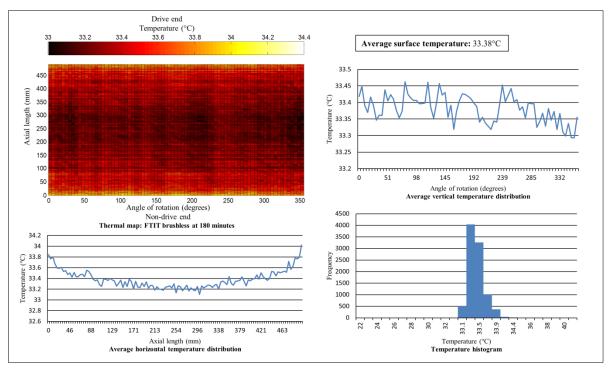
Figure F.7: Temperature data analysis for FTIT with brushes removed at 180 minutes
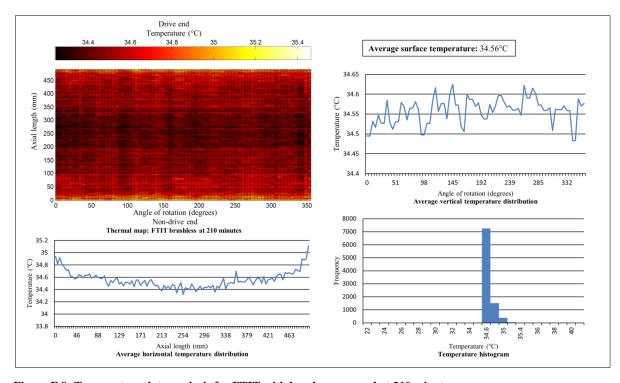
Figure F.8: Temperature data analysis for FTIT with brushes removed at 210 minutes
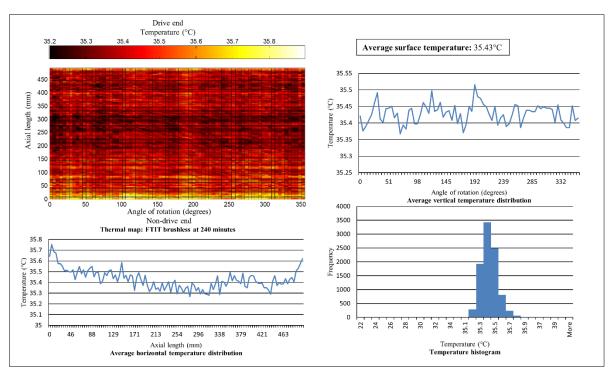
Figure F.9: Temperature data analysis for FTIT with brushes removed at 240 minutes
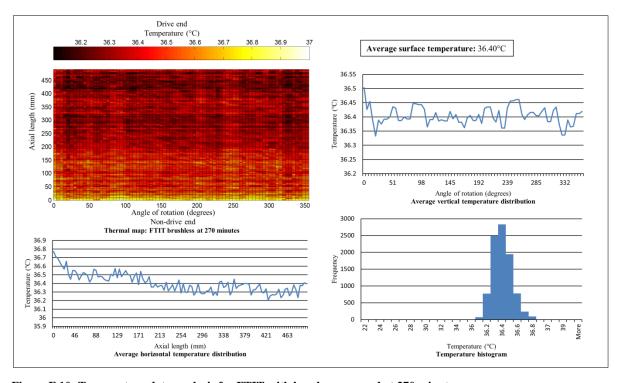
Figure F.10: Temperature data analysis for FTIT with brushes removed at 270 minutes

132
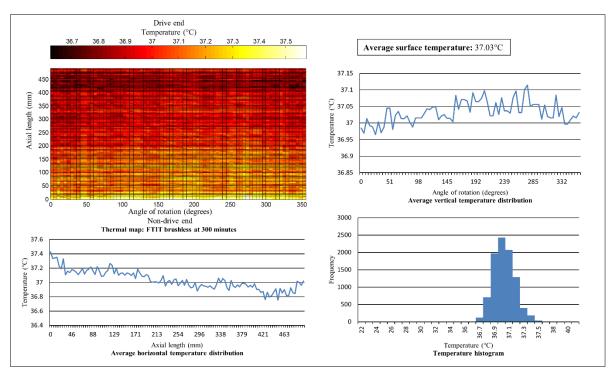
Figure F.11: Temperature data analysis for FTIT with brushes removed at 300 minutes
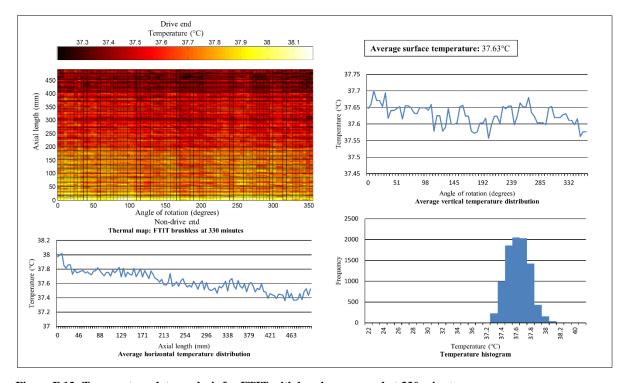
Figure F.12: Temperature data analysis for FTIT with brushes removed at 330 minutes

133
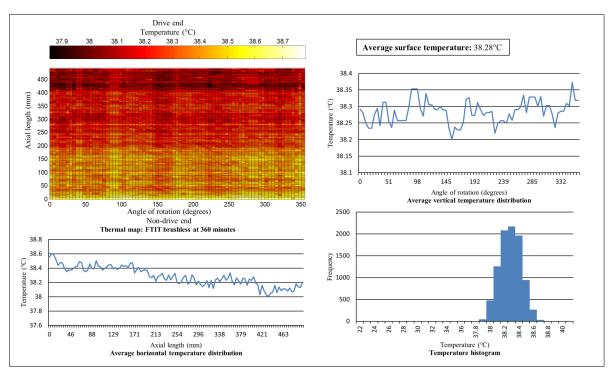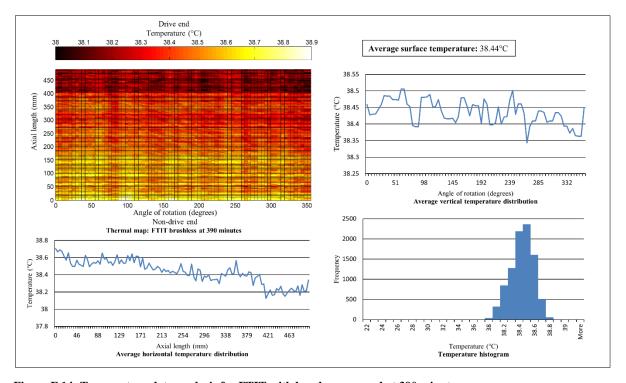
Figure F.13: Temperature data analysis for FTIT with brushes removed at 360 minutes

Figure F.14: Temperature data analysis for FTIT with brushes removed at 390 minutes
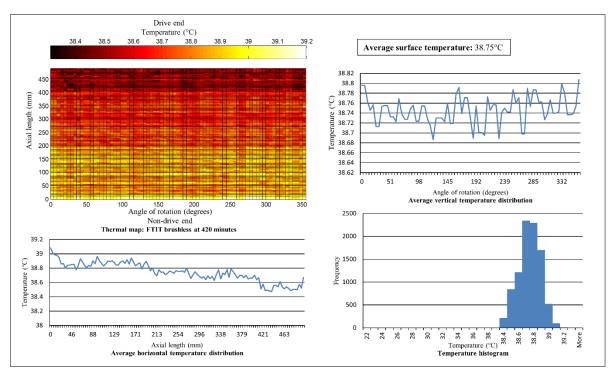
Figure F.15: Temperature data analysis for FTIT with brushes removed at 420 minutes
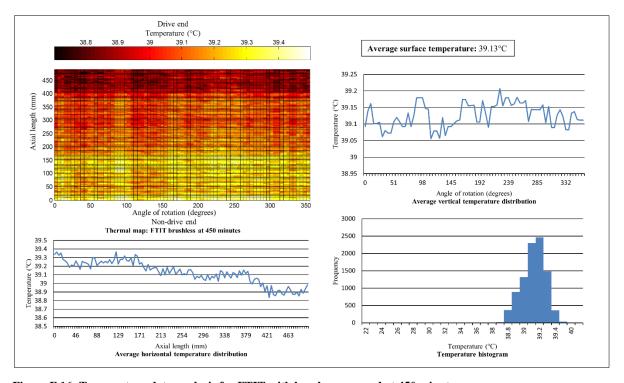
Figure F.16: Temperature data analysis for FTIT with brushes removed at 450 minutes
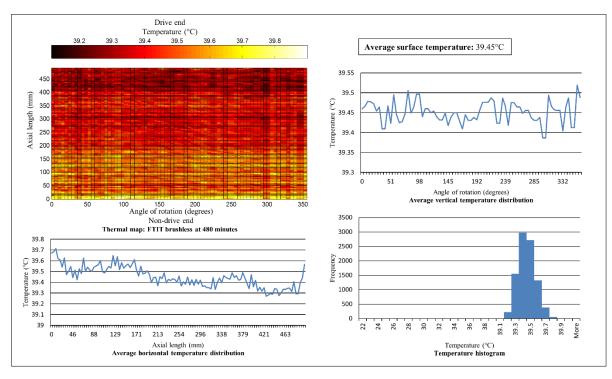
Figure F.17: Temperature data analysis for FTIT with brushes removed at 480 minutes

Appendix G | CTIT temperature data analysis

Figure G.1: Temperature data analysis for CTIT at 0 A, 0 minutes

**Figure G.2: Temperature data analysis for CTIT at 5 A, 10 minutes**

137
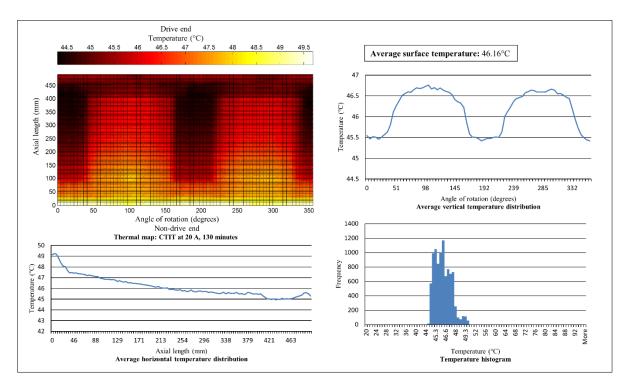
Figure G.3: Temperature data analysis for CTIT at 5 A, 20 minutes

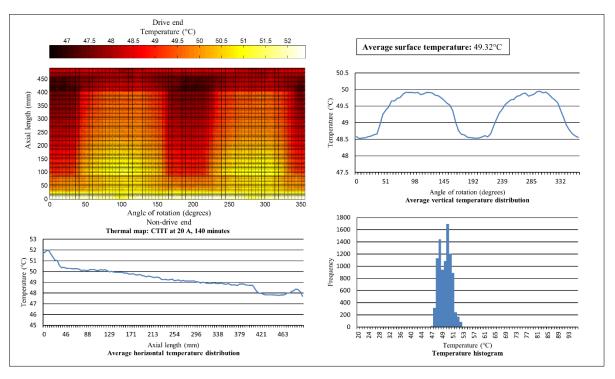**Figure G.4: Temperature data analysis for CTIT at 5 A, 30 minutes**

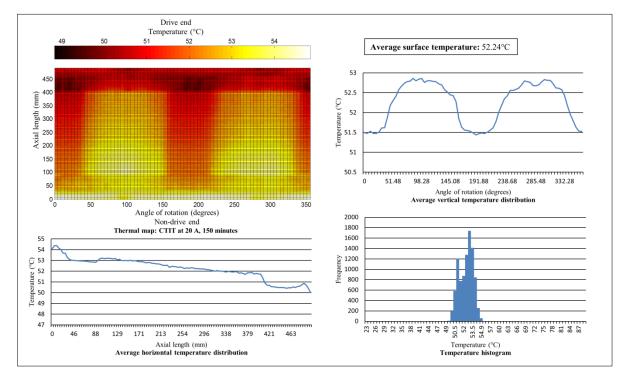**Figure G.5: Temperature data analysis for CTIT at 5 A, 40 minutes**

Figure G.6: Temperature data analysis for CTIT at 5 A, 50 minutes
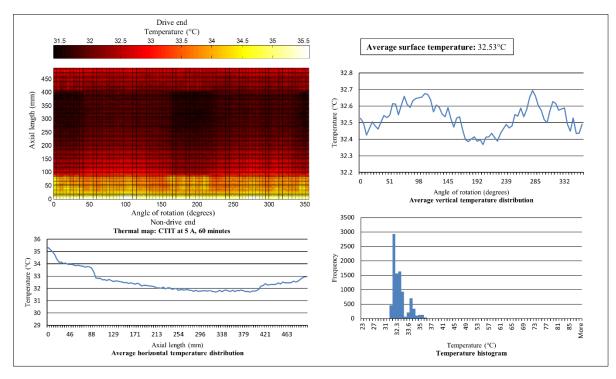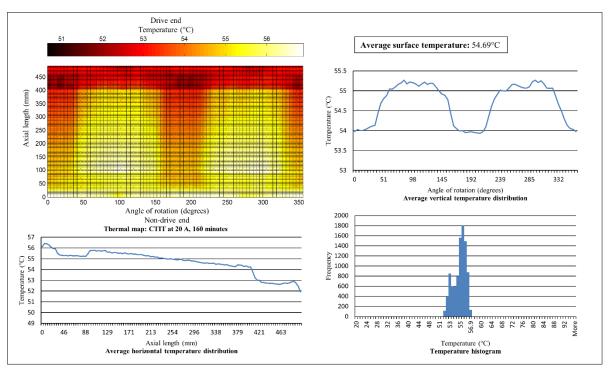
Figure G.7: Temperature data analysis for CTIT at 5 A, 60 minutes
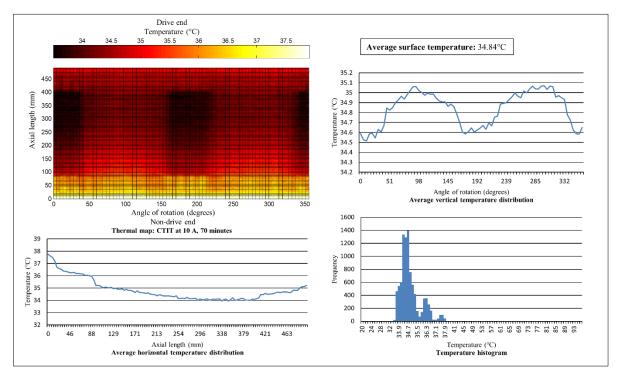
Figure G.8: Temperature data analysis for CTIT at 10 A, 70 minutes
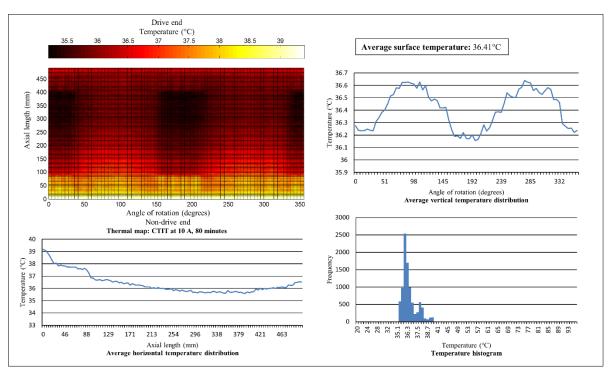
Figure G.9: Temperature data analysis for CTIT at 10 A, 80 minutes
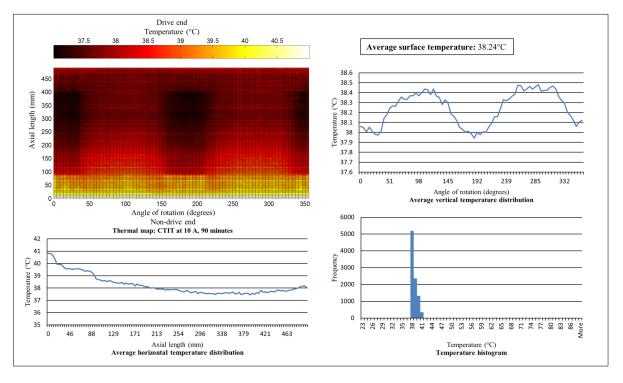
Figure G.10: Temperature data analysis for CTIT at 10 A, 90 minutes
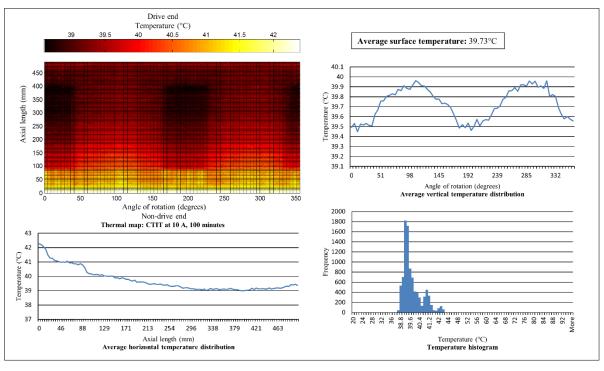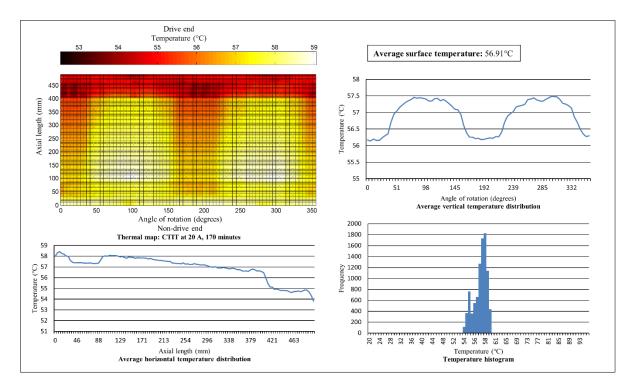
Figure G.11: Temperature data analysis for CTIT at 10 A, 100 minutes
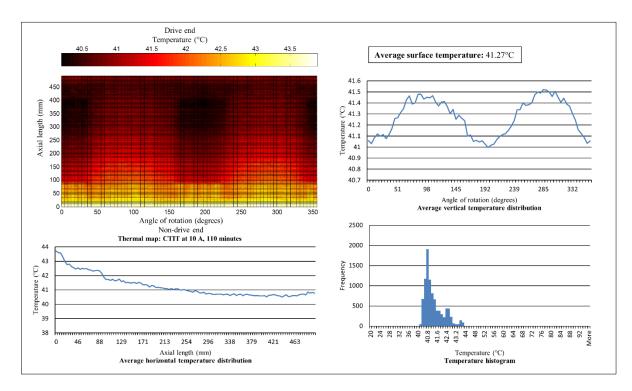
Figure G.12: Temperature data analysis for CTIT at 10 A, 110 minutes
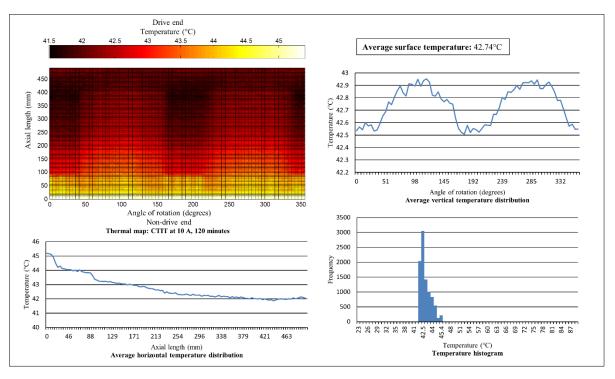
Figure G.13: Temperature data analysis for CTIT at 10 A, 120 minutes

Figure G.14: Temperature data analysis for CTIT at 20 A, 130 minutes

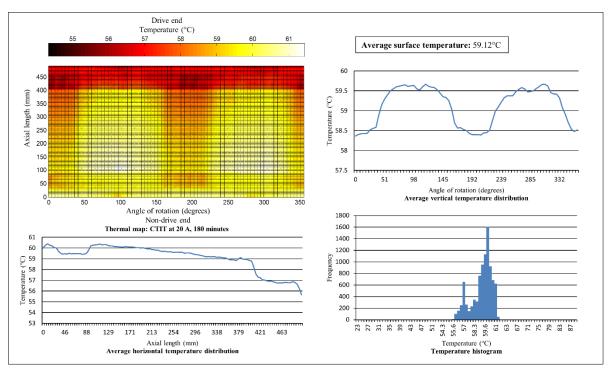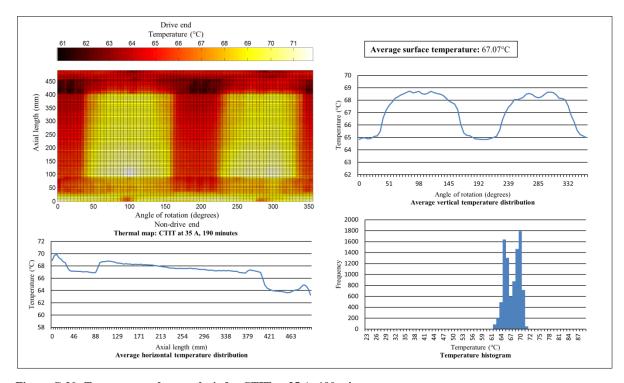**Figure G.15: Temperature data analysis for CTIT at 20 A, 140 minutes**

Figure G.16: Temperature data analysis for CTIT at 20 A, 150 minutes

Figure G.17: Temperature data analysis for CTIT at 20 A, 160 minutes

Figure G.18: Temperature data analysis for CTIT at 20 A, 170 minutes

Figure G.19: Temperature data analysis for CTIT at 20 A, 180 minutes

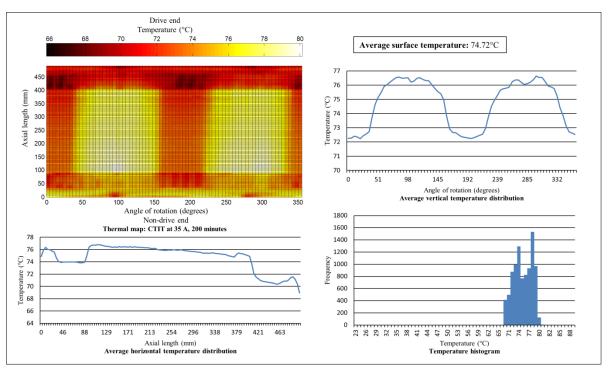**Figure G.20: Temperature data analysis for CTIT at 35 A, 190 minutes**

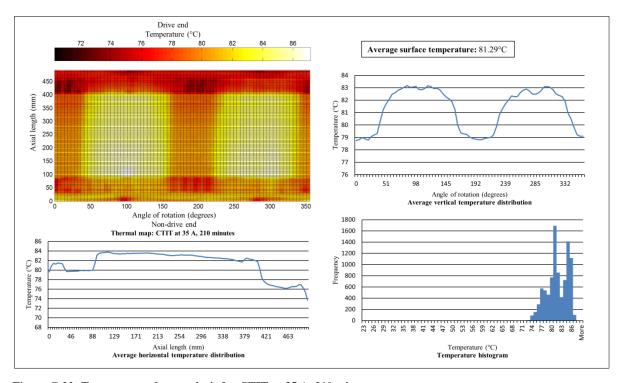**Figure G.21: Temperature data analysis for CTIT at 35 A, 200 minutes**

Figure G.22: Temperature data analysis for CTIT at 35 A, 210 minutes